The Dissertation Committee for Mei Shen Certifies that this is the approved version of the following dissertation:

The Electrogenerated Chemiluminescence of Novel Organic Donor-Acceptor Emitters as well as Study Heterogeneous Electron Transfer Kinetics using Scanning Electrochemical Microscopy

Committee:

Allen J. Bard, Supervisor

Richard M. Crooks

Keith J. Stevenson

David A. Vandenbout

Arumugam Manthiram

The Electrogenerated Chemiluminescence of Novel Organic Donor-Acceptor Emitters as well as Study Heterogeneous Electron Transfer Kinetics using Scanning Electrochemical Microscopy

by

Mei Shen, B.S.; M.S.

Dissertation

Presented to the Faculty of the Graduate School of

The University of Texas at Austin

in Partial Fulfillment

of the Requirements

for the Degree of

Doctor of Philosophy

The University of Texas at Austin

August 2011

Dedication

To my parents who have endlessly supported me to pursue my dream as well as my brothers Wei and Jie, my grandparents, my aunts and uncles.

To my friends, professors and teachers

Acknowledgements

I would like to express my deepest gratitude to Professor Allen J. Bard for giving me the opportunity to work with him, to learn from him, for his guidance and advice, for creating such a multicultural environment and providing me with so many personal and professional growth opportunities and for teaching me to think Big.

I would like to thank Dr. Fu-Ren (Frank) Fan for his help especially in instrumental problems. I would like to thank Joaquin and Alec for spending the graduate time together. I give special thanks to Joaquin for being such a great teacher. I would like to thank Drs. Chongyang Liu and Joy Chen for technical assistance.

I would like to thank Professor Richard M. Crooks for giving me the most important lesson about scientifically oral presentation. I also would like to thank other committee members, Professors Arumugam Manthiram, Keith J. Stevenson, David A. Vandenbout for kindly serving in my defense committee.

I would like to give many thanks to Angie Nelson as well as Penny Kile, Betsy Hamblen, Dr. Jennifer S Brodbelt for the support in my every day activities, and all of collaborators and the Bard group members through the years.

The Electrogenerated Chemiluminescence of Novel Organic Donor-Acceptor Emitters as well as Study Heterogeneous Electron Transfer Kinetics using Scanning Electrochemical Microscopy

Publication No._____

Mei Shen, Ph.D.

The University of Texas at Austin, 2011

Supervisor: Allen J. Bard

New modalities and novel emitters were investigated for the production of electrogenerated chemiluminescence (ECL). In annihilation ECL, a light-emitting excited state is formed upon reaction of two electrochemically generated species, typically a radical anion and a radical cation. Donor-acceptor (DA) molecules provide a means of generating these two reactive species within the same molecule but where the oxidized and reduced centers are separated; furthermore, they allow one to explore the ECL properties of multiply charged radical ions. Three new efficient ECL-emitting donor-acceptor molecules were investigated.

The effects of conjugation in the electrochemistry of diphenylaminospirobifluorenylfumaronitrile (FPhSPFN), which has the structure of D-X-A-A-X-D, where X is a linker, as well as the effects of the stability of its (multiply charged) radical ions on its red ECL emission (λ_{max}= 708 nm) were studied; the molecule

shows solvatochromism and different emission yields on both photoluminescence and ECL in benzene:acetonitrle mixtures. The possibility of generating ECL through multiply charged radical ions was further tested with the very efficient 1b emitter (4,7-bis(4-(4-sec-butoxyphenyl)-5-(3,5-di(1-naphthyl)phenyl)thiophen-2-yl)-2,1,3-benzothiadiazole). Two reversible oxidations and one reduction were observed. The more sluggish reduction is proposed to be a consequence of a long distance electron transfer to the buried acceptor center; further confirmation of this effect was pursued by application of the scanning electrochemical microscope (SECM) to model systems. 1b emits intense ECL with λ_{max}= 635 nm and with an efficiency 330% of the ECL standard 9, 10-diphenylanthracene and similar intensity to the red emitting standard tris(2,2′-bipyridine)ruthenium(II) perchlorate (Rubpy). The generation of asymmetric chronoamperometric ECL pulses upon generation of radical anion-radical dication annihilation events was explained by the use of digital simulation, and proven to be a consequence of asymmetry in the amount of generated charges rather than instability of the electrogenerated species. ECL was also produced from a film of a red fluorophore **1a** (4,7-bis(4-(n-hexyl)-5-(3,5-di(1-naphthyl)phenyl)thiophen-2-yl)-2,1,3-benzothiadiazole) with a coreactant in PBS buffer solution.

The electrochemical synthesis of carbon quantum Dots (C QDs) in inert atmosphere was explored using highly oriented pyrolytic graphite as the starting material, for its later use in the production of ECL in the radical annihilation mode. FT-IR (ATR), mass spectrometry (desorption chemical ionization), Raman and TEM analysis were used to characterize the C QDs.

Table of Contents

List of Tables

List of Figures

Chapter 1. Introduction to Electrogenerated Chemiluminescence and Scanning Electrochemical Microscopy

1.1 Annihilation ECL

Electrogenerated Chemiluminescence (ECL) is the generation of light through electrochemical processes. Luminescence during electrolysis was first observed in the 1920s when Grignard compounds were oxidized at several hundred volts,[1] and again when luminol was electrochemically oxidized in an alkaline solution.[2] In 1964, Hercules showed that a square wave potential pulse could be used to generate light in the absence of oxygen.[3] Many developments have occurred in the field of ECL following these early experiments, including the use of coreactants, which made aqueous ECL possible. The low detection limit ECL has made it an ideal analysis tool. It is especially popular in the area of bioanalysis, where it has been used in enzyme detection, immunosensors, and DNA probes. While its applications are primarily biological, ECL studies are also performed on organic compounds in organic solvent in the absence of oxygen and water. This has led to the observation of many interesting phenomena from the electrochemistry and spectroscopy of a variety of unique compounds.

Annihilation ECL includes the process of generation of an excited singlet state (S-route) through the electron transfer between electrochemically generated species and the following emission of light.[4, 5] This process can be represented in a general way as shown below:

Scheme 1:

$A + e^- \rightarrow A^{-\cdot}$ (reduction at electrode) (1.1.1)

$D - e^- \rightarrow D^{+\cdot}$ (oxidation at electrode) (1.1.2)

$A^{-\cdot} + D^{+\cdot} \rightarrow {}^1A^* + D$ (excited singlet state formation) (1.1.3)

${}^1A^* \rightarrow A + h\nu$ (light emission) (1.1.4)

where A and D are electroactive species and denote acceptor and donor respectively. A and D can belong to different molecules as in mixed ECL systems, but often represent energy levels (i.e., LUMO and HOMO) within the same molecule that are accessible electrochemically to generate a radical cation and a radical anion. ECL can be obtained in this way from species such as aromatic heterocycles or hydrocarbons.[6] A typical case is the efficient ECL emitter 9,10-diphenylanthracene (DPA).[7, 8]

The excited singlet state is not always formed directly during the annihilation reaction. When the energy of the annihilation reaction is significantly smaller than the energy of the emitting singlet state, a triplet excited state could be formed. In this case, the process of triplet-triplet annihilation (T-route) outlined in Scheme 2 follows to form the emitting singlet.

Scheme 2:

$A^{-\cdot} + D^{+\cdot} \rightarrow {}^3A^* + D$ (excited triplet state formation) (1.1.5)

${}^3A^* + {}^3A^* \rightarrow {}^1A^* + A$ (triplet-triplet annihilation) (1.1.6)

${}^1A^* \rightarrow A + h\nu$ (light emission) (1.1.7)

1.2 COREACTANT ECL

Coreactants are also used in ECL studies when one of the generated radical species are unstable or cannot be generated within the solvent window. A coreactant is a compound that can become a strong oxidizing or reducing agent upon reduction or oxidation, respectively. The most common coreactants are benzoyl peroxide (BPO), persulfate, tripropylamine (TPrA) and oxalate. BPO and persulfate can be reduced to create oxidizing agents, while TPrA and oxalate can be oxidized to make reducing agents. For example, in the case when BPO is used as a coreactant, the excited state is generated as follows:

Scheme 3:

$$BPO + e^- \rightarrow BPO^{-\cdot} \quad (1.2.1)$$

$$BPO^{-\cdot} \rightarrow C_6H_5CO_2^- + C_6H_5CO_2^{\cdot} \quad (1.2.2)$$

$$C_6H_5CO_2^{\cdot} + A^{-\cdot} \rightarrow C_6H_5CO_2^- + {}^1A^* \quad (1.2.3)$$

Notice that in both Schemes 1 and 2, the mechanism through which the excited state is formed involves an annihilation reaction between the molecule under study that may give rise to the formation of excimers; the coreactant scheme typically gives rise to emissive states devoid of this particular complication and as such has been used to distinguish spectral differences between ECL and photoluminescence (PL).[9, 10]

1.3 INTRODUCTION TO SECM

SECM involves the measurement of the current through an ultramicroelectrode (UME) (an electrode with a radius, *a*, of the order of a few nm to 25 μm) when it is held or moved in a solution in the vicinity of a substrate. Substrates, which can be solid surfaces of different types (e.g., glass, metal, polymer, biological material) or liquids (e.g., mercury, immiscible oil), perturb the electrochemical response of the tip, and this perturbation provides information about the nature and the properties of the substrate. [11]

A voltammogram was produced on an UME, and the current eventually limits to a value that is completely controlled by the rate of mass transfer by diffusion of electroactive species O from the bulk solution to the electrode surface. For a conductive disk with radius *a*, this limiting current when the tip is far away from the substrate is given by:

$$i_{T,\infty} = 4nFDC^*a \qquad (1.3.1)$$

where *n* is the number of electron transferred, *D* is the diffusion coefficient of O, *C** is concentration of O. When the tip is brought close to a substrate, a positive feedback or a negative feedback will be observed depending on the nature of the substrate. If the substrate is an insulator, like a piece of glass or plastic, the substrate blocks some of the diffusion of O to the tip and the current will decrease compared to $i_{T,\infty}$. The closer the tip gets to the substrate, the smaller i_T becomes. At the limit when the distance between the tip and the substrate, *d*, approaches zero, i_T also approaches zero. This decrease in current with distance is called negative feedback. When the tip is brought near an electrically conductive substrate, like a platinum electrode, while there is still blockage of diffusion

of O to the tip by the substrate, there is also the oxidation of the product R back to O. This O generated at the substrate diffuses to the tip and causes an increase in the flux of O compared with $i_{T,\infty}$. In the limit as d approaches zero, the tip will move into a regime where electron tunneling can occur and the tip current will get very large. This increase of current with distance is called positive feedback. A plot of i_T versus d, as a tip is moved in the z direction, is called an approach curve. Schemes when the tip is far away from the substrate as well as when the tip is close to an insulator substrate and a conductive substrate along with approach curves are shown in Figure 1.1.

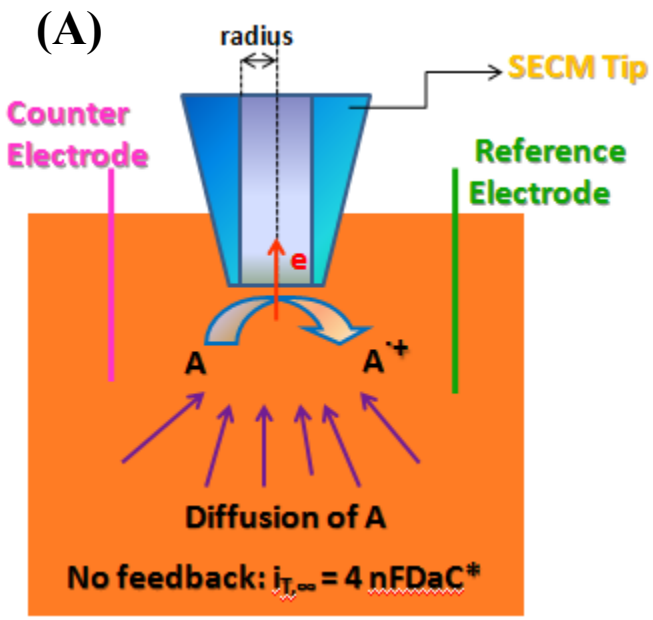

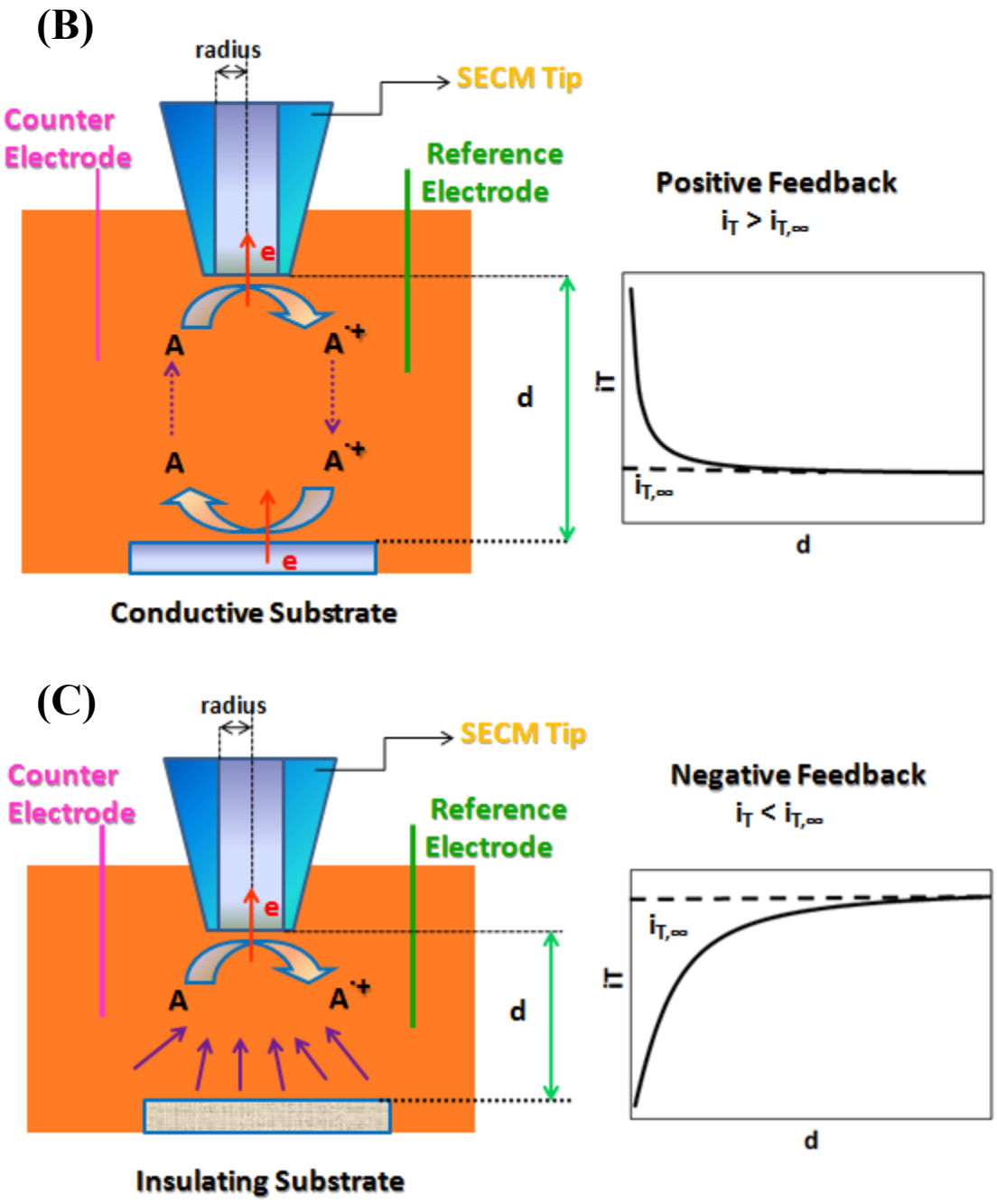

Figure 1.1. Schematic representation of the SECM experiment when the electroactive species are A and oxidation occurs on the tip,.

(A) Steady-state diffusion to the tip far from substrate. (B)Tip is near a conductive substrate, Positive feedback. (C) Tip is near an insulating substrate, Negative feedback**.**

1.4 KINETIC STUDY USING SECM FEEDBACK MODE

There are two approaches to measure heterogeneous electron transfer kinetics at electrodes by SECM. One approach is to measure kinetics at the tip electrode above a conductive substrate by taking advantage of the increased mass transfer to the tip, the reaction on the substrate is mass transfer controlled. The alternative approach is to examine heterogeneous electron transfer kinetics on the substrate by holding the tip at a potential where the reaction is mass transfer controlled and studying the approach curve as a function of substrate potential.[12] For the case when kinetics are measured at the tip, Equations 1.4.1 to 1.4.4 are useful (RG = 10): [13, 14]

$$I_T(E, L) = \frac{0.68+\frac{0.78377}{L}+ 0.3315\, e^{-\frac{1.0672}{L}}}{\theta+\frac{1}{\kappa}} \qquad (1.4.1)$$

$$\kappa = \frac{k^0 e^{-\alpha n f(E-E^{0\prime})}}{m_O} \qquad (1.4.2)$$

$$m_O = \frac{4D_o}{\pi a}\left(0.68 + \frac{0.78377}{L} + 0.3315e^{-1.0672/L}\right) \qquad (1.4.3)$$

$$\theta = 1 + \frac{D_o}{D_R}\, e^{\left(nf\left(E-E^{0\prime}\right)\right)} \qquad (1.4.4)$$

Where κ is the kinetic parameter and m_o is the effective mass-transfer coefficient.

Equations 1.4.1 to 1.4.4 can be used to determine the standard rate constant and the transfer coefficient for a sluggish tip reaction. For a system with no kinetic complications at the tip, the CV response of the tip will simply be:

$$I_T(E, L) = \frac{0.68 + \frac{0.78377}{L} + 0.3315\, e^{-\frac{1.0672}{L}}}{\theta} \qquad (1.4.5)$$

where θ has been described in Equation 1.4.4.

1.5 REFERENCES

[1] Dufford, R. T.; Nightingale, D.; Gaddum, W. L. *J. Am. Chem. Soc.* **1927**, *49*, 1858.

[2] Harvey, N. *J. Phys. Chem.* **1929**, *33*, 1456.

[3] Hercules, D. M. *Science.* **1964**, *145*, 808.

[4] Bard, A. J. in *Electrogenerated Chemiluminescence*; Bard, A. J., Ed.; Marcel Dekker: New York, 2004.

[5] For reviews on ECL, see: (a)Ref 2. (b) Richter, M. M. *Chem. Rev*. **2004**, *104*, 3003-3036. (c) Knight, A. W.; Greenway, G. M. *Analyst* **1994**, *119*, 879-890. (d) Faulkner, L. R.; Bard, A. J. *Electroanalytical Chemistry*; Marcel Dekker: New York, 1977; Vol. 10, p 1. (e) Bard, A. J.; Debad, J. D.; Leland, J. K.; Sigal, G. B.; Wilbur, J. L.; Wohlstadter, J. N. in *Encyclopedia of Analytical Chemistry: Applications, Theory and Instrumentaion*; Meyers, R. A., Ed.; John Wiley & Sons: New York, 2000; Vol. 11, p 9842.

[6] Forry, S. P.; Wightman, R. M. in *Electrogenerated Chemiluminescence*; Bard, A. J., Ed.; Marcel Dekker: New York, 2004; p 277.

[7] Maloy, J. T. in *Electrogenerated Chemiluminescence*; Bard, A. J., Ed.; Marcel Dekker: New York, 2004; p 159.

[8] Keszthelyi, C. P.; Tokel-Takvoryan, N. E.; Bard, A. J. *Anal. Chem*. **1975**, *47*, 249-256.

[9] Sartin, M. M.; Zhang, H. Y.; Zhang, J. Y.; Zhang, P.; Tian, W. J.; Wang, Y.; Bard, A. J. *J. Phys. Chem. C* **2007**, *111*, 16345-16350.

[10] Choi, J.-P.; Wong, K.-T.; Chen, Y.-M.; Yu, J.-K.; Chou, P.-T.; Bard, A. J. *J. Phys. Chem. B.* **2003**, *107*, 14407-14413.

[11] Bard, A. J. In *Scanning Electrochemical Microscopy*; Bard, A. J.; Mirkin, M. V., Eds,; Marcel Dekker: New York, 2001, pp 1.

[12] Borgwarth, K.; Heinze, J. In *Scanning Electrochemical Microscopy*; Bard, A. J.; Mirkin, M. V., Eds,; Marcel Dekker: New York, 2001, pp 217-219.

[13] Mirkin, M. V.; Richards, T. C.; Bard, A. J. *J. Phys. Chem.* **1993**, *97*, 7672-7677.

[14] *Scanning Electrochemical Microscopy*; Bard, A. J.; Mirkin, M. V., Eds,; Marcel Dekker: New York, 2001.

Chapter 2. Electrochemistry and Electrogenerated Chemiluminescence of Diphenylaminospirobifluorenylfumaronitrile

2.1 INTRODUCTION

Donor-acceptor based molecules include the cases in which the donor and acceptor are either directly covalently connected[1-3]or through a linker[4]. The first case can be represented as D-A and the second case as D-X-A, where X is the linker. Diphenylaminospirobifluorenylfumaronitrile (FPhSPFN) red fluorophore is a donor-acceptor based molecule. The fumaronitrile moiety is a good electron acceptor (A)[5] and triphenylamine based molecules are good electron donors (D)[6,7-9]. Spirobifluorene has been used extensively in molecular design as a linker because of its structural rigidity.[10-12] FPhSPFN has a configuration of D-X-A-X-D, where a fumaronitrile group as A and two substituted diphenylamines as D, linked through a spirobifluorene linker X. FPhSPFN emits in the red region and exhibits a high solid state fluorescence quantum yield (46% at 646 nm)[13] and was designed for use in organic light emitting devices (OLED).

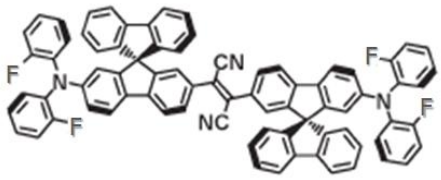

FPhSPFN

We report an electrochemical and spectroscopic study of a novel donor-acceptor-based molecule, i.e., FPhSPFN red fluorophore, as well as its electrogenerated chemiluminescence (ECL) that results from the annihilation reaction between the radical anions and radical cations generated during electrochemical reduction and oxidation.

2.2 EXPERIMENTAL

Solutions for electrochemical measurements consisted of 0.5 mM FPhSPFN in 2.33:1 (by volume) MeCN/PhH mixture as the solvent and 0.1 M $TBAPF_6$ as the supporting electrolyte. Anhydrous acetonitrile (MeCN) and benzene (PhH) were obtained from Aldrich (St. Louis, MO) and transferred directly into a helium atmosphere drybox (Vacuum Atmospheres Corp., Hawthorne, CA) without further purification. Electrochemical grade tetra-*n*-butylammonium hexafluorophosphate ($TBAPF_6$) was obtained from Fluka and used as received. Benzoyl peroxide (BPO) was from Aldrich and was used as received. FPhSPFN was synthesized according to literature procedure.[13]

The same electrochemical cell (Figure 2.1) was used for both cyclic voltammetry and ECL transient experiments; it consisted of a coiled Pt wire (0.5 mm in diameter) as a counter electrode, a Ag wire (0.5 mm in diameter) as a quasi-reference electrode, and a Pt disk inlaid in glass bent at a 90^o angle (for the disk to face the detector) as a working electrode. The area of the Pt disk electrode was 0.019 cm^2 unless specifically noted. After each experiment, the potential of the Ag wire was calibrated with ferrocene (taken as 0.342 V vs SCE**)**.[14] Before each experiment, the working electrode was polished on a felt pad with 0.3 μm alumina (Buehler, Ltd., Lake Bluff, IL), sonicated in Milli-Q deionized water and then in ethanol. The counter and reference electrodes were cleaned by rinsing and sonicating in acetone, water and ethanol. Finally, all the electrodes were rinsed with acetone, dried in the oven and transferred into the drybox. For chronoamperometry experiments, a 25 μm (in diameter) gold ultramicroelectrode (UME) was used as working electrode. The cleaning of the UME followed the same procedure as the cleaning of the macro working electrode.

(A)

(B)

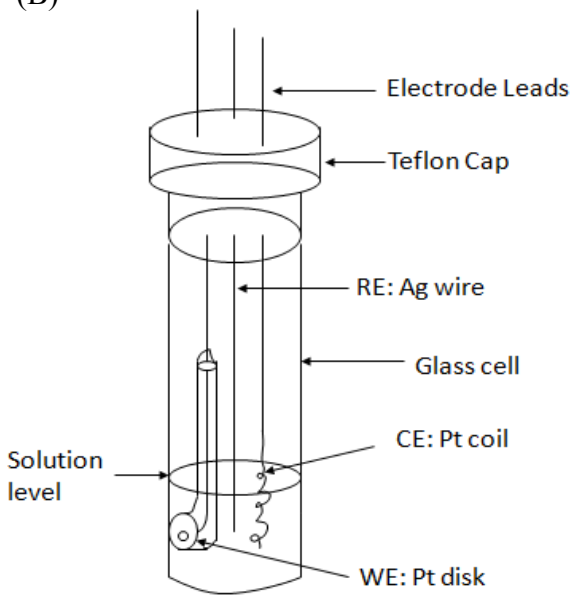

Figure 2.1. (A) Picture and (B) Diagram of the electrochemical cell.

All solutions were prepared inside the drybox. For measurements made outside of the box, the electrochemical cell was closed with a Teflon cap that had a rubber O-ring to form an airtight seal. Stainless steel rods driven through the cap formed the electrode connections. Cyclic voltammograms (CVs) were obtained on a CH Instruments electrochemical workstation (CHI 660, Austin, TX). Spectroscopic experiments were done in a 1 cm path length quartz cell. Absorbance spectra were obtained on a Milton Roy spectronic 3000 array spectrophotometer. Fluorescence spectra were collected on a QuantaMaster spectrofluorimeter (Photon Technology International, Birmingham, NJ). The excitation source was a 70 W xenon lamp (LPS-220B Lamp power supply), and the excitation and emission slits were set to 0.5 mm (2 nm bandwidth).

The ECL spectra were obtained on Princeton SPEC-10 Instruments using a charge-coupled device (CCD) camera (Trenton, NJ) cooled to -100^{o}C with an Acton SpectraPro-150 monochromator (Acton, MA) as detector. ECL spectra were calibrated using Hg/Ar pen-ray lamp from Oriel (Stratford, CT). ECL intensity-time curves were collected on an Autolab potentiostat (Ecochemie, Netherlands) connected to a photomultiplier tube (PMT, Hamamatsu, R4220p, Japan). The PMT was supplied with -750 V from a Kepco (New York) or a series-225 Bertan (Bertan High Voltage Corp., Hucksville, NY) high voltage power supply. Relative ECL intensity was calculated with respect to DPA in 2.33:1 MeCN/PhH by comparison of the maximum intensities in ECL spectra.

2.3 ELECTROCHEMISTRY

The reversibility, diffusion coefficient and number of electrons transferred as well as the stability of the radical cations and anions of FPhSPFN were investigated using

cyclic voltammetry (CV). A CV showing both reduction and oxidation is shown in Figure 2.2; two reduction waves and one overall oxidation wave were observed. The experimental values obtained for the standard potentials of the reductions are $E^{o}_{1,\ red}$ = -1.09 V vs SCE and $E^{o}_{2,\ red}$ = -1.50 V vs SCE. Simulation was done to further investigate the oxidation peak. The results will be shown and discussed later.

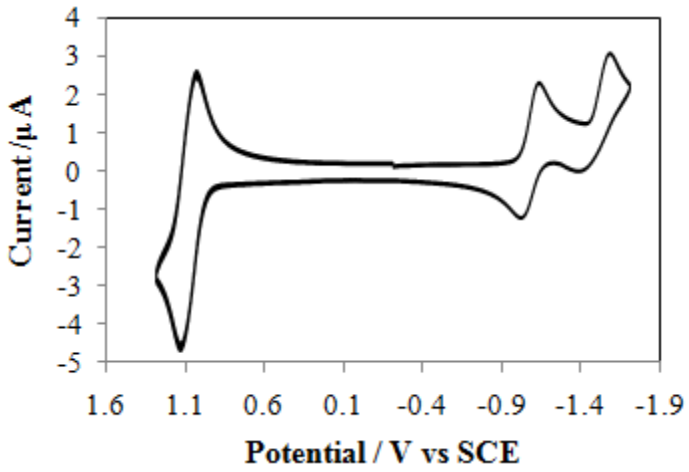

Figure 2.2. Cyclic voltammogram of 0.5 mM FPhSPFN in 2.33:1 MeCN/PhH with 0.1 M $TBAPF_6$.

Scan rate = 100 mV/s. Area of electrode is 0.019 cm^2.

The scan rate (v) was changed to study the reversibility of the reduction and oxidation of FPhSPFN. Scan rate dependent CVs for the first reduction peak and oxidation are presented in Figure 2.3. Peak splittings (ΔE_p) for first reduction and oxidation of 0.5 mM FPhSPFN are presented in Table 2.1. As a reference, ΔE_p for ferrocene performed under the same experimental conditions with different v are also included in Table 2.1.

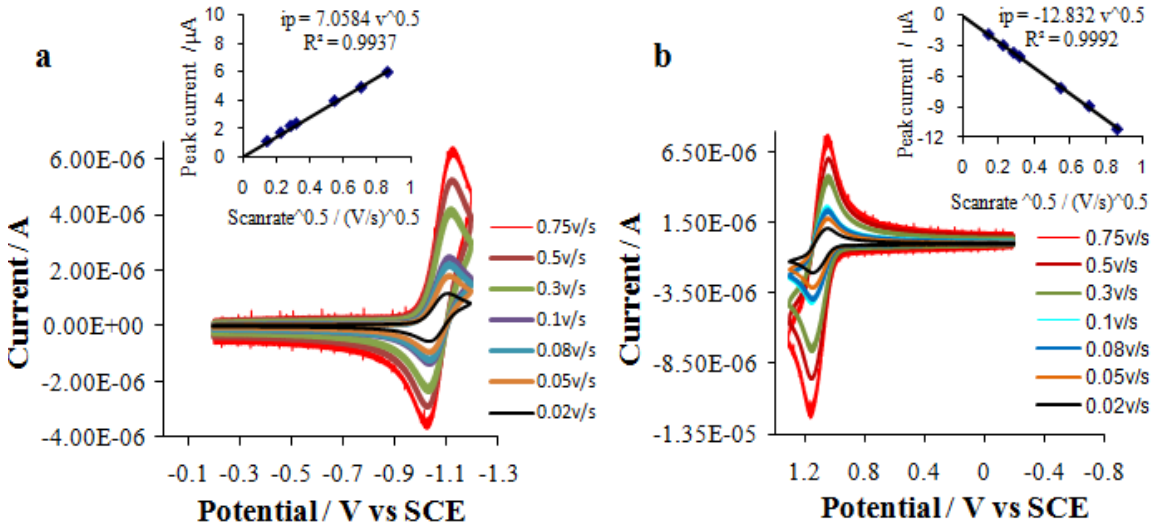

Figure 2.3. (a) Reduction voltammogram of first reduction peak of 0.5 mM FPhSPFN in 2.33:1 MeCN/PhH at various *v*.

Inset: First reduction peak current versus $v^{1/2}$. (b) Oxidation CV of 0.5 mM FPhSPFN in 2.33:1 MeCN/PhH at various scan rates. Inset: Oxidation peak current versus $v^{1/2}$.

Table 2.1. Peak splitting (mV) for the first reduction peak and the overall oxidation peak of 0.5 mM FPhSPFN and 1 mM ferrocene in 2.33: 1 MeCN/PhH and 0.1 M $TBAPF_6$ at various scan rates.

	0.02 V/s	**0.05 V/s**	**0.08 V/s**	**0.1 V/s**	**0.3 V/s**	**0.5 V/s**	**0.75 V/s**
First reduction	73	77	73	81	87	93	101
Overall oxidation	101	102	97	103	109	115	117
Ferrocene	73	73	71	75	85	87	95

From Figure 2.3, it can be seen that the peak current changed linearly with the square root scan rate for both the first reduction ($i_{p,r1}$) and the overall oxidation ($i_{p,o}$), indicating diffusion control of the current. The results in Table 2.1 show that at small *v*, the ΔE_p for the first reduction peak is larger than ~59 mV expected for a nernstian wave.

However, ferrocene, a known nernstian system studied under the same experimental conditions shows a similar ΔE_p value. The similarity of peak splitting to ferrocene indicates that the first reduction peak is nernstian under the experimental conditions and most likely only affected by uncompensated resistance. However, for the oxidation peak, a larger peak splitting than ferrocene is observed, thus the oxidation is not a single one-electron transfer process and, as shown below, involves a multi- electron transfer.

Chronoamperometry at an UME was used to determine the number of electrons, *n*, exchanged in each electrochemical process observed. The methodology used consists of determining the diffusion coefficient, *D*, independently from *n* and with only prior knowledge of the bulk concentration, *C** and the radius of the UME, *a*, by normalizing a short time transient with respect to the limiting steady state current, $i_{d,ss}$.[15] This normalized response is plotted against $t^{-1/2}$ where linear fitting should yield a slope equal to $(2/\pi^{3/2})aD^{-1/2}$. After determining *D*, *n* can be calculated based on Eq. 2.1 for $i_{d,ss}$:

$$i_{d,ss} = 4\,n\,F\,D\,C^{*}a \qquad (2.1)$$

where *F* is Faraday's constant (96,485 C/mol). Before the chronoamperometry study, the linear scan voltammetry of FPhSPFN at a gold UME was studied. Voltammograms before subtracting background for FPhSPFN and of the background are shown in Figure 2.4. The background processes observed in this figure correspond to oxidation and reduction reactions occurring at the extremes of the potential window and that have a slight impact in the surface condition of the electrode. Background subtraction allows a clear observation of the purely diffusional processes occurring during the measurement.

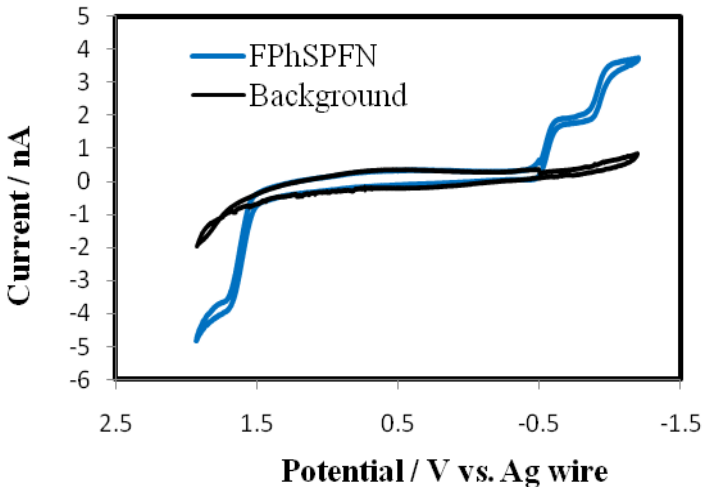

Figure 2.4. Cyclic voltammogram before subtracting background for FPhSPFN and of the background on gold UME.

Solution of FPhSPFN contains 0.5 mM FPhSPFN in 2.33:1 acetonitrile/benzene and 0.1 M $TBAPF_6$, background solution contains only 0.1 M $TBAPF_6$ in 2.33:1 acetonitrile/benzene, gold UME has a radius of a = 12.5 μm. Scan rate = 100 mV/s.

The background subtracted voltammogram is shown in Figure 2.5. Two well separated reduction peaks and a single oxidation peak were observed, consistent with the CV results at a macroelectrode. The value of the steady state current for oxidation was twice value of steady state current of each reduction wave.

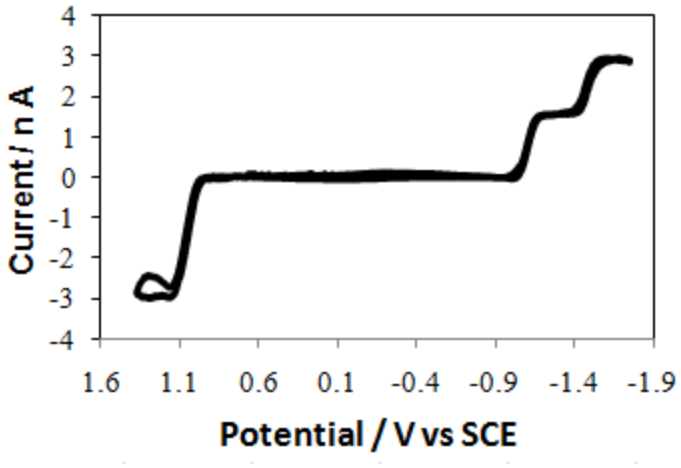

Figure 2.5. Background subtracted cyclic voltammogram.

For 0.5 mM FPhSPFN in 2.33:1 MeCN/PhH and 0.1 M $TBAPF_6$ on gold UME, radius *a* = 12.5 μm. Scan rate = 100 mV/s.

Chronoamperometry results for the first reduction (step potential, E_{SP} = -1.18 V vs SCE) and overall oxidation (E_{SP} = 1.18 V vs SCE) are shown in Figure 2.6. In Figure 2.6, $i(t)/i_{ss}$ were plotted versus $t^{-1/2}$ **,** experimental data show that $i(t)/i_{ss}$ are linearly dependent on $t^{-1/2}$. Linear regression was used to calculate the slope and intercept. The intercepts obtained from all of these cases are very close to 1. The intercept and the linear dependence agree well with the theoretical prediction in a reasonably short time region (≥ 0.3 s). [15]

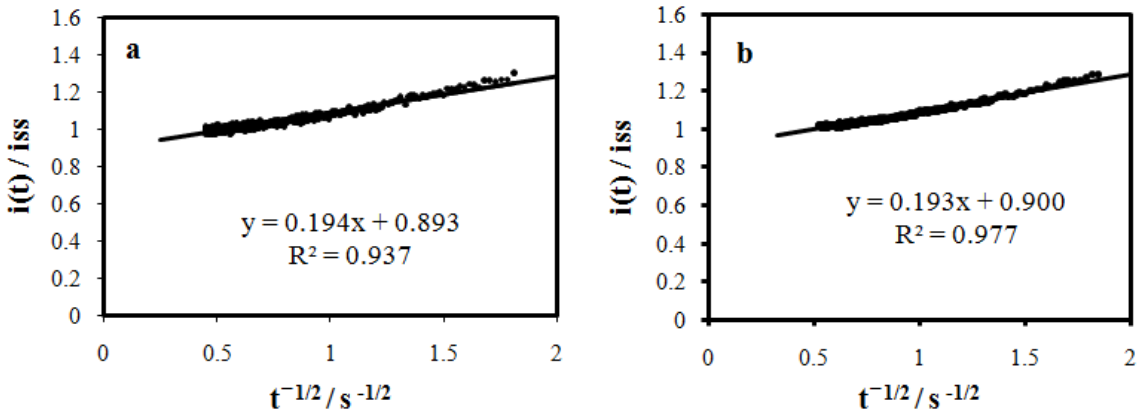

Figure 2.6. Plot of the experimental ratio $i_d(t)/i_{d,ss}$ against the inverse square root of time.

For 0.5 mM FPhSPFN in 0.1 M $TBAPF_6$ with 12.5 μm radius Au UME in 2.33:1 MeCN/PhH. (a) First reduction at step potential E_{SP} = -1.18 V vs SCE (b) Overall oxidation at E_{SP} = 1.18 V vs SCE.

The diffusion coefficients and number of electrons calculated from all of the above cases are summarized in Table 2.2.

Table 2.2. *D* and *n* values for the first reduction and overall oxidation of 0.5 mM FPhSPFN in 0.1M $TBAPF_6$. Solvent: 2.33:1 MeCN/PhH. Electrode radius a=12.5 μm.

Reaction	i_{ss} **/ nA**	$10^6 D$ **/ cm^2 s^{-1}**	***n***
First reduction	1.33	5.34	1.04
Overall oxidation	2.5	5.41	1.79

Based on the results from chronoamperometry, the reduction involves two one-electron transfer processes, while two electrons are transferred during the oxidation process. These results can be rationalized from the chemical structure of FPhSPFN, which comprises a single fumaronitrile group symmetrically linked through a spirobifluorene

group to two triphenylamine groups. Fumaronitrile is a good electron acceptor and triphenylamine is a good electron donor. The two reduction peaks are thus assigned to the stepwise reduction of the fumaronitrile moiety to form the radical anion $A^{-\bullet}$, then reduction to $A^{2-\bullet}$ occurs as observed in the absence of water.[16] The electron-donating triphenylamine moieties are separated by two spirobifluorene moieties and one fumaronitrile moiety, so the two oxidation centers are far apart and not well conjugated. Thus, in the case of oxidation, the loss of an electron from one triphenylamine group to form the radical cation does not greatly influence the oxidation of the second triphenylamine group, so that a single two-electron wave is observed for the oxidation. This observation is consistent with similar cases in which two unconjugated 9, 10-diphenylanthracence groups separated by a spirobifluorene linker show a single oxidation peak.[14] Furthermore, if the two triphenylamine groups are separated by a shorter, conjugated linker, they do show the appearance of two one-electron waves.[4] In the experiment, no spirobifluorene redox peaks were observed within the potential window of the solvent used. This also occurs when other more easily oxidizable groups are attached to this moiety; the direct reduction of unsubstituted spirobiflourene has been shown to be as negative as -2.85 V vs SCE and its oxidation to yield an irreversible voltammogram at 1.54 V vs SCE.[4]

Digital simulations of the experimental CVs of the oxidation shown in Figure 2.8 were carried out to obtain a better estimate of the degree of splitting of the oxidation wave. The double layer capacitance and the uncompensated resistance used in the simulation are calculated experimentally from plot of charging current versus scan rate (Figure 2.7). The charging current was measured at 0.4 V and Table 2.3 summarizes the charging currents at different scan rates. Figure 2.7 shows a linearized plot from which the slope indicates the differential capacitance of the macroelectrode in farads. The

double layer capacitance was calculated to be 0.8 μF (42.1 μF/cm^2) and the uncompensated resistance as 1000 Ω.

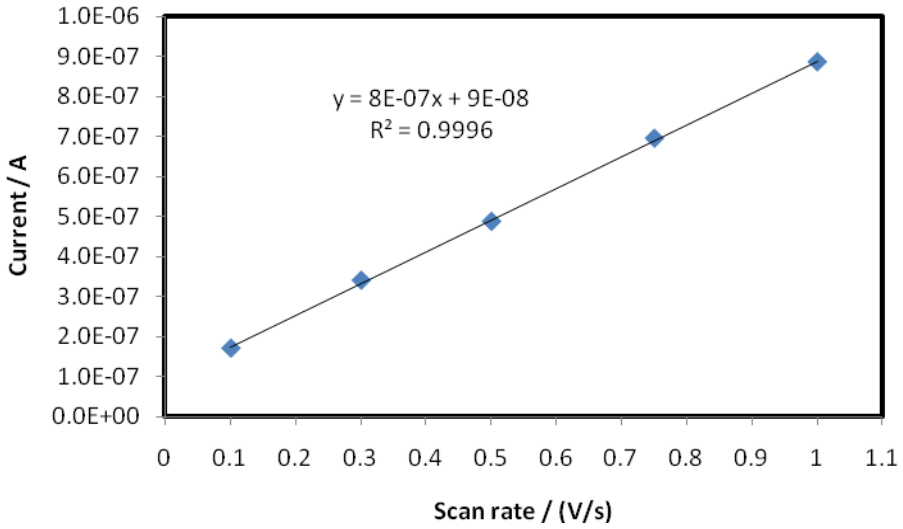

Figure 2.7. Plot of charging current *vs*. scan rate.

Table 2.3. Charging current under different scan rates.

Scan rate /(V/s)	Charging current/A
0.1	1.70E-07
0.3	3.40E-07
0.5	4.87E-07
0.75	6.95E-07
1	8.86E-07

The CV simulation mechanism assigned two reversible, one-electron processes for the oxidation with a ΔE^o between the two waves to be 63 mV, and $D = 8.75 \times 10^{-6}$ cm^2/s, $E^o_{1,\,ox}$ = 1.05 V vs SCE, $E^o_{2,\,ox}$ = 1.11 V vs SCE. The plots in Figure 2.8 indicate good fits between experimental and simulated oxidation CVs performed at various scan rates from 0.05 V/s to 0.75 V/s.

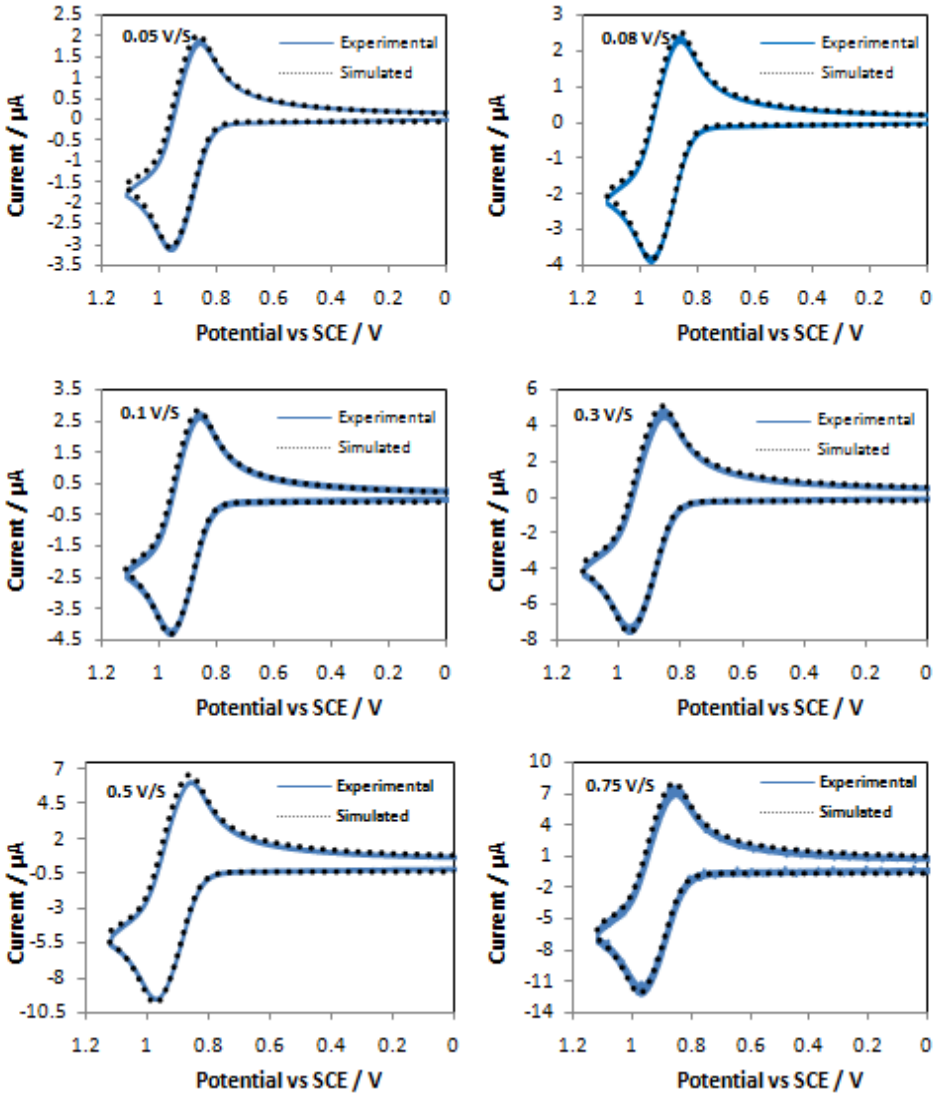

Figure 2.8. Simulation of 0.5 mM $FPhSPF_6$ oxidation.

At (a) 0.05 V/s (b) 0.08 V/s (c) 0.1 V/s (d) 0.3 V/s (e) 0.5 V/s (f) 0.75 V/s. Simulation mechanism is two one-electron oxidations with D = 8.75 x 10^{-6} cm^2/s, $E^o_{1,\,ox}$ = 1.05 V vs SCE, $E^o_{2,\,ox}$ = 1.11 V vs SCE, k^o = 10^4 cm/s, α=0.5, uncompensated solution resistance R_u = 1000 Ω, and double layer capacitance C_{dl} = 0.8 µF.

2.4 ELECTROGENERATED CHEMILUMINESCENCE

The same solvent was used for spectroscopic as for electrochemical measurements. The absorption spectrum, in Figure 2.9 shows absorption maxima at 310 nm and 456 nm. The absorption at 310 nm is close to that observed for the spirobifluorene group.[17] The molar extinction coefficient calculated at 310 nm is 4.59×10^4 $M^{-1}s^{-1}$ and at 456 nm is 2.65×10^4 $M^{-1}s^{-1}$.

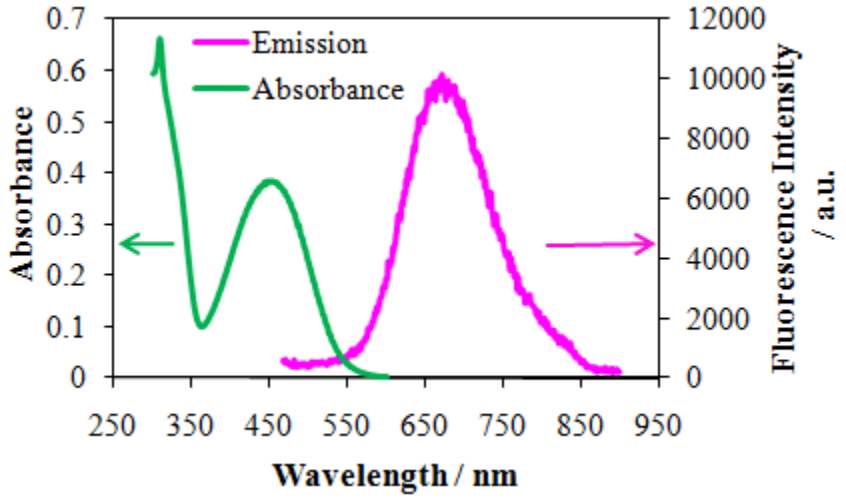

Figure 2.9. Absorbance and fluorescence emission spectra of solution of 14.5 μM FPhSPFN in 2.33:1 MeCN/PhH.

Excitation wavelength, 456 nm.

The photoluminescence with excitation at 456 nm, also shown in Figure 2.9, produces an emission maximum at 673 nm. The large Stokes shift of 217 nm is consistent with significant structural rearrangement and a large dipole moment change upon excitation and emission of FPhSPFN.[18]

Figure 2.10 shows the ECL spectrum obtained by pulsing between reduction and oxidation potentials that gave similar electrochemical currents in order to have an approximate stoichiometry of 1:1 radical anions with radical cations (80 mV past the first reduction peak and at the half-wave oxidation potential, respectively), and the photoluminescence spectrum, both for the solvent composition of 2.33:1 MeCN/PhH.

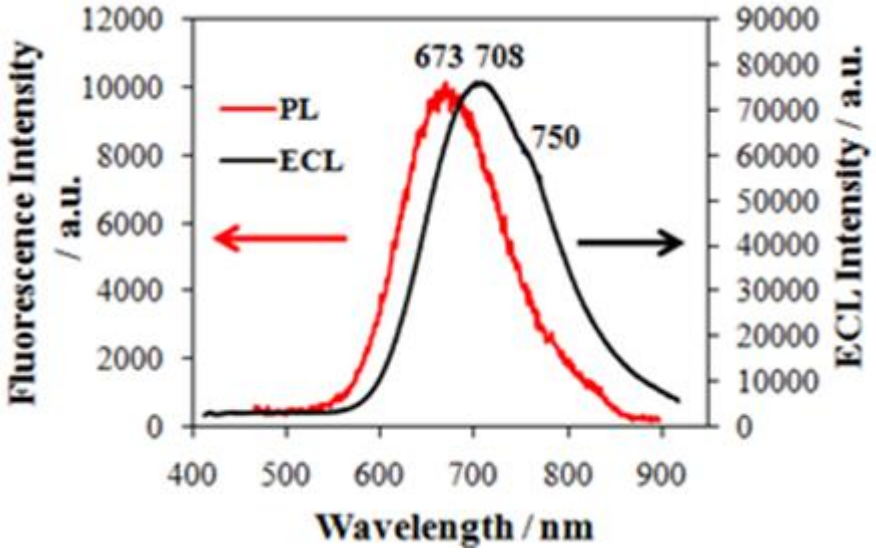

Figure 2.10. Fluorescence or photoluminescence (PL) spectra of 14.5 μM FPhSPFN in 2.33:1 MeCN/PhH and ECL spectra of 0.5 mM FPhSPFN in 0.1 M $TBAPF_6$ in 2.33:1 MeCN/PhH.

ECL spectrum was generated by pulsing between +1.02 V and -1.18 V (vs SCE) (half oxidation and 80 mV past the first reduction peak potential). ECL spectra were integrated for 1 min using a 1 mm slit width. (Excitation wavelength for fluorescence emission: 456 nm)

A red shift of 35 nm was observed for ECL as compared with PL. Note that because of the large Stokes shift, FPhSPFN shows very little absorbance within the wavelength range of PL and ECL (Figure 2.9), so although the concentration of FPhSPFN is much smaller in the PL experiment, absorption of the emitted light in ECL is not significant. We have also carried out ECL experiments with similar concentrations of FPhSPFN as used in PL (e.g., 20 μM), and the normalized ECL spectra show the same shape and location as in the more concentrated cases with the same peak shift. These results suggest that the red shift of ECL spectra is not due to self absorbance or an inner filter effect as is often seen in ECL when compared to PL. There is also the possibility that systematic errors in the spectroscopy can account for some of the difference, since the PL and ECL spectra were taken with different instruments. However our extensive experience with these measurements in previous ECL studies indicates that this would result, at most, in a shift of 10 to 15 nm.

The energy of excited singlet state is calculated based on the equation E_s (in eV) = 1239.81/λ (in nm)[19], where λ is the wavelength at maximum PL emission. The calculated excited singlet state energy is 1.83 eV. The energy of the annihilation reaction, $-\Delta H^o = E^o_{ox} - E^o_{red} - T\Delta S$, based on the difference between the thermodynamic potentials of the overall oxidation and the first reduction waves in the cyclic voltammogram ($E^o_{ox} - E^o_{red}$ = 2.17 eV) with an estimated entropy effect (~ 0.1 eV) subtracted out, is about 2.07 eV. The energy of the annihilation reaction (2.07 eV) is greater than the energy needed to directly populate the singlet excited state (1.83 eV), thus the singlet-excited states can be directly populated upon radical ion annihilation.[19] It has been suggested that in systems with large Stokes shifts, a more correct calculation of the energy of the excited singlet state energy can be estimated by considering the wavelength where the absorbance and emission curves cross,[19] in our case this would yield an excited singlet state energy of

2.33 eV (at 531 nm) for which our estimated $-\Delta H^o$ =2.07 eV would be insufficient to populate it. Experimentally we observe that upon pulsing into the second reduction process (Figure 2.14), where $-\Delta H^o$ =2.48 eV and the calculated singlet state energy is surpassed, the ECL emission profile is maintained, suggesting that in this excess-energy scenario the same excited state is formed, and thus, energy sufficient even for the first reduction-whole oxidation case; building up on the uncertainties presented by each calculation method, we then believe that it is sufficient to describe the energetics of the system by considering the maximum of the PL emission, as it has been traditionally done for ECL systems.[2]

Figure 2.10 reveals a shoulder near 750 nm clearly seen for ECL. In order to understand better the origin of this shoulder, both ECL and PL experiments were done in solvents with different ratios of benzene (PhH) to acetonitrile (MeCN) to change the polarity of the solvent medium without compromising our ability to carry out electrochemical measurements (because of increasing solution resistance with addition of PhH).The results of PL with various MeCN/PhH ratios are shown on absolute and normalized scales in Figure 2.11a and b, respectively. In general, the system shows solvatochromism, with increasing fluorescence intensity and a blue shift in the peak wavelength with decreasing solvent polarity (increase in the fraction of benzene). This strongly suggests that the excited state has a high dipole moment, thus it is less stabilized by a non polar solvent such as benzene, yielding a shorter radiative lifetime of the excited state (which results in faster radiative decay that is less prone to quenching or radiationless decay) and a smaller Stokes shift.[20,21] Figure 2.11b also reveals that the PL spectra broaden and show the growth of a very low intensity shoulder between 750 nm and 850 nm with increasing solvent polarity (ca. 30% of the main peak height when larger fractions of acetonitrile were used).

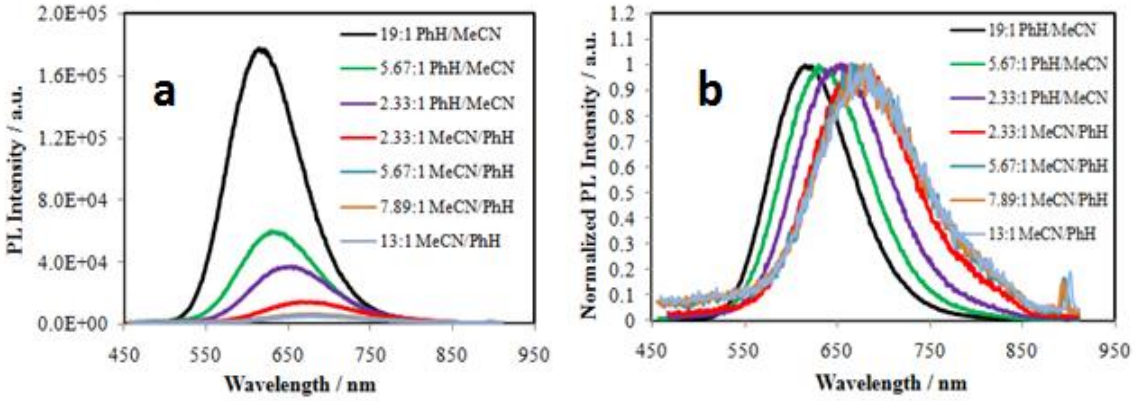

Figure 2.11. Fluorescence spectra of 14.5 μM FPhSPFN in solvents of different MeCN/PhH ratios.

a) Before normalization. b) After normalization.

Correspondingly, the ECL spectra with different PhH to MeCN ratios are presented in Figures 2.12a and b, in an absolute scale and normalized scales. The same trend was observed as in PL, peak intensities increased and peak wavelengths blue-shifted as the solvent polarity decreased. Thus, there is some correlation between the behavior of PL and ECL, suggesting that similar excited states are involved. The normalized ECL spectra (Figure 2.12b) show more clearly that the shoulder around 750 nm relatively increased in intensity with increasing solvent polarity.

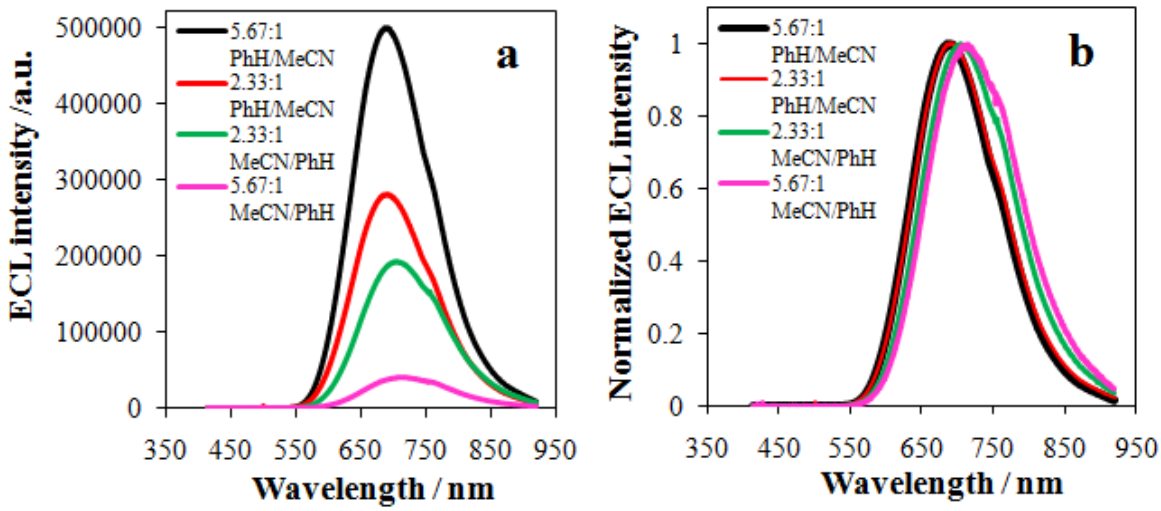

Figure 2.12. ECL spectra of 0.5 mM FPhSPFN in solvents of different MeCN/PhH ratios.

With pulsing between +1.18 V and -1.18 V (vs SCE) (80 mV over the whole oxidation and first reduction peak potentials). a) Before normalization. b) After normalization. ECL spectra were integrated for 1 min using a 1 mm slit width. Supporting electrolyte: 0.1 M $TBAPF_6$. Electrode area: 0.028 cm^2. In the case of 5.67:1 MeCN/PhH, 0.25 mM FPhSPFN was used because of its limited solubility.

Further ECL experiments were carried out to test possibilities for the origin of this shoulder, such as the formation of excimers. When the ECL spectrum is obtained by the use of a correactant, such as BPO as shown in Figure 2.13, the shoulder is still present in the same proportions as in the annihilation case; while this is not strictly conclusive, it does suggest strongly that the formation of an excimer is not the reason for the observation of the shoulder. A mechanistic note worth considering in the case of FPhSPFN, is that the presence of two oxidizable and two reducible moieties may lead to unusual charged excited states by virtue of the annihilation of multiply charged species,

e.g., a dication with an anion radical. As can be seen in Figure 2.14, the normalized ECL spectra for the comparison of the annihilation reactions of the dication-anion and cation-anion pairs (produced by judicious choice of the oxidation stepping potential) are essentially the same. One other possibility for the origin of this peak may lie in the formation of an internal charge transfer state, as has been suggested with certain ECL systems,[22,23] however the broadness of the overall emission and the degree of overlapping with the main emission prevent us from drawing further conclusions in this case.

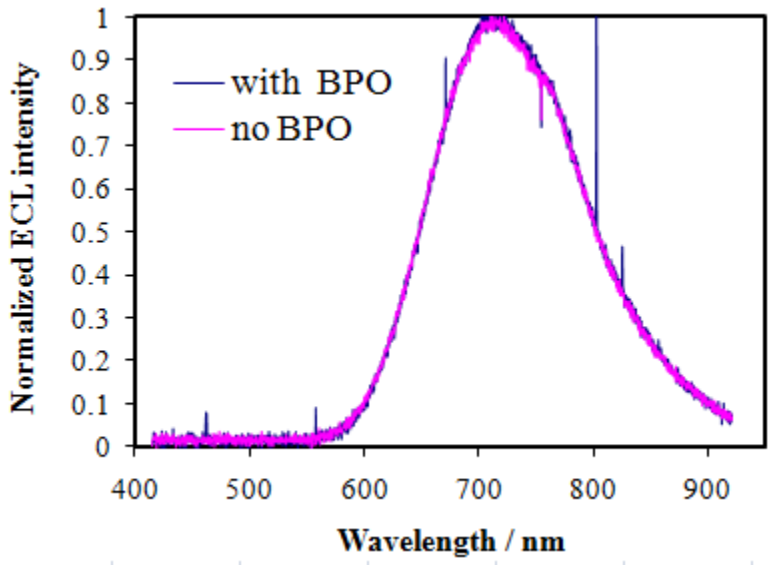

Figure 2.13. Normalized ECL spectra of FPhSPFN with the presence of BPO coreactant and without BPO coreactant.

In 13:1 MeCN/PhH when pulsing between +1.18 V and -1.18 V (vs SCE) (80 mV over the whole oxidation and first reduction peak potentials). ECL spectra were integrated for 1 min using a 1 mm slit width.

Based on results of Figure 2.12a, a comparison of the relative ECL intensity of 0.5 mM FPhSPFN in different solvents with respect to 0.5 mM DPA is shown in Table 2.4.

Table 2.4. Maximum ECL Emission Wavelength λ_{max}^{ECL}, Intensity at λ_{max}^{ECL} and Relative Intensity with respect to DPA.

Solvent	**λ_{max}^{ECL} (nm)**	**$I_{\lambda max}^{ECL}$ (a.u.)**	**Relative Intensity w.r.t. DPA** *
PhH/MeCN 5.67:1	687	5.0×10^5	16 %
PhH/MeCN 2.33:1	690	2.8×10^5	8.7 %
MeCN/PhH 2.33:1	708	1.9×10^5	6%

* Calculated by comparing of $I_{\lambda max}^{ECL}$ of FPhSPFN with respect to that of DPA in MeCN/PhH 2.33:1.

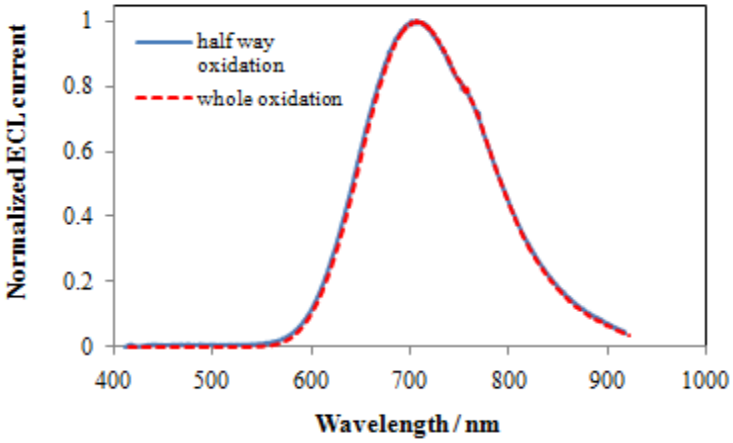

Figure 2.14. Normalized ECL spectra obtained when stepping between the first reduction wave at -1.18 V (vs SCE) and the half-wave oxidation potential at +1.02 V (vs SCE) or the overall oxidation wave at +1.18 V (vs SCE).

Slit width: 1 mm; Integration time: 1 min. Solution: 0.5 mM FPhSPFN in 2.33:1 acetonitrile/benzene and 0.1 M $TBAPF_{6.}$

A comparison of the ECL spectra collected with the first reduction and second reduction is shown in Figure 2.15.

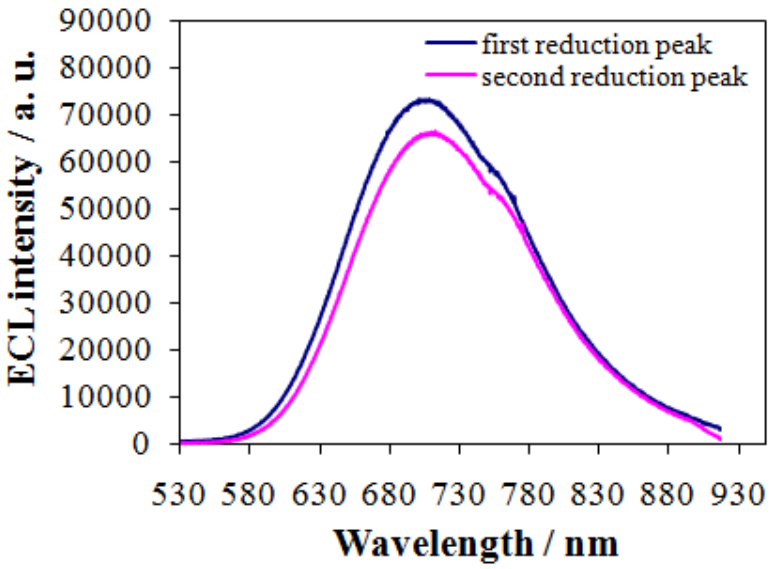

Figure 2.15. ECL spectra for different reduction potential.

For 0.5 mM FPhSPFN in 0.1 M $TBAPF_6$ in 2.33:1 MeCN/PhH obtained by pulsing between +1.02 V vs SCE and two different cathodic potentials (-1.18 V vs SCE and -1.638 V vs SCE). ECL spectra were integrated for 1 min using a 1 mm slit width.

A potential excursion into the second reduction process to generate the radical di-anion showed a decrease in the ECL intensity. We believe that a following chemical

process consumes in part the radical dianion, as evidenced by the lack of reversibility observed in the CV when going into the second reduction peak. The observed formation of a film on the electrode when stepping into such reduction potentials may also play a role in this ECL intensity decrease.

2.5 TRANSIENT ELECTROGENERATED CHEMILUMINESCENCE

Observation of the ECL transients during potential pulsing with different pulse durations can provide information about the ECL process and reactant stability.[24] For example, when the radical ions are generated under mass transfer controlled conditions and are stable during a pulse, the ECL emission pulses are of equal height and constant with pulsing. Instability of one of the radical ion species results in unequal heights for the anodic and cathodic pulses and a decay of the ECL emission with time.

During the reduction and oxidation of FPhSPFN, four kinds of radical ions can be formed, the dianion (D-X-$A^{2-\cdot}$-X-D), the radical anion (D-X-$A^{-\cdot}$-X-D), the dication ($D^{+\cdot}$-X-A-X-$D^{+\cdot}$), and the radical cation ($D^{+\cdot}$-X-A-X-D). We investigated what combinations of these species produce stable and intense ECL. For this purpose we observed the ECL transients with a PMT while pulsing the potential between certain combinations of potentials for oxidation and reduction. Figure 2.16 shows the results of this technique for the relevant combinations of generated species. Figure 2.16a, in which approximately the same amounts of anion and cation radicals are produced in each pulse, shows that the ECL response is fairly symmetrical, but with a slightly lower ECL intensity in the anodic pulse. Often, this behavior suggests instability of the formed radical anions, however no indication of this type of effect is provided in the well-behaved electrochemistry already described for FPhSPFN. The electrochemical control of the stoichiometry of the

annihilation reaction in the case presented in Figure 2.16a is more difficult than in the simpler case where only the radical anion and cation is generated, as there is always uncertainty about how much of the radical dication is being produced concurrently with the radical cation (either by direct generation or by disproportionation of the radical cations). Figure 2.16b shows the more controllable production of an excess of radical cation equivalents upon anodic stepping into the overall oxidation wave. It was observed that in this situation, a more long lasting ECL signal was obtained, as evidenced in Figure 2.16b during the cathodic pulse. Integration of the transients in Figures 2.16a and 2.16b for one cycle, *i.e.*, an oxidation and a reduction step, showed a four-fold increase in the ECL intensity when stepping into the whole oxidation wave compared to the case of only half of the oxidation wave. Finally Figure 2.16c shows that upon stepping to the second reduction wave, the emission observed in the anodic pulses is greatly reduced, thus confirming the instability of the dianion, which is consistent with the shape of the second reduction wave in the cyclic voltammetry and the decrease in the intensity of the ECL response shown in Figure 2.15 when stepped into the second reduction wave.

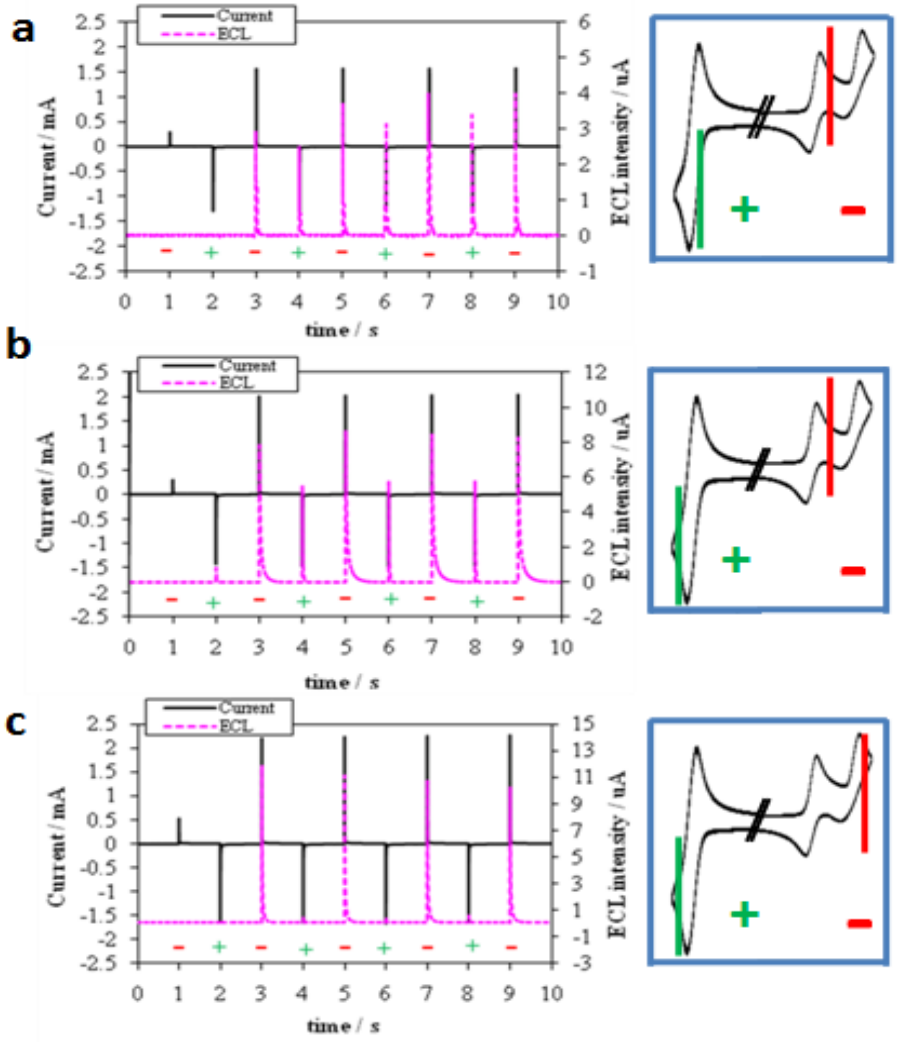

Figure 2.16. Electrochemical current (black, solid) and ECL (pink, dotted) transients.

With pulsing time of 1s, for 0.5 mM FPhSPFN in 2.33:1 MeCN/PhH pulsed between a) first reduction and half oxidation, b) first reduction and whole oxidation, and c) second reduction and whole oxidation. Panels on the right show schematically the potentials used and the polarity of the step as indicated in the graphs.

2.6 CONCLUSIONS

We report here the electrochemistry and ECL of a novel red emitting OLED compound, the donor-linker-acceptor-linker-donor molecule FPhSPFN. The presence of fumaronitrile moiety as electron acceptors and triphenylamine moiety as electron donors allows the generation of ECL without the addition of a coreactant or a second compound. The nonplanar-bulky spirobifluorene linker prevents the delocalization of charges through the whole molecule and favors the localization of the negative charge of the radical anions on fumaronitrile group and of the positive charge of the radical cations on each triphenylamino group. The wavelengths and intensities of ECL and PL vary significantly with solvent polarity, indicative of the formation of emissive excited states having high dipole moments. The instability of the dianion gives rise to low ECL intensity upon radical ion annihilation. Energy of this annihilation reaction is sufficiently high to generate the singlet excited state and the corresponding ECL emission. The compound shows an increase of ECL intensity with decreasing solvent polarity and has a relative ECL intensity between 6% and 16% of DPA. The results demonstrate the possibility of designing donor-acceptor based molecules as for efficient ECL.

2.7 REFERENCES

[1] Lai, R. Y.; Kong, X. X.; Jenekhe, S. A.; Bard. A. J. *J. Am. Chem. Soc.* **2003**, *125*, 12631-12639.

[2] Lai, R.Y.; Fabrizio, E. F.; Lu, L.; Jenekhe, S. A.; Bard, A. J. *J. Am. Chem. Soc.* **2001**, *123,* 9112-9118.

[3] Izadyar, A.; Omer, K. M.; Liu, Y. Q.; Chen, S. Y.; Xu, X. J.; Bard, A. J. *J. Phys. Chem. C* **2008**, *112*, 20027-20032.

[4] Fungo, F.; Wong, K.-T.; Ku, S.-Y.; Hung, Y.-Y.; Bard, A. J. *J. Phys. Chem. B* **2005**, *109*, 3984-3989.

[5] Pan, Y.; Zhao, J. S.; Ji, Y. Y.; Yan, L.; Yu, S. Q. *Chem. Phys*. **2006**, *320*, 125-132.

[6] Izadyar, A.; Omer, K. M.; Liu, Y. Q.; Chen, S. Y.; Xu, X. J.; Bard, A. J. *J. Phys. Chem. C* **2008**, *112*, 20027-20032.

[7] Chiu, K.Y.; Su, T. X.; Li, J. H.; Lin, T.-H.; Liou, G.-S.; Cheng, S.-H. *J. Electroanal. Chem*. **2005**, *575*, 95-101.

[8] Zou, Y. P.; Sang, G. Y.; Wan, M. X.; Tan, S. T.; Li, Y. F. *Macromol. Chem. Phys.*, **2008**, *209*, 1454-1462.

[9] Hancock, J. M.; Gifford, A. P.; Zhu, Y.; Lou, Y.; Jenekhe, S. A. *Chem. Mater*. , **2006**, *18*, 4924-4932.

[10] Sartin, M. M.; Shu, C. F.; Bard, A. J. *J. Am. Chem. Soc*. **2008**, *130*, 5354-5360.

[11] Fungo, F.; Wong, K.-T.; Ku, S.-Y.; Hung, Y.-Y.; Bard, A. J. *J. Phys. Chem. B* **2005**, *109*, 3984-3989.

[12] Natera, J.; Otero, L.; D'Eramo, F.; Sereno, L.; Fungo, F.; Wang, N.-S.; Tsai, Y.-M.; Wong, K.-T. *Macromolecules*, **2009**, *42*, 626-635.

[13] Lee, Y.-T.; Chiang, C.-L.; Chen, C.-T. *Chem. Commun.* **2008**, 217–219.

[14] Sartin, M. M.; Shu, C. F.; Bard, A. J. *J. Am. Chem. Soc*. **2008**, *130*, 5354-5360.

[15] Denuault, G.; Mirkin, M. V.; Bard, A. J. *J. Electroanal. Chem*. **1991**, *308*, 27-38.

[16] Grimshaw, J. *Electrochemical Reactions and Mechanisms in Organic Chemistry*. Elsevier: Amsterdam, 2000; P 66.

[17] Rashidnadimi, S.; Hung, T. H.; Wong, K.-T.; Bard, A. J. *J. Am. Chem. Soc*. **2008**, *130*, 634-639.

[18] Berlman, I. B. *Handbook of Fluorescence Spectra of Aromatic Molecules*, 2nd ed.; Academic Press: New York, 1971.

[19] Bard, A. J. in *Electrogenerated Chemiluminescence*; Bard, A. J., Ed.; Marcel Dekker: New York, 2004.

[20] Lakowicz, J. R. *Principles of Fluorescence Spectroscopy*, 3rd ed; Springer Science + Business Media: New York, 2006.

[21] Nigam, S.; Rutan, S. *Appl. Spectrosc*. **2001**, *55*, 362A-370A.

[22] Kapturkiewicz, A.; Herbich, J.; Nowacki, J. *Chem. Phys. Lett*. **1997**, *275*, 355-362.

[23] Itaya, K.; Toshima, S. *Chem. Phys. Lett*. **1977**, *51*, 447-452.

[24] (a) Ref. 19, Chapters 2 (Fan, F.-R. F.) and 3 (Maloy, J. T.); (b) Cruser, S. A; Bard, A. J. *J. Am. Chem. Soc.* **1969**, *91*, 267.

Chapter 3. Electrochemistry and Electrogenerated Chemiluminescence of Dithienylbenzothiadiazole Based Molecules: Differential Reactivity of Donor and Acceptor Groups and Simulations of Radical Cation-Anion and Dication- Radical Anion Annihilations

3.1 INTRODUCTION

We report the electrochemistry and electrogenerated chemiluminescence (ECL) of two red fluorescent dithienylbenzothiadiazole derivatives, (4,7-bis(4-(n-hexyl)-5-(3,5-di(1-naphthyl)phenyl)thiophen-2-yl)-2,1,3-benzothiadiazole, compound **1a**) and (4,7-bis(4-(4-sec-butoxyphenyl)-5-(3,5-di(1-naphthyl)phenyl)thiophen-2-yl)-2,1,3-benzothiadiazole, compound **1b**), which are reported to have a high photoluminescence quantum yield (44% of Rhodamine B) and have been studied as red-emitting electroluminescent and laser dyes.[1]

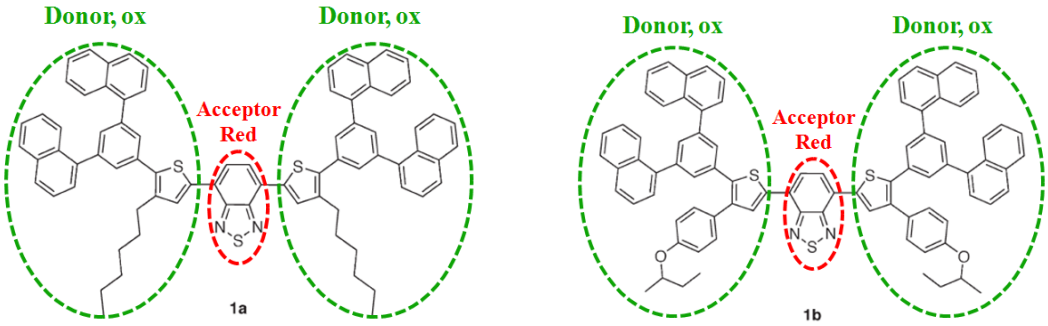

Their ECL results from the annihilation reactions between the radical anions and radical cations generated during electrochemical reduction and oxidation. Since they both have two oxidation sites, ECL can also be generated through annihilation reactions between the radical anions and dications. The comparison between simulation and

experiment of the transient ECL emission of compound **1b** for the multiply charged radical ion annihilation reactions was reported. Compound **1a** is reported to have a high photoluminescence quantum yield in solid (62% in solid measured in an integrating sphere under 325nmlaser excitation).[1] ECL of **1a** film was studied, which results from the coreactant reaction between **1a** film and TPrA (coreactant) in PBS buffer solution. **1a** film was prepared by dropping cast **1a** in dichloromethane on Fluorine-doped Tin Oxide (FTO).

Compound **1a** and **1b** has the configuration of donor-acceptor-donor, with a 2,1,3-benzothiadiazole moiety as the electron acceptor in the center connected directly to two donors at the ends. For compound **1b**, each donor is a thiophene moiety substituted in position 2 by 3,5-di(1-naphthyl)phenyl and in position 3 by 4-*sec*-butoxyphenyl; for compound **1a**, each donor is a thiophene moiety substituted in position 2 by 3,5-di(1-naphthyl)phenyl and in position 3 by n-hexyl.

There are two dominant pathways through which ECL can be produced, namely the annihilation and coreactant pathways.[2] Annihilation ECL process of generation of an excited singlet state (S-route) occurs through electron transfer between electrochemically generated species followed by the emission of light.[3,4] The S-route ECL process can be represented in a general way as shown below:

$A + e^- \rightarrow A^{-\cdot}$ (reduction at electrode) (3.1)

$D - e^- \rightarrow D^{+\cdot}$ (oxidation at electrode) (3.2)

$A^{-\cdot} + D^{+\cdot} \rightarrow {}^1A^* + D$ (excited singlet state formation) (3.3)

${}^1A^* \rightarrow A + h\nu$ (light emission) (3.4)

where A and D are electroactive species and denote acceptor and donor, respectively. A and D can be the same molecule as in the case of efficient ECL emitter 9,10-diphenylanthracene (DPA).[5,6] They can also be different moieties within the same molecule, as in a donor-acceptor organic molecule. One molecule may have multiple donors or acceptors. A number of donor-acceptor molecules have been the target of ECL studies, for example metal complexes,[7] like the widely-used $[Ru(bpy)_3]^{2+}$,[8] in which electrochemical oxidation occurs in the Ru(II) center while three possible reductions can occur in the bipyridine ligands, the emitting state being a metal to ligand charge transfer (MLCT) state.[9] Combination of organic based D-A motifs allows the design of efficient ECL emitters;[10] high ECL efficiencies have been reported[11-13] and the possibility of increasing the light yield by multiple, chemically reversible, D or A units has been suggested.[14]

Coreactants are also used in ECL studies when one of the generated radical species are unstable or cannot be generated within the solvent window. [4] In the case when benzoyl peroxide (BPO), is used as a coreactant, a simplified mechanism follows in Scheme 2:[15]

$$BPO + e^- \rightarrow BPO^{-\cdot} \quad (3.5)$$

$$BPO^{-\cdot} \rightarrow C_6H_5CO_2^- + C_6H_5CO_2^{\cdot} \quad (3.6)$$

$$C_6H_5CO_2^{\cdot} + A^{-\cdot} \rightarrow C_6H_5CO_2^- + {}^1A^* \quad (3.7)$$

One interesting aspect of the molecule **1a** and **1b** is that the acceptor group is "buried" between the two large donor groups. In such structures, heterogeneous electron transfer kinetics depends on the extent to which the electroactive center is physically removed from the immediate vicinity of the electrode surface, for example, when a

molecule is substituted by a long chain or bulky moiety.[16] In compound **1a** and **1b**, we would expect that the rate constant for reduction, k_r^o, would be smaller than in the unsubstituted parent 2,1,3-benzothiadiazole molecule. Moreover, one can compare in the same molecule the electron transfer kinetics for the reduction with those for the oxidation, k_o^o, of the more exposed donor groups (the thiophene groups). Cyclic voltammetry (CV) studies at different scan rates coupled with digital simulation demonstrate that the electron transfer rates for the reduction and oxidation processes are indeed different.

Transient ECL generated by alternating potential steps can provide information about the stability of the precursor species (radical anions, radical cations, dications). When the radical ions are generated under mass transfer controlled conditions and are stable during a pulse, the ECL emission pulses are of equal height during anodic and cathodic pulses and constant with pulsing. Instability of one of the radical ion species results in unequal heights for the anodic and cathodic pulses and decay of the ECL emission with time.[17] We show a comparison between transient ECL of **1b** generated through radical anion-radical cation and also radical anion-dication annihilations and simulations of this transient ECL were carried out. Transient methods for the characterization of ECL, along with a comparison to simulation models can aid in developing an understanding of the optimum conditions for generating strong and stable ECL emission.[18]

3.2 EXPERIMENTAL

Materials. Anhydrous acetonitrile (MeCN), dichloromethane (CH_2Cl_2 or DCM) and tripropylamine (TPrA) were obtained from Aldrich (St. Louis, MO) and transferred

directly into a helium atmosphere drybox (Vacuum Atmospheres Corp., Hawthorne, CA) without further purification. Electrochemical grade tetra-*n*-butylammonium hexafluorophosphate ($TBAPF_6$) and 9,10-diphenylanthracene (DPA) were obtained from Fluka and used as received. Tris(2,2'-bipyridine)ruthenium (II) perchlorate (Rubpy) was obtained from GFS Chemicals, Inc. (Powell, OH). Compound **1a** and **1b** were synthesized as reported recently.[1] Characterization details (mass spectrometry, NMR) is contained in the Supporting Information of this reference.

Characterization. The same electrochemical cell was used for both CV and ECL experiments. The electrochemical cell consisted of a coiled Pt wire (0.5 mm in diameter) as a counter electrode, a Ag wire (0.5 mm in diameter) as a quasi-reference electrode, and a Pt disk inlaid in glass bent at a 90^o angle (for the disk to face the light detector) as a working electrode. The geometric area of the Pt disk electrode was 0.028 cm^2. The electrode area was calibrated with 1mM ferrocenemethanol in 0.1 M KCl with diffusion coefficient of $D = 6.7\times10^{-6}$ cm^2/s. Different scan rates and corresponding peak currents for oxidation of ferrocenemethanol were shown in Table 3.1. And Figure 3.1 shows the plot of peak current versus square root of scan rate. Then D was calculated from the slope.

(A)

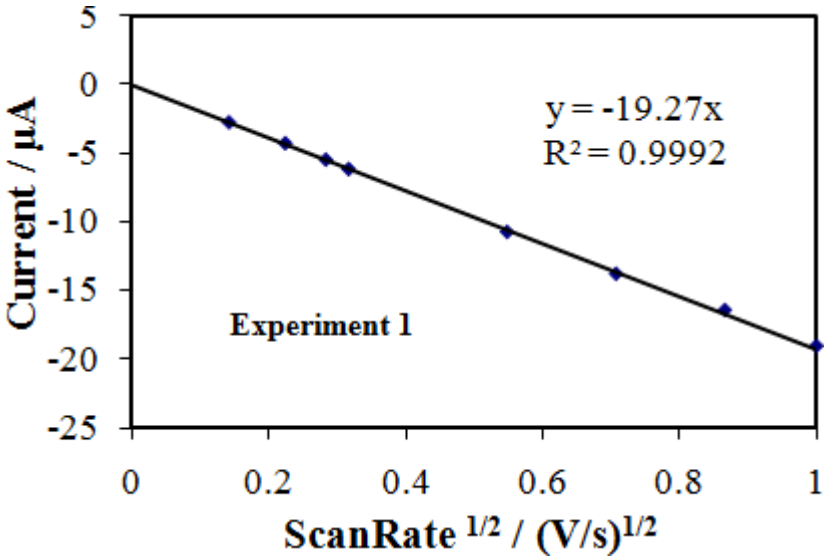

(B)

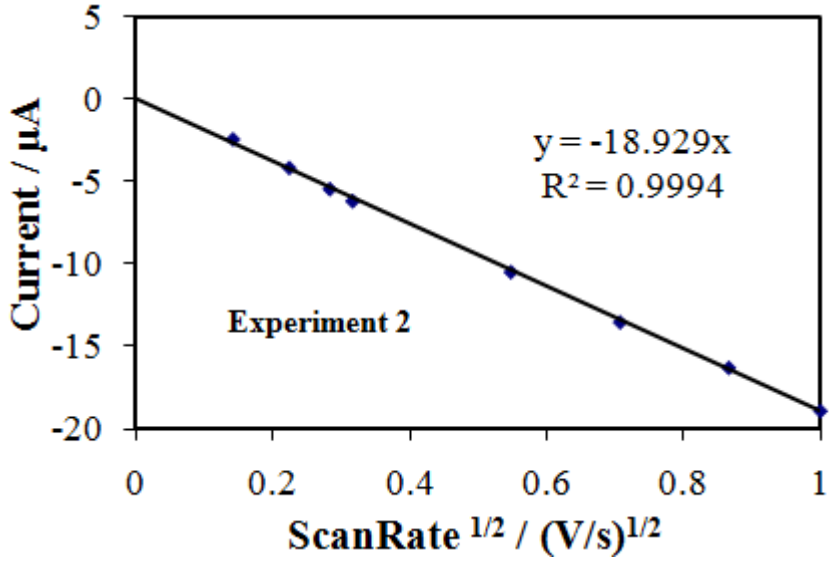

Figure 3.1. Peak current versus square root of scan rate for ferrocenemethanol oxidation.

Table 3.1. Scan rates and peak current for oxidation of ferrocenemethanol in 0.1 M KCl.

Scan Rate (V/s)	Scan Rate$^{1/2}$ $(V/s)^{1/2}$	i_{peak} / µA (experiment 1)	i_{peak} / µA (experiment 2)
0.02	0.1414	-2.8	-2.4
0.05	0.2236	-4.3	-4.2
0.08	0.2828	-5.5	-5.4
0.1	0.3162	-6.2	-6.2
0.3	0.5477	-10.8	-10.5
0.5	0.7071	-13.8	-13.5
0.75	0.8660	-16.5	-16.3
1	1	-19.1	-18.9

After each experiment, the potential of the Ag wire was calibrated with ferrocene (taken as 0.342 V vs SCE).[19] Before each experiment, the working electrode was polished on a felt pad with 0.3 μm alumina (Buehler, Ltd., Lake Bluff, IL), sonicated in Milli-Q deionized water and then in ethanol. The counter and reference electrodes were cleaned by rinsing and sonicating in acetone, water and ethanol. Finally, all the electrodes were rinsed with acetone, dried in the oven and transferred into the glove box.

Solutions for electrochemical measurements consisted of 0.5 mM **1a/1b** in CH_2Cl_2 as the solvent and 0.1 M $TBAPF_6$ as the supporting electrolyte. All solutions were prepared inside the glove box. For measurements made outside of the box, the electrochemical cell was closed with a Teflon cap that had a rubber O-ring to form an airtight seal. Stainless steel rods driven through the cap formed the electrode connections.

For study of **1a** film**,** the same counter electrode was used and cleaned as described above, a Ag/AgCl reference electrode was used, the working electrode was FTO electrode with 1a film on it.**1a** film was prepared by dropping cast 25 µL 0.5mM **1a** in DCM on FTO, sit dry.

Cyclic voltammograms (CVs) were obtained on a CH Instruments electrochemical workstation (CHI 660, Austin, TX). Digital simulations of CV were performed using Digisim software (Bioanalytical Systems). Spectroscopic experiments for 1a in solution were done in a 1 cm path length quartz cell. Absorbance of 1a film on FTO was measured with the same FTO without 1a film as background. Absorbance spectra were obtained on a Milton Roy spectronic 3000 array spectrophotometer. Fluorescence spectra were collected on a QuantaMaster spectrofluorimeter (Photon Technology International, Birmingham, NJ). The excitation source was a 70 W xenon lamp (LPS-220B Lamp power supply), and the excitation and emission slits were set to 0.5 mm (2 nm bandwidth).

The ECL spectra were obtained on Princeton SPEC-10 Instruments using a charge-coupled device (CCD) camera (Trenton, NJ) cooled to -100 ^{o}C with an Acton SpectraPro-150 monochromator (Acton, MA) as detector. The wavelength scale of the CCD camera and grating system were calibrated using Hg/Ar pen-ray lamp from Oriel (Stratford, CT). ECL intensity-time curves were collected on an Autolab potentiostat (Ecochemie, Netherlands) connected to a photomultiplier tube (PMT, Hamamatsu, R4220p, Japan). The PMT was supplied with -750 V with a Kepco (New York) high voltage power supply. ECL efficiency was determined with respect to DPA and Rubpy in MeCN by comparing the maximum intensities and emission area in the ECL spectra, respectively.

3.3 ELECTROCHEMISTRY

*CV of **1a** in solution with digital simulation.* A CV of **1a** in CH_2Cl_2 showed one reduction and two oxidation waves (Figure 3.2). CVs for reduction and oxidation with different scan rate were shown Figure 3.3 and Figure 3.4, respectively.

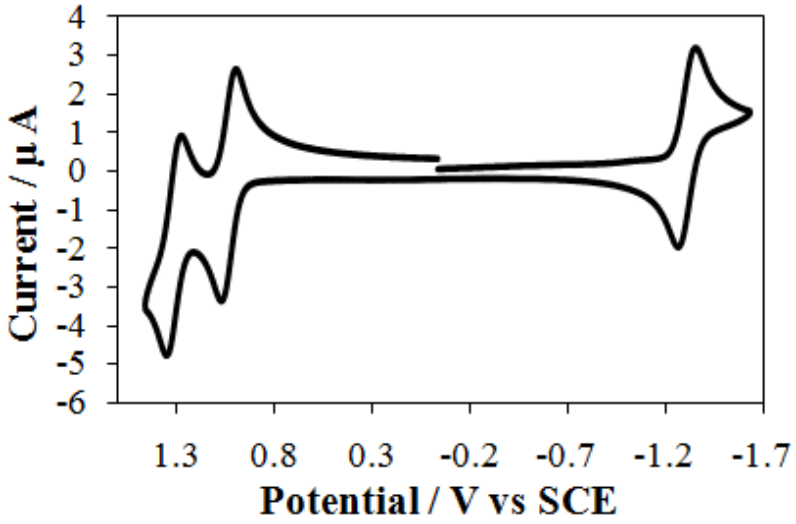

Figure 3.2. Cyclic voltammogram of 0.5 mM **1a** in dichloromethane with 0.1 M $TBAPF_6$.

Scan rate = 100 mV/s. Area of electrode is 0.028 cm^2.

(A)

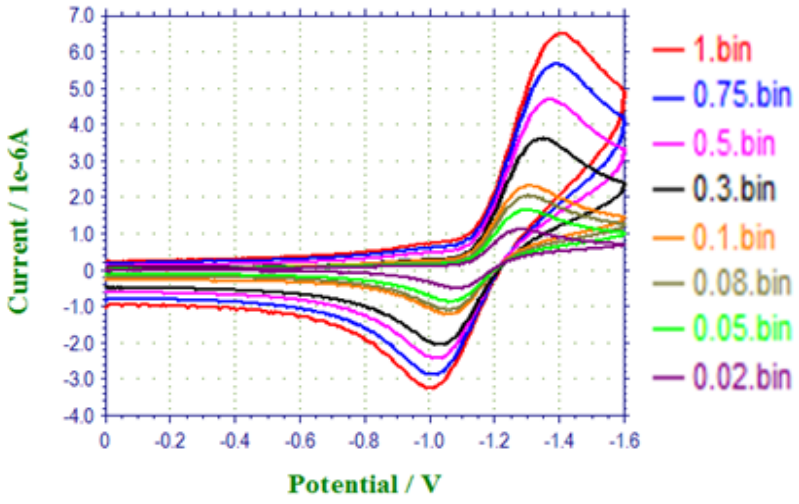

(B)

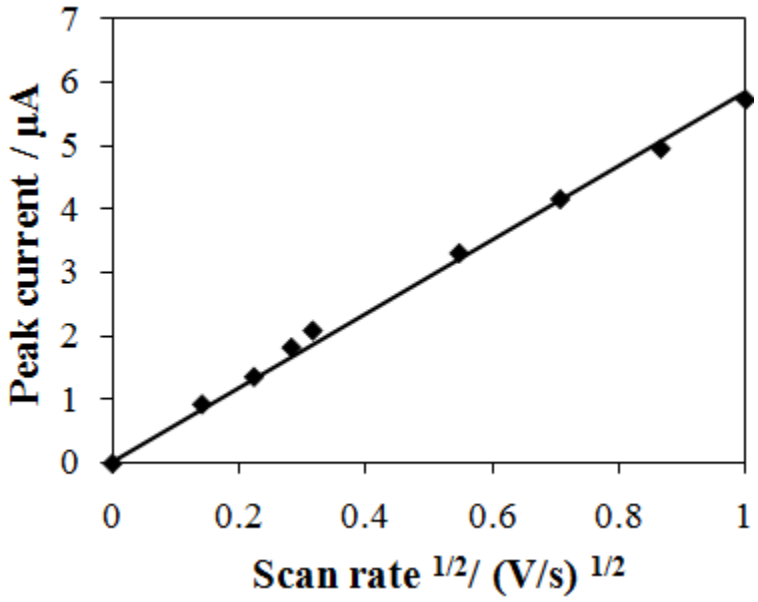

Figure 3.3. (A) Cyclic voltammogram of 0.5 mM **1a** reduction in dichloromethane with different scan rate. (B)Peak current of **1a** reduction versus square root of scan rate.

(A)

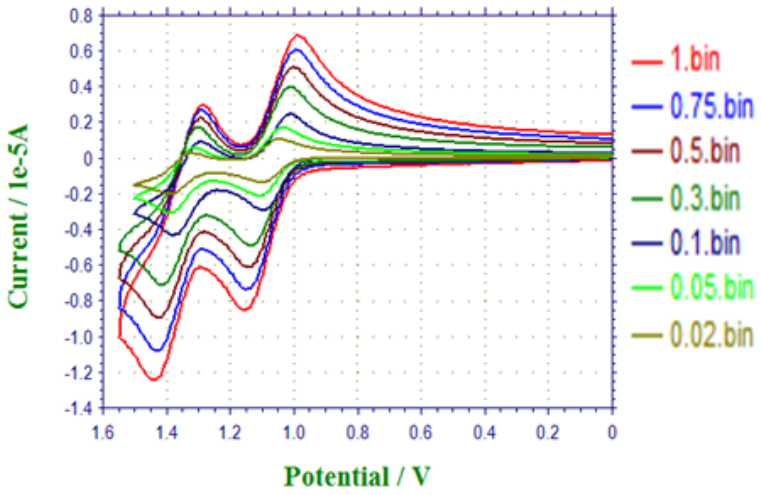

(B)

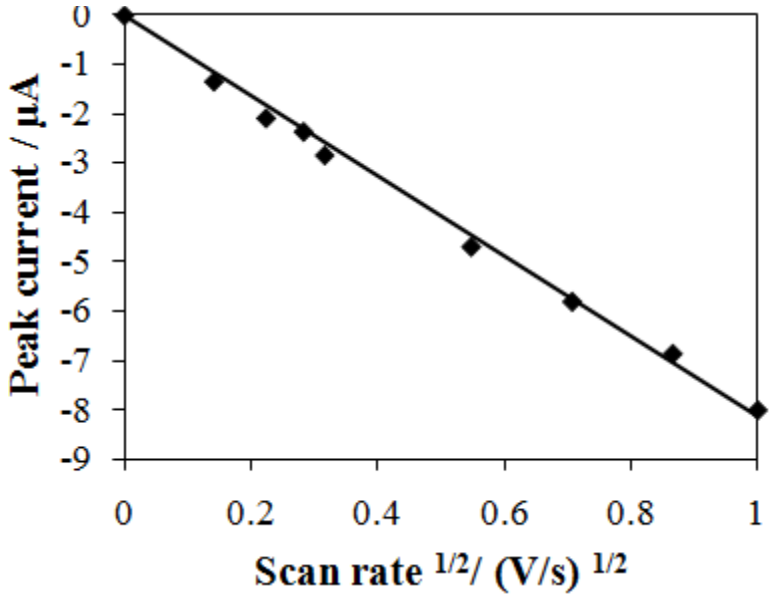

Figure 3.4. (A) Cyclic voltammogram of 0.5 mM **1a** oxidation in dichloromethane with different scan rate. (B)Peak current of **1a** oxidation versus square root of scan rate.

Plots of peak current versus square root of scan rate were also shown in Figure 3.3 (B) and Figure 3.4 (B), which indicate diffusion control of the reduction and oxidation currents. Digital simulations of the experimental CVs for the reduction and oxidation are shown in Figures 3.5 and 3.6, respectively. Experimental and simulated CVs for both reduction and oxidation performed at various scan rates from 0.02V/s to 1.0 V/s fits very well. The double layer capacitance and the uncompensated resistance used in the simulation were measured from a potential step in the region with only double layer charging occurred, i.e. at 0 V vs SCE. The best fit for the CV simulation suggests a single 1e reduction with E^{o}_{red} = -1.18V vs SCE, $D = 6 \times 10^{-6}$ cm^2/s and $k^o = 0.6 \times 10^{-3}$ cm/s; and two 1e oxidations with $E^{o}_{oxi,1}$ = 1.01 V vs SCE, $E^{o}_{oxi,2}$ = 1.24 V vs SCE, $D = 6 \times 10^{-6}$ cm^2/s and k^o = 0.02 cm/s.

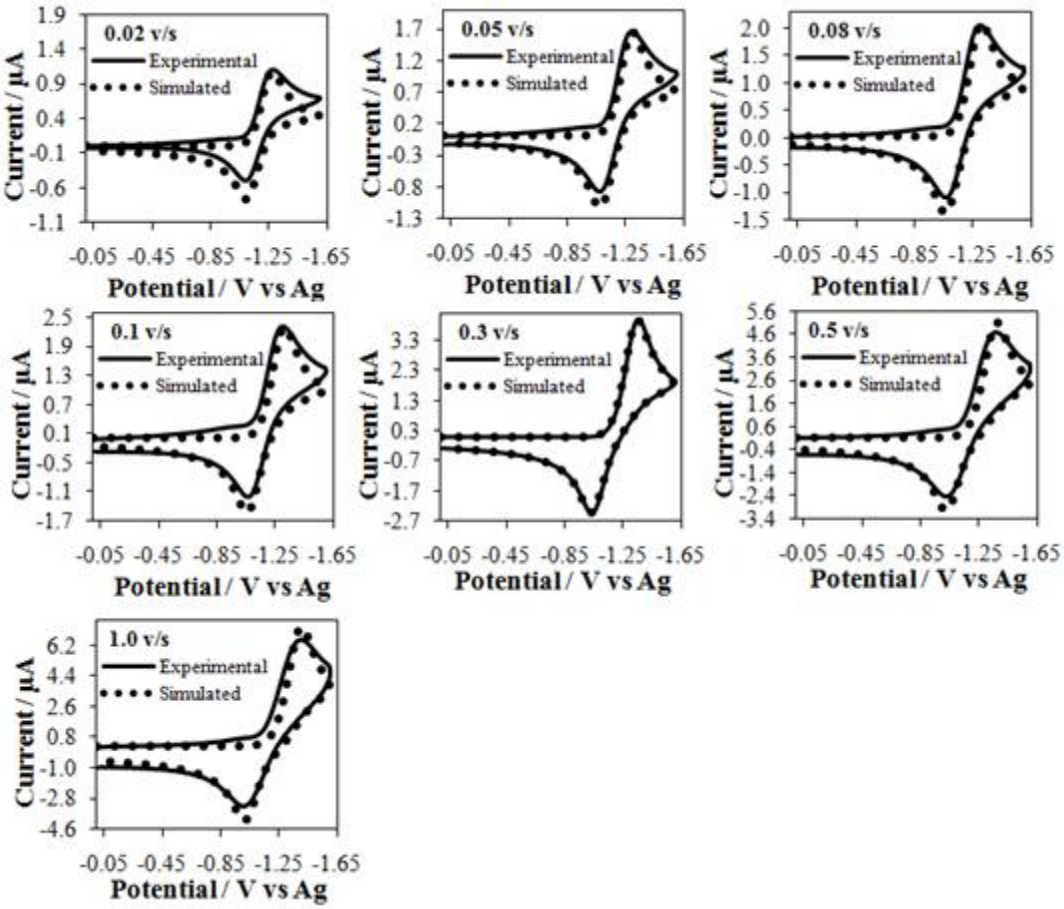

Figure 3.5. Simulation of 0.5 mM **1a** reduction in dichloromethane.

(a) 0.02 V/s (b) 0.05 V/s (c) 0.08 V/s (d) 0.1 V/s (e) 0.3 V/s (f) 0.5 V/s (g) 1 V/s. Simulation mechanism is one-electron reduction with D = 6×10^{-6} cm^2/s, E^o_{red} = –1.18V vs SCE, $k^o = 0.6 \times 10^{-3}$ cm/s, $\alpha = 0.5$, uncompensated solution resistance R_u = 1972 Ω, and double layer capacitance C_{dl} = 0.25 µF.

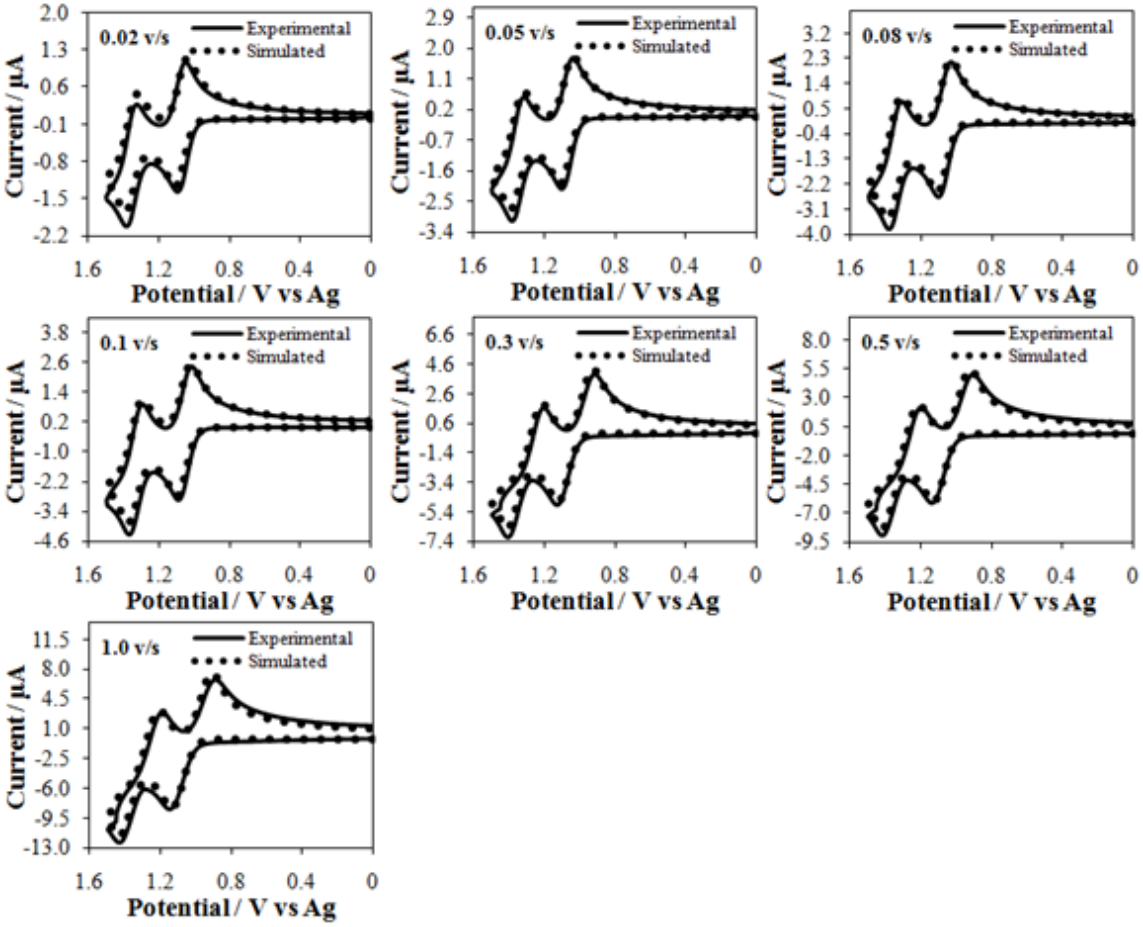

Figure 3.6. Simulation of 0.5 mM **1a** oxidation in dichloromethane.

(a) 0.02 V/s (b) 0.05 V/s (c) 0.08 V/s (d) 0.1 V/s (e) 0.3 V/s (f) 0.5 V/s (g) 1 V/s. Simulation mechanism is two stepwise 1e oxidations with D = 6×10^{-6} cm^2/s, $E^o_{1,ox}$ = 1.01 V vs SCE, $E^o_{2,ox}$ = 1.24 V vs SCE, k^o = 0.02 cm/s, α=0.5, uncompensated solution resistance R_u = 1972 Ω, and double layer capacitance C_{dl} = 0.25 µF.

The CV results can be rationalized from the chemical structure of **1a**, which comprises a 2, 1, 3-benzothiadiazole moiety as the reduction center (A−group) and two bulky substituted thiophene end groups as donor groups (D−group). After gaining 1e in the center (A−group), only a single 1e reduction wave is observed. The two end groups are connected directly to the acceptor center, each capable of losing an electron. The splitting between the oxidation waves of 0.23 V shows that after the loss of 1e from one end D−group, it is more difficult to lose the second electron in the molecule. This indicates that considerable conjugation exists between these two D−groups; CV of other ECL D-A systems have shown that for molecules with two D-groups, the presence of a bulky, non-conjugated spirobifluorene linker between them causes a smaller peak splitting in the 2e oxidation process (~ 0.06 V),[19, 20] as opposed to a larger splitting observed when the two D-groups are connected through a conjugated linker (~ 0.18 V).[21] In all of these cases a doubly charged ion is generated, but the electrostatic repulsive interaction could only account for about a third of what is observed here.

*CV of **1b** in solution with digital simulation.* A CV of **1b** in CH_2Cl_2 showed one reduction and two oxidation waves (Figure 3.7).

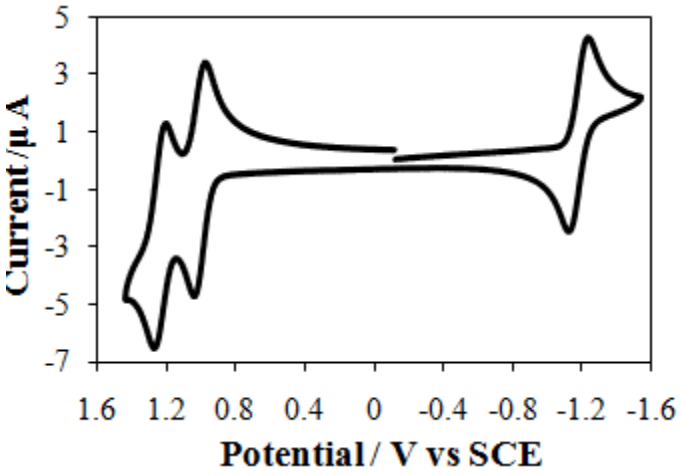

Figure 3.7. Cyclic voltammogram of 0.5 mM **1b** in dichloromethane with 0.1 M $TBAPF_6$.

Scan rate = 100 mV/s. Area of electrode is 0.028 cm^2.

Digital simulations of the experimental CVs for the reduction and oxidation are shown in Figures 3.8 and 3.9, respectively. These indicate good fits between experimental and simulated CVs for both reduction and oxidation performed at various scan rates from 0.05 V/s to 0.75 V/s. The double layer capacitance and the uncompensated resistance used in the simulation were measured from a potential step in the region with only double layer charging occurred, i.e. at 0 V vs SCE. The best fit for the CV simulation suggests a single 1e reduction with $D = 1.0(\pm 0.1) \times 10^{-5}$ cm^2/s and $k^o = 1.5 \times 10^{-3}$ cm/s; and two 1e oxidations with $D = 1.1(\pm 0.1) \times 10^{-5}$ cm^2/s and $k^o > 0.1$ cm/s.

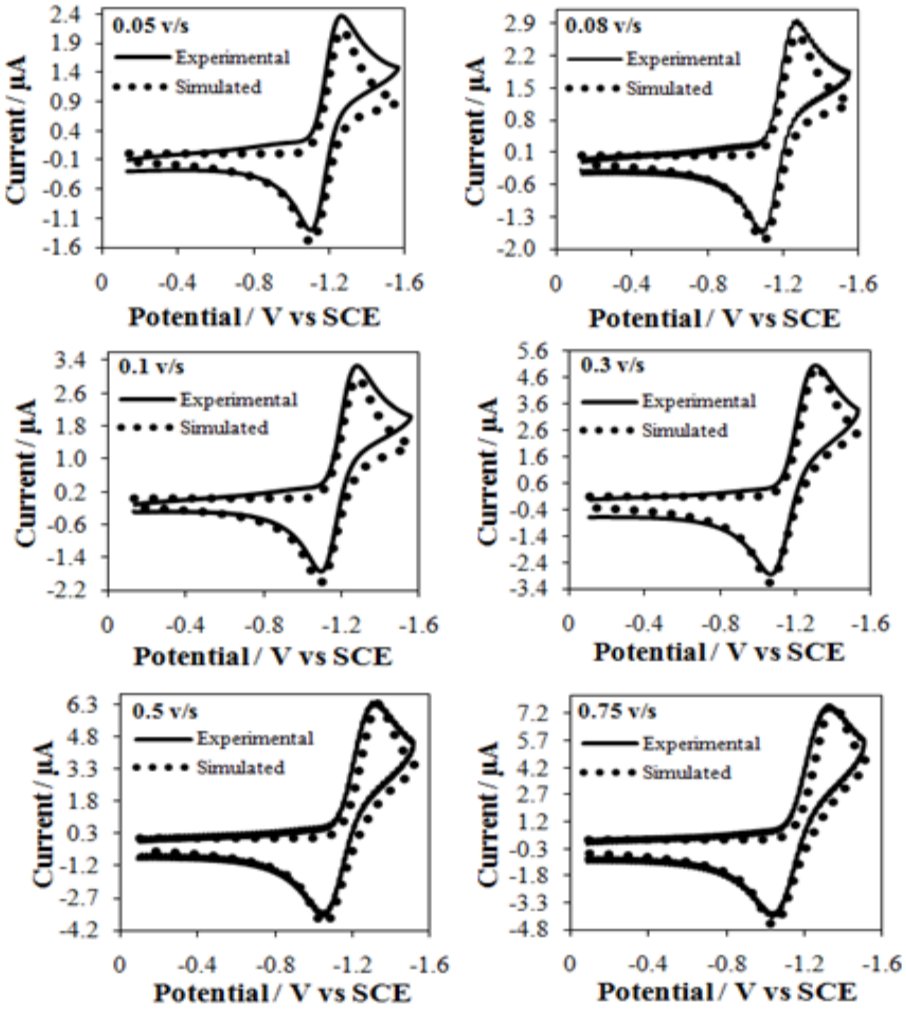

Figure 3.8. Simulation of 0.5 mM **1b** reduction in dichloromethane.

(a) 0.05 V/s (b) 0.08 V/s (c) 0.1 V/s (d) 0.3 V/s (e) 0.5 V/s (f) 0.75 V/s. Simulation mechanism is one-electron reduction with D = 1.0×10^{-5} cm^2/s, E^o_{red} = –1.18 V vs SCE, $k^o = 1.5 \times 10^{-3}$ cm/s, $\alpha = 0.5$, uncompensated solution resistance R_u = 1972 Ω, and double layer capacitance C_{dl} = 0.25 µF.

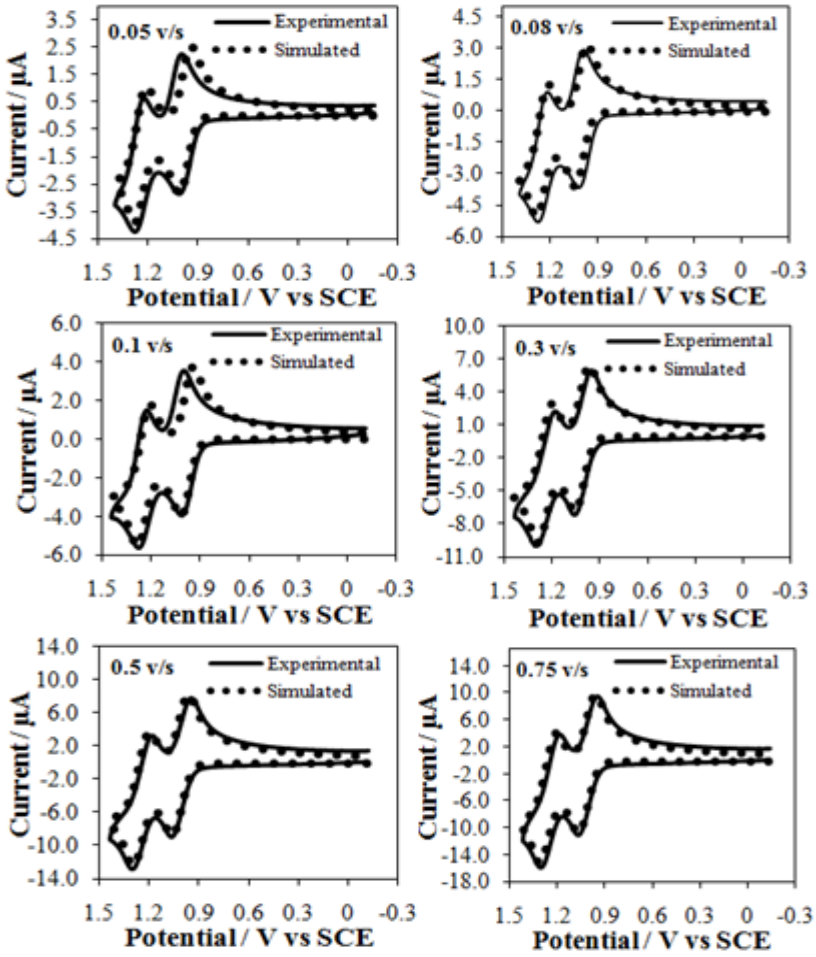

Figure 3.9. Simulation of 0.5 mM **1b** oxidation in dichloromethane.

(a) 0.05 V/s (b) 0.08 V/s (c) 0.1 V/s (d) 0.3 V/s (e) 0.5 V/s (f) 0.75 V/s. Simulation mechanism is two stepwise 1e oxidations with D = 1.1 × 10^{-5} cm^2/s, $E^o_{1,ox}$ = 1.01 V vs SCE, $E^o_{2,ox}$ = 1.24 V vs SCE, k^o > 0.1 cm/s, α=0.5, uncompensated solution resistance R_u = 1972 Ω, and double layer capacitance C_{dl} = 0.25 µF.

Heterogeneous Electron Transfer Kinetics. As stated earlier, the structures of **1a** and **1b** suggest that the reduction of the benzothiadiazole center should be more hindered than that of a free benzothiadiazole molecule and also slower than the rate of oxidation of the external D–groups. This expectation is confirmed by the CV results. As shown by the simulations in Figures 3.5 and 3.6 for **1a**, a smaller heterogeneous electron transfer rate constant, k_r^o = 0.6 × 10^{-3} cm/s, was calculated for the reduction occurring in the acceptor center compared to the oxidations occurring at the two donor ends of the molecule with k^o = 0.02 cm/s. The same trend was observed for **1b**, as shown by the simulations in Figures 3.8 and 3.9**,** a smaller heterogeneous electron transfer rate constant, k_r^o = 1.5 × 10^{-3} cm/s, was calculated for the reduction occurring in the acceptor center compared to the oxidations occurring at the two donor ends of the molecule with k^o > 0.1 cm/s. Note that the slower measured kinetics for the reduction center cannot be accounted on the basis of uncompensated resistance, R_u, because (1) this was taken into account in the simulation from the measured R_u and (2) the same value was used for the oxidation and reduction steps. A similar CV study and measurement of the heterogeneous rate constant was carried out for 2,1,3-benzothiadiazole itself (structure is shown below). CVs and digital simulations are shown in Figure 3.10. Because of the poor solubility of this species in CH_2Cl_2, the electrochemical study was carried out in MeCN. In the CV study, only one reduction peak and no oxidation peaks were observed. The CV simulation mechanism assigned a one-electron process for the reduction with E^o_{red} = –1.56 V vs SCE, D = 3.6 × 10^{-5} cm^2/s and k^o > 0.1 cm/s. The larger D value is consistent with the smaller size of this molecule compared to **1a** and **1b**.

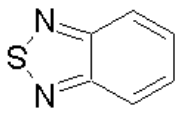

2, 1, 3-Benzothiadiazole

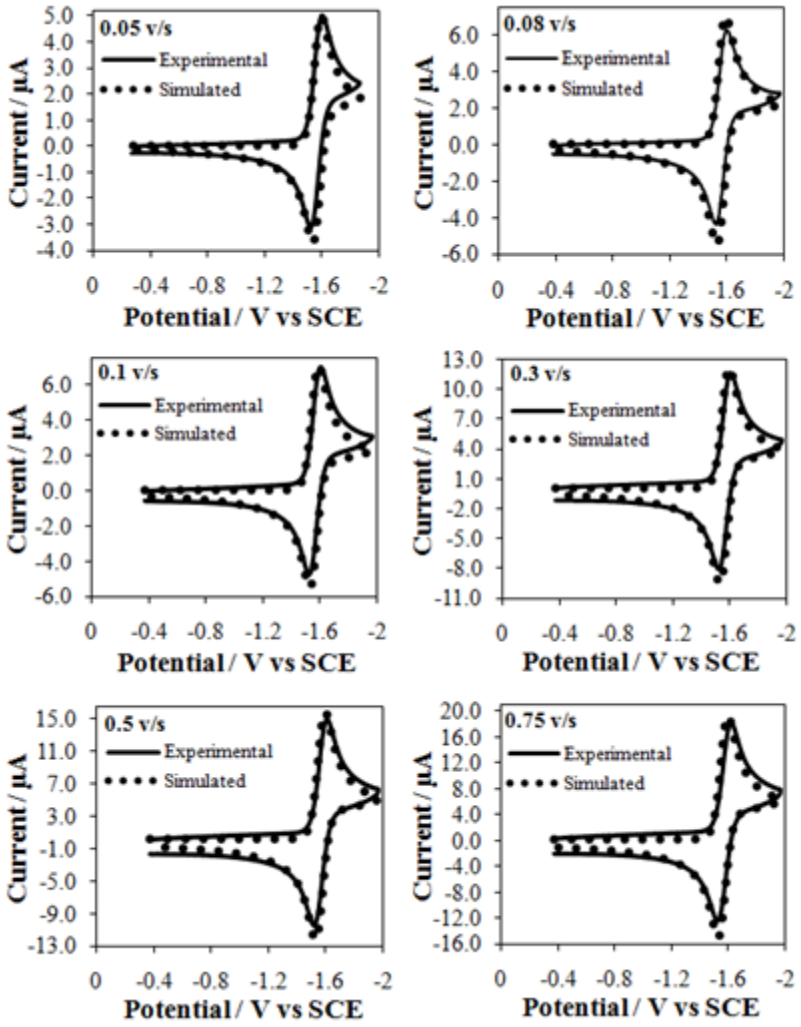

Figure 3.10. Simulation of 0.5 mM 2,1,3-benzothiadiazole reduction in MeCN.

(a) 0.05 V/s (b) 0.08 V/s (c) 0.1 V/s (d) 0.3 V/s (e) 0.5 V/s (f) 0.75 V/s. Simulation mechanism is one-electron reduction with D = 3.6 x 10^{-5} cm^2/s, E^o_{red} = -1.56 V vs SCE, k^o > 0.1 cm/s, α = 0.5, uncompensated solution resistance R_u = 264 Ω, and double layer capacitance C_{dl} = 0.28 µF.

The slow electron transfer rate of the reduction center can be attributed to it being blocked by the two bulky end groups.[16] In fact, when 2, 1, 3-benzothiadiazole was connected to a small end group (*t*-butylphenyl), a faster electron transfer rate for reduction was observed,[22] in contrast to **1a/1b** where blocking occurs. The distortion of the shape of the reduction CV of **1a/1b** (when compared to the ideal nernstian case) cannot be attributed to a following reaction, as shown by the CV behavior and also by the fact that, as described below, the ECL efficiency is high.[3, 4] The slow electron transfer of the A−group can be thought of as a forced longer distance electron transfer because of the blockage (a nonadiabatic effect) or the fact that reduction via the accessible thiophene groups would occur at a significantly more negative potential (< −2 V) , thus causing a large energy of activation for the reduction. Kojima and Bard[23] studied the heterogeneous electron transfer kinetics for the reduction of 16 aromatic compounds and found that the total activation energies for reorganization and solvation for all were in the range of 0.1 to 0.2 eV. Such small activation energies, e.g. for dibenzothiophene, cannot account for the small rate of reduction found here, suggesting that a steric (longer distance) electron transfer is more reasonable.

3.4 ELECTROGENERATED CHEMILUNINESCENCE

Figure 3.11 shows the ECL spectra of **1a** generated by pulsing the electrode potential between the reduction and two possible oxidations. Fluorescence and absorbance spectra are also shown in Figure 3.11. Maximum PL emission of **1a** occurs at 612 nm and maximum ECL emission occurs at 630 nm. There is a 18 nm red shift of the ECL spectrum compared to the fluorescence spectrum.

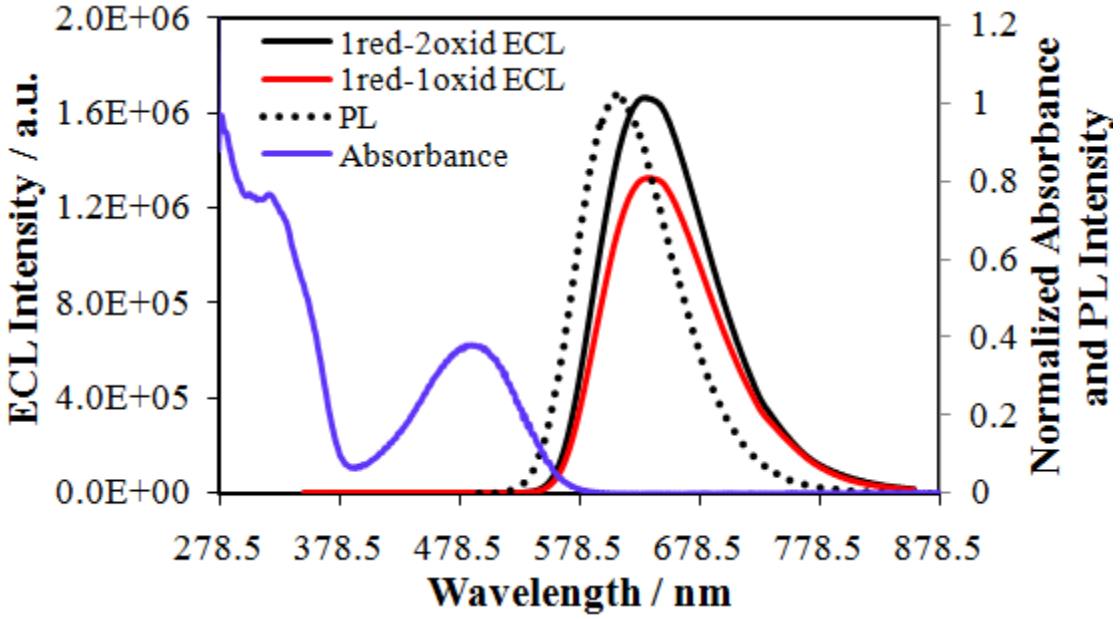

Figure 3.11. ECL spectra of 0.5 mM **1a** in 0.1 M $TBAPF_6$ in dichloromethane.

Obtained by pulsing between 80 mV past the reduction peak potential and two different anodic potentials, 80 mV past the first oxidation peak potential and 80 mV over the second oxidation peak potential as well as normalized absorbance and normalized fluorescence or photoluminescence (PL) spectrum of 7 μM **1a** in dichloromethane. ECL spectra were integrated for 30 s using a 0.5 mm slit width. (Excitation wavelength for fluorescence emission: 485nm).

The ECL spectra of **1b** generated by pulsing the electrode potential between the reduction and the two possible oxidations are shown in Figure 3.12. Absorption and photoluminescence spectra were also shown in Figure 3.12. There is a 17-nm red shift of the ECL spectrum compared to the fluorescence spectrum.

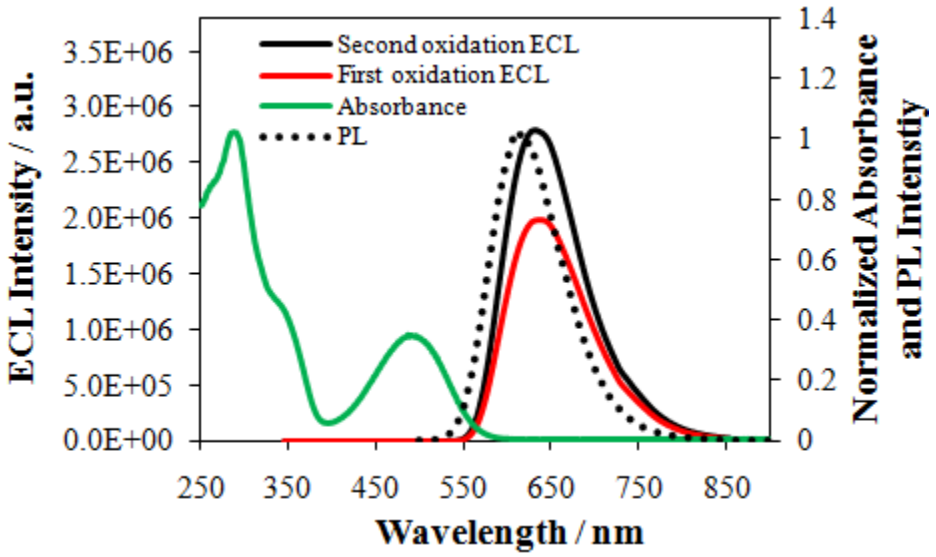

Figure 3.12. ECL spectra of 0.5 mM **1b** in 0.1 M $TBAPF_6$ in dichloromethane.

Obtained by pulsing between 80 mV past the reduction peak potential and two different anodic potentials, 80 mV past the first oxidation peak potential and 80 mV over the second oxidation peak potential as well as normalized absorbance and normalized fluorescence or photoluminescence (PL) spectrum of 7 μM **1b** in dichloromethane. ECL spectra were integrated for 30 s using a 0.5 mm slit width. (Excitation wavelength for fluorescence emission: 491 nm).

Compound **1a** has a Stokes shift of 127 nm and compound **1b** has a Stokes shift of 120 nm and they both show some absorbance within the wavelength range of photoluminescence (PL) and ECL; the concentration of **1a/1b** in the ECL experiments (0.5 mM) was much higher than in the PL experiment (7 μM), thus absorption of the emitted light in ECL could account for a small inner filter effect that red shifts the observed ECL emission with respect to that of PL. Systematic errors in the spectroscopy can also account for some of the difference, since the PL and ECL spectra were taken with different instruments and different slit widths; in our experience the accumulated errors typically result in a shift of 10 to 15 nm. Despite these small discrepancies, the same excited emissive state is probably formed in ECL and in PL.

For both **1a** and **1b,** the ECL generated when stepping into the second oxidation showed a higher intensity for reasons discussed below. Taken together with the results of CV, which showed no indication of decomposition of the radical cation or the dication, and the fact the ECL spectrum is close to the fluorescence spectrum with no additional emission peaks, the precursor stability is high, which is not seen in similar donor-acceptor systems.[19]

The energy of the excited singlet state can be estimated from the fluorescence emission maximum by the equation E_s (in eV) = 1239.81/λ (in nm)[3], where λ is the wavelength at maximum emission. The calculated excited singlet state energy for **1b** is 2.03 eV. The energy of the annihilation reaction, $-\Delta H^o = E^o_{ox} - E^o_{red} - T\Delta S$, based on the difference between the thermodynamic potentials of the first oxidation and the second oxidation and the reduction in the cyclic voltammogram ($E^o_{1,\,ox} - E^o_{red}$ = 2.19 eV, $E^o_{2,\,ox}$ –

E^{o}_{red} = 2.42 eV) with an estimated entropy effect (~ 0.1 eV) subtracted out, is about 2.09 eV and 2.32 eV. The energy of the annihilation reaction (2.09 eV and 2.32 eV) is greater than the energy needed to directly populate the singlet excited state (2.03 eV), and thus the ECL reaction probably proceeds via the S-route where the singlet-excited state is directly populated upon radical ion annihilation. With a large Stokes shift, a more correct calculation of the energy of the excited singlet state energy can be estimated by considering the wavelength where the absorbance and emission curves cross; in our case, this would yield an excited singlet state energy of 2.27 eV (at 546 nm), for which our estimated $-\Delta H^{o}$ = 2.09 eV for reduction and first oxidation would be insufficient to populate it. Experimentally, we observe that upon pulsing into the second oxidation process, where $-\Delta H^{o}$ = 2.32 eV and the calculated singlet state energy is higher, the ECL emission profile is maintained, suggesting that in this excess energy scenario, the same excited state is formed and is thus energy-sufficient even for the reduction-first oxidation case. Given the apparent high ECL efficiency, even with the uncertainties presented in the calculations, we assign it to an energy sufficient system.[20]

Based on the calculation procedure above, the calculated excited singlet state energy for **1a** is 2.03 eV. The calculated energy of the annihilation reaction, the difference between the thermodynamic potentials of the first oxidation and the second oxidation and the reduction in the cyclic voltammogram ($E^{o}_{1,\,ox} - E^{o}_{red}$ = 2.26 eV, $E^{o}_{2,\,ox} - E^{o}_{red}$ = 2.54 eV) with an estimated entropy effect (~ 0.1 eV) subtracted out, is about 2.16 eV and 2.44 eV. The energy of the annihilation reaction (2.16 eV and 2.44 eV) is greater than the energy needed to directly populate the singlet excited state (2.03 eV), and thus

the ECL reaction probably proceeds via the S-route where the singlet-excited state is directly populated upon radical ion annihilation. With a large Stokes shift, a more correct calculation of the energy of the excited singlet state energy can be estimated by considering the wavelength where the absorbance and emission curves cross; in our case, this would yield an excited singlet state energy of 2.27 eV (at 546 nm), for which our estimated $-\Delta H^{o}$ = 2.16 eV for reduction and first oxidation would be insufficient to populate it. Experimentally, we observe that upon pulsing into the second oxidation process, where $-\Delta H^{o}$ = 2.44 eV and the calculated singlet state energy is higher, the ECL emission profile is maintained, suggesting that in this excess energy scenario, the same excited state is formed and is thus energy-sufficient even for the reduction-first oxidation case. Given the apparent high ECL efficiency, even with the uncertainties presented in the calculations, we assign it to an energy sufficient system.[20]

The relative intensities of **1b** with respect to DPA and Rubpy, efficient and widely investigated ECL molecules, are shown in Table 3.2. ECL intensities of **1b** are stronger than that of DPA and comparable with that of Rubpy when stepping to both the first oxidation and second oxidation, indicating that **1b** is a strong ECL emitter.

Table 3.2. Maximum ECL Emission Wavelength λ_{max}^{ECL}, Intensity at λ_{max}^{ECL} and Relative Intensity with respect to DPA and Rubpy.

Pulsing Potentials	λ_{max}^{ECL} (nm)	I (λ_{max}^{ECL}) (a.u.)	Relative Intensity vs. DPA[a]	Relative Intensity vs. Rubpy[b]
Reduction and First Oxidation	637	2.0×10^6	330 %	110 %
Reduction and Second Oxidation	633	2.8×10^6	470 %	150%

[a] Calculated by comparing the $I_{\lambda max}^{ECL}$ of **1b** with that of DPA in MeCN.

[b]Calculated by comparing the $I_{\lambda max}^{ECL}$ of **1b** with that of Rubpy in MeCN generated by oxidation and first reduction.

The ECL of **1a** was compared to Rubpy and **1b** and the results are shown in Table 3.3. The comparison of ECL was made in terms of maximum intensity and integrated area of ECL spectra.

Table 3.3. Maximum ECL Emission Wavelength λ_{max}^{ECL} and Relative Intensity with respect to Rubpy and 1b under conditions of Figure 4.

Pulsing Potentials	λ_{max}^{ECL} (nm)	Relative Intensity vs. 1b[a]	Relative Intensity vs. Rubpy[b]	Integrated Area vs. 1b[a]	Integrated Area vs. Rubpy[b]
Reduction and First Oxidation*	633	(21 ± 5) %	(17 ± 3) %	(22 ± 5) %	(42 ± 6) %
Reduction and Second Oxidation*	631	(41 ± 5) %	(31 ± 3) %	(19 ± 4) %	(33 ± 3) %

[a] Calculated by comparing the $I\lambda max^{ECL}$ and integrated area of ECL spectrum of **1a** with that of 1b in DCM.

[b]Calculated by comparing the $I\lambda max^{ECL}$ and integrated area of ECL spectrum of **1a** with that of Rubpy in MeCN.

*For reduction-first oxidation of 1a, comparison was made with reduction-first oxidation of 1b and first reduction-oxidation of Rubpy; for reduction-second oxidation of 1a, comparison was made with reduction-second oxidation of 1b and second reduction-oxidation of Rubpy.

3.5 EXPERIMENTAL AND SIMULATED TRANSIENT ECL

In transient ECL experiments, the behavior of the ECL emission is monitored versus time during multi potential-step chronoamperometry;[3] this programming alternates the potential of the working electrode between a cathodic potential (radical anion generation) and an anodic potential (radical cation generation). Electrogenerated reactants in excess from pulse *j*-1 react with freshly electrogenerated reactants generated during

pulse *j*, and so forth. When the radical ions are generated under mass transfer controlled conditions and at equal time intervals, i.e. the cathodic pulse is of equal length to the anodic pulse, the ECL emission will show a characteristic decay which is a product of the Cottrell decay along with the consumption of the radical ions by the annihilation reaction. Provided the radical ions are stable, the ECL transient during a cathodic and anodic step should exhibit the same shape and the intensity of the emission should not decrease with increasing number of steps (after complete development of a quasi steady state diffusion layer).[17, 24] Much of the early ECL literature included the analysis of these transients for the extraction of kinetic and mechanistic parameters, e.g. through the use of Feldberg plots.[25] However, the complexity of the ECL process has limited its applicability.[3] Our approach in this work is to use transient ECL as an evidence of the stability of the radical ions and also to show a particular case in which unequal transients can also be caused by the reactant stoichiometry. Despite the existence of a vast literature on ECL transients and the study of mixed systems,[26] e.g. systems in which D and A in equations 1 and 2 are located on different molecules and where possibly different stoichiometric amounts of D and A could be used, to the best of our knowledge this case has not been simulated previously and compared to experimental results.[27]

Experimental ECL transients. Three kinds of ions can be formed during the reduction and oxidation of **1b**, the radical anion $\mathbf{1b}^{-\cdot}$, the radical cation $\mathbf{1b}^{+\cdot}$ and the dication $\mathbf{1b}^{2+\cdot}$. Figure 3.13 is a schematic of the polarity and selection of the potential steps for the production of the different ions, and shows the results of transient ECL generated by different combinations of these: Figure 3.13 a, in which ECL was generated by radical anion and radical cation annihilation (1-1 case), and Figure 3.13 b, in which ECL was generated by radical anion and dication annihilation (1-2 case). Both cases show that the ECL responses are fairly stable in that the transient response does not

decrease with the number of steps thus indicating, as grasped from the chemical reversibility in the cyclic voltammetry shown in Figure 3.7, no evident loss of **1b** or its electrochemically reduced/oxidized species due to chemical decomposition into other products. This feature is characteristic of strongly emitting ECL systems.

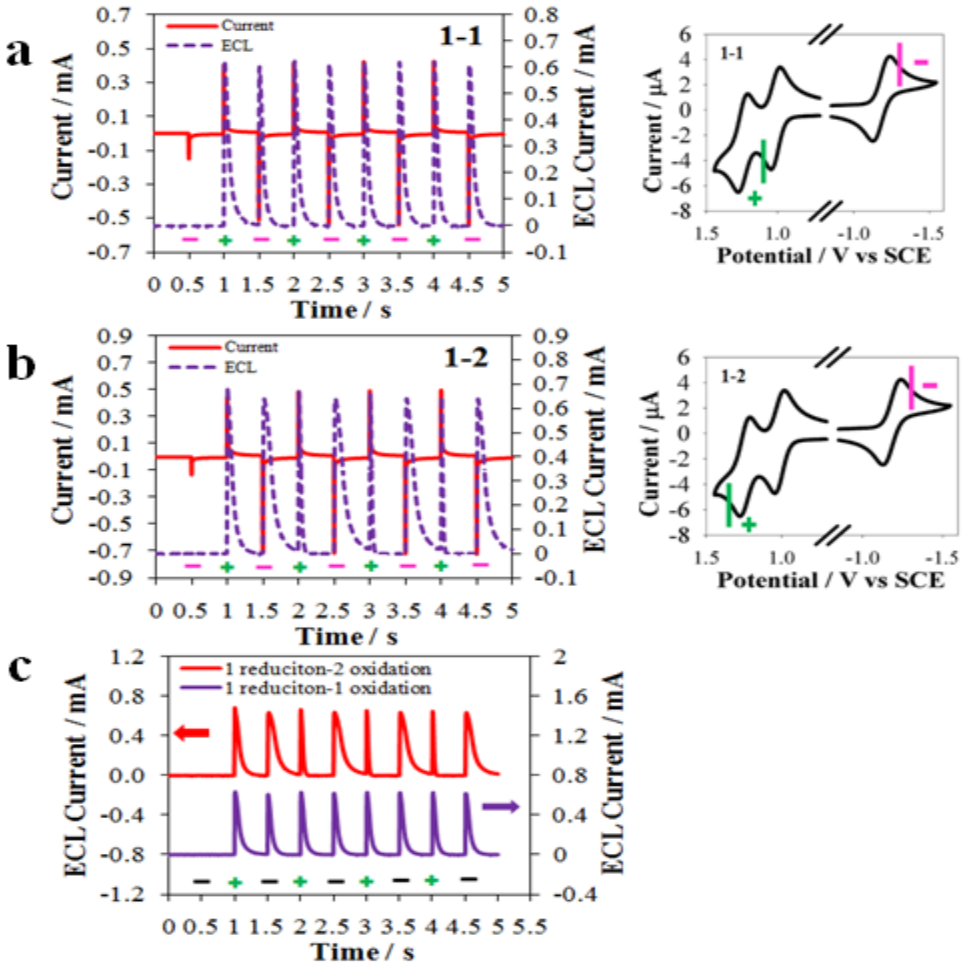

Figure 3.13. Current (red, solid) and ECL (purple, dotted) transients with 0.5 s pulsing time for 0.5 mM **1b** in dichloromethane.

Pulsed between a) reduction and first oxidation, b) reduction and second oxidation, and c) comparison of transient ECL generated through a) (purple, solid) and b) (red, solid).

Panels on the right show schematically the potentials used and the polarity of the step as indicated in the graphs. + indicates an anodic step or production of radical cations, - indicates a cathodic step or production of radical anions. For 1:1 case, an oxidation potential of 1.12 V and a reduction potential of −1.32 V were applied; for 1:2 case: an oxidation potential of 1.36 V and a reduction potential of−1.32 V were applied (vs SCE).

As shown in Figure 3.13a, the ECL transient generated by radical anion-cation annihilation exhibits a symmetrical response during the anodic and cathodic pulses; in Figure 3.13b, however, where ECL is generated by anion-dication annihilation, a broader ECL signal was obtained during the cathodic pulse compared to the anodic pulse. This can be more clearly observed in the comparison made in Figure 3.13c between the two experimental cases. A possible misinterpretation of the shape of the transients in Figure 3.13b without taking into account the effects of the stoichiometry of the reaction could suggest that the radical anion is chemically unstable, so that upon anodic stepping (production of dications), the ECL intensity decays faster in time as a consequence of the decomposition of the anions.[17] This explanation is contrary to the stability observed in the transients of Figure 3.13a for the 1-1 case, and also because the overall ECL emission is increased when comparing the 1-2 case with respect to the 1-1 case; Furthermore, the CV of **1b** does not suggest any chemical instability. The difference in the shape of the 1-2 case with respect to the 1-1 case in Figure 3.13c can be better explained by the following arguments that take into account the stoichiometry of the reactants. In the first cathodic pulse (t = 0.5 s, j), $\mathbf{1b}^{\cdot-}$ is produced; since no radical cations are initially present in the system, there is no ECL emission at t = 0.5 s. In the following first anodic pulse (t = 1 s, j+1) $\mathbf{1b}^{+\cdot}$ or $\mathbf{1b}^{2+\cdot}$ (for the 1-2 case) is freshly produced and reacts with $\mathbf{1b}^{\cdot-}$ produced in

step *j* and ECL emission is observed; **1b** $^{-\cdot}$ is the limiting species in both cases, so the same ECL emission profile is produced for the first anodic pulse as evidenced in Figure 3.13c at *t* = 1s. Since in the 1-2 case a larger amount of charge is injected for the generation of **1b**$^{2+\cdot}$ at pulse *j*+1 compared to the 1-1 case, more radical cations are left to react with **1b** $^{-\cdot}$ for the following cathodic pulse (*t* = 1.5 s, *j*+2), thus a broader peak is observed for the 1-2 case; after the cathodic pulse at 1.5 s, less **1b** $^{-\cdot}$ is left for the following anodic pulse (t = 2 s, *j*+3) as a consequence of a larger amount of radical cations having been consumed during pulse *j*+2, thus a narrower ECL signal is seen in pulse *j*+3 compared to the 1-1 case; the following pulses can be described by these same arguments. To understand and quantify the observed differences, simulation of transient ECL was performed and the results are shown below.

Digital simulation of transient ECL. Electrochemical and ECL digital simulations were carried out using the COMSOL Multiphysics ® Software v.3.2 which uses a finite element method (FEM) to treat diffusion and reaction kinetics. The problem was solved in the transient mode and a 1D approach was used to model planar diffusion to the electrode. While the use of an exponentially expanding grid has been criticized for ECL simulations using the finite difference method,[28] it did provide the necessary stability and memory efficiency required to treat the coupled homogeneous and heterogeneous electrochemical conditions in this FEM simulation.

(A) Reactions

$m + \bar{e} \rightleftarrows r1$ Radical anion formation with E^0_{red} and k^0_{red} (3.8)

$o1 + \bar{e} \rightleftarrows m$ Radical cation formation with $E^0_{ox,1}$ and $k^0_{ox,1}$ (3.9)

$o2 + \bar{e} \rightleftarrows o1$ Radical dication formation with $E^0_{ox,2}$ and $k^0_{ox,2}$ (3.10)

$r1 + o1 \xrightarrow{kann} me + m$ Radical ion annihilation with k_{ann} (3.11)

$r1 + o2 \xrightarrow{kann} me + o1$ Radical ion annihilation with k_{ann} (3.12)

$o2 + m \xrightarrow{ktr} 2o1$ Radical dication charge transfer to parent molecule (3.13)

$me \xrightarrow{kem} m + b(light)$ Light emission from excited state with k_{em} (3.14)

(B) Simulation space

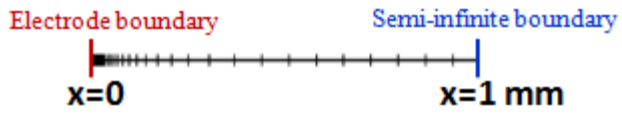

(C) Potential vs. time program

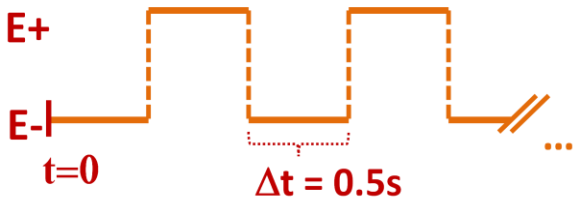

Species	(D) Diffusion and kinetics	
Parent molecule **m** = 1b	$\frac{\partial c_m(x,t)}{\partial t} = D_m \frac{\partial^2 c_m(x,t)}{\partial x^2} + k_{ann} c_{o1} c_{r1} - k_{tr} c_{o2} c_m + k_{em} c_{me}$	(3.15)
Radical anion **r1** = $1b^{-\cdot}$	$\frac{\partial c_{r1}(x,t)}{\partial t} = D_{r1} \frac{\partial^2 c_{r1}(x,t)}{\partial x^2} - k_{ann} c_{o1} c_{r1} - k_{ann} c_{o2} c_{r1}$	(3.16)
Radical cation **o1** = $1b^{+\cdot}$	$\frac{\partial c_{o1}(x,t)}{\partial t} = D_{o1} \frac{\partial^2 c_{o1}(x,t)}{\partial x^2} - k_{ann} c_{o1} c_{r1} + k_{ann} c_{o2} c_{r1} + 2k_{tr} c_{o2} c_m$	(3.17)
Radical dication **o2** = $1b^{2+\cdot}$	$\frac{\partial c_{o2}(x,t)}{\partial t} = D_{o2} \frac{\partial^2 c_{o2}(x,t)}{\partial x^2} - k_{ann} c_{o2} c_{r1} - k_{tr} c_{o2} c_m$	(3.18)
Excited state of m **me** = $1b^*$	$\frac{\partial c_{me}(x,t)}{\partial t} = D_{me} \frac{\partial^2 c_{me}(x,t)}{\partial x^2} + k_{ann} c_{o1} c_{r1} + k_{ann} c_{o2} c_{r1} - k_{em} c_{me}$	(3.19)

Species	(E) Flux condition at electrode	
Parent molecule **m** = 1b	$J = (k^0_{ox,1} e^{-\alpha f(E-E^0_{ox,1})} c_{o1} - k^0_{ox,1} e^{(1-\alpha) f(E-E^0_{ox,1})} c_m) - (k^0_{red} e^{-\alpha f(E-E^0_{red})} c_m - k^0_{red} e^{(1-\alpha) f(E-E^0_{red})} c_{r1})$	(3.20)
Radical anion **r1** = $1b^{-\cdot}$	$J = k^0_{red} e^{-\alpha f(E-E^0_{red})} c_m - k^0_{red} e^{(1-\alpha) f(E-E^0_{red})} c_{r1}$	(3.21)
Radical cation **o1** = $1b^{+\cdot}$	$J = -(k^0_{ox,1} e^{-\alpha f(E-E^0_{ox,1})} c_{o1} - k^0_{ox,1} e^{(1-\alpha) f(E-E^0_{ox,1})} c_m) + (k^0_{ox,2} e^{-\alpha f(E-E^0_{ox,2})} c_{o2} - k^0_{ox,2} e^{(1-\alpha) f(E-E^0_{ox,2})} c_{o1})$	(3.22)
Radical dication **o2** = $1b^{2+\cdot}$	$J = -(k^0_{ox,2} e^{-\alpha f(E-E^0_{ox,2})} c_{o2} - k^0_{ox,2} e^{(1-\alpha) f(E-E^0_{ox,2})} c_{o1})$	(3.23)
Excited state of m **me** = $1b^*$	$J = 0$	(3.24)

(F)

Initial and semi-infinite boundary conditions:

$c_m = 0.5$ mM , $c_{r1} = c_{o1} = c_{o2} = c_{me} = 0$

$D_m = D_{r1} = D_{o1} = D_{o2} = D_{me} = 1\times10^{-9}$ m^2/s

Figure 3.14. Summary of simulation model used for transient ECL.

(A) Chemical and electrochemical reactions used, Equations 3.8-3.14; (B) 1D simulation space showing the spatial simulation elements and the relevant boundaries; (C) Programming used for the electrode potential vs time; (D) Coupled diffusion and kinetics used in the simulation space for each species, Equations 3.15-3.19; (E) Butler-Volmer expressions for the flux to the electrode boundary for each species, Equations 3.20-3.24; (F) Initial and semi-infinite boundary conditions used.

Figure 3.14 shows a summary of the simulation model, where the required reactions for the ECL process, Panel (A) of Figure 3.14, have been expanded from those shown in equations 3.1-3.4 to account also for the possibility of electrogeneration of a dication in addition to the radical cation and radical anion, the annihilation reaction between a dication and a radical anion, and the non-trivial oxidation of the parent molecule by the dication (comproportionation). Panel (B) of Figure 3.14 shows the discretization of the simulation space; this was performed using an exponentially expanding grid with a base box length of Δx_0 =15 nm and an element growth factor of 1.2 (β = 0.2, where $\Delta x_k = \Delta x_0 e^{k\beta}$, Δx_k being the size of simulation element k). For a simple

potential step at a diffusion limited potential and following Cottrell behavior, the size of the simulation space should accommodate at least 6 to 7 times the extension of the diffusion layer δ, where $\delta \approx (2Dt)^{1/2}$, D is the diffusion coefficient of the species and t is the length of the potential step. While in transient ECL the potential is being stepped to different values, δ can be safely approximated using the total time of the experiment. For our typical simulations and experiments, $t \approx 10$ s and $D = 1\times10^{-5}$ cm^2/s as explained earlier in the text, so $7\delta \approx 989$ μm; as shown in panel (B) of Figure 3.14, we decided to use a simulation space 1 mm in length (55 simulation elements), where the region closest to the electrode is meshed the finest.

The potential versus time programming used for the electrode boundary is shown in panel (C) of Figure 3.14; the simulated stepping was accomplished by setting a time dependent sine wave as the argument of a step function that alternated between an oxidizing and a reductive potential, E^+ and E^-, respectively, thus resulting in a square wave with a potential step length of 0.5 s as described experimentally in Figure 3.13. The use of Butler-Volmer (*B-V*) kinetics to describe the flux of electroactive species with respect to the electrode boundary allows relating the potential programming to the operation of the electrode (Equations 3.20-3.24). As well, the use of Fick's second law of diffusion including reaction kinetics allows the description of the following chemical reaction mechanisms necessary for the ECL process in the simulated space (Equations 3.15-3.19). The respective equations for these two processes are shown in panel (D) of Figure 3.14 for each participating species; species that can either be both reduced and oxidized, e.g. the parent molecule and the radical cation, required the use of more than one *B-V* expression to be described. Panel (D) in Figure 3.14 also shows the initial and semi-infinite boundary conditions, which indicate that only the parent molecule is present at the beginning of the experiment and in the bulk of the solution.

For the evaluation of the model equations in Figure 3.14, all second-order kinetics were assumed to be fast and to proceed close to diffusion limitation such that $k_{ann} = k_{tr} = 1\times10^{9}$ $M^{-1}s^{-1}$ and the radiative decay of the excited state of the parent molecule was assumed to have a life time of 1 ns, such that $k_{em} = 1\times10^{9}$ s^{-1}, a typical value for fluorescence emission.[29] For the evaluation of the *B-V* kinetics, we assumed that the transfer coefficient α is 0.5, that $f = 38.94$ V^{-1} (where $f = F/RT$, the Faraday constant F = 96,485 C/mol, the gas constant R = 8.314 J/mol and the temperature T = 298 K) and that the standard rate constant k^0 for the two reversible oxidations was $k^0_{ox,1} = k^0_{ox,2} = 10$ cm/s and for the reduction, $k^0_{red} = 1.5\times10^{-3}$ cm/s, in accordance to the text. For the evaluation of the potential expressions in the *B-V* model, a simplification was used in order to avoid very large numbers in the evaluation of the exponentials, which led to instabilities in the numerical evaluation. Such simplification consisted in decreasing the potential gap between $E^0_{ox,1}$ (first oxidation) and E^0_{red} (first reduction) to manageable values without affecting the accuracy of the results, i.e. the experimental energetic gap of 2.19 V between $E^0_{ox,1}$ and E^0_{red} was reduced to 0.6 V. The used standard potentials used were $E^0_{ox,1} = 0.3$V, $E^0_{ox,2} = 0.53$V and $E^0_{red} = -0.3$V and the selected stepping potentials, which operate under diffusion limited conditions, were $E^+ = 0.36$ V and $E^+ = 0.59$ V for the first and second oxidation processes respectively and $E^- = -0.36$ V for the reduction process. The values chosen for the stepping and standard potentials for the oxidation reactions at the electrode are in accordance with the potential separation between the first and second oxidations observed experimentally in order to accurately compare simulation and experiment.

The simulated ECL signal was obtained by two approaches, the first one by integration of the rate of emission of the excited state, Equation 3.14 in Figure 3.14(A), across the simulation space at specified intervals (time stepping = 1 ms) and the second

one by modeling the emitted light (species *b* in Figure 3.14(A), Equation 3.14) as a pseudoparticle with extremely high diffusion coefficient (e.g. $D = 10^7$ cm^2/s) and integrating its flux at the electrode boundary to obtain a "photonic current".[21] While the units of the ECL signal are arbitrary (i.e. do not include effects from the quantum efficiency of emission, geometry of photon collection or response of the detector), the relative intensities and shape of the response were consistent upon comparison of both transients (e.g. by overlapping them on the same scale). Comparison of the simulated and experimental results was done in the same fashion and is shown in Figure 3.15 for the two cases of interest, i.e. the reaction of the radical anion generated at E^- and either the radical cation (1-1 case) or dication (1-2 case) generated at E^+.

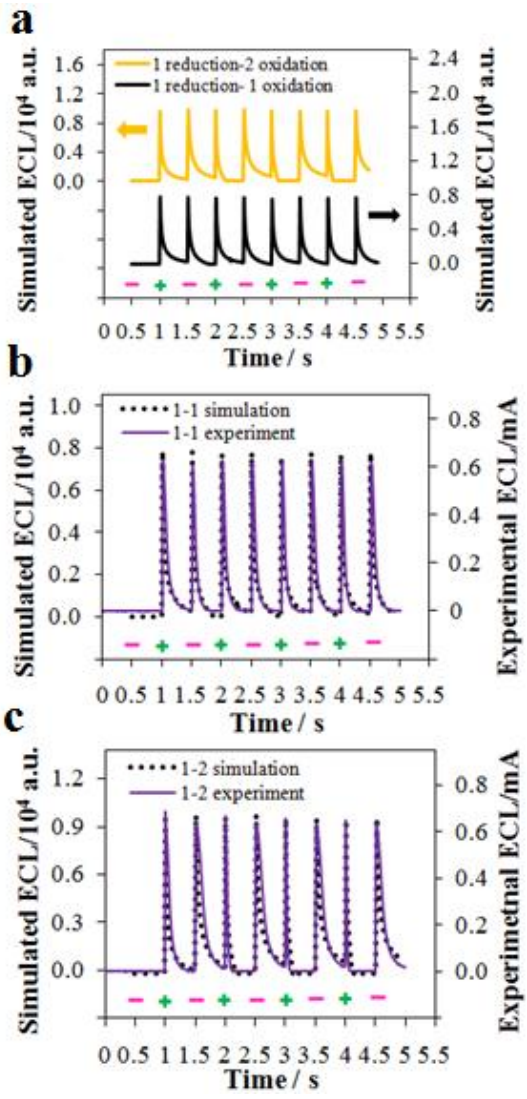

Figure 3.15. Comparison between simulated and experimental results for transient ECL.

a) simulated transients for the 1-1 (black) and 1-2 (yellow) case, – and + signs indicate cathodic and anodic stepping respectively, all other conditions as explained in the text; b) comparison for the 1-1 case between simulation (dotted) and experimental (continuous) transients on the same scale; c) same as b) but for the 1-2 case. Simulated transients neglect the first 5 ms of each step.

Figure 3.15a shows the comparison of the two simulation results, 1-1 case and 1-2 case, and Figures 3.15b and 3.15c show the comparison of the corresponding experimental and simulated results. Qualitatively there is a very good agreement between the experimental and simulated results; the simulation effectively recreates the following features: 1) there is a predicted difference in the shape of the ECL transients when comparing the 1-1 case to the 1-2 case, that is, upon change of the stoichiometry of the problem without the need to include other effects such as instability of the radical ions; 2) the relative widths and intensities of the curves agree well with the experimental ones, the simulation predicts in the 1-2 case narrower transients for the anodic pulses and wider ones for the cathodic pulses when compared to the 1-1 case; 3) the first transient, i.e. t = 1 s, shows no difference between the 1-1 and 1-2 case due to the role of **1b**$^{\cdot-}$ as the limiting reactant, as explained in the discussion of Figure 3.13. The fit is satisfactory, considering the simplifications of the mechanism used (Figure 3.14).

The goodness of the fit between the experimental and simulated results for **1b** was further tested quantitatively; this can be done by comparing the relative integrated intensities of both experimental and simulated transients. Table 3.4 shows the results for relevant comparisons of the features exhibited by the ECL transients of **1b** and ruthenium tris-bipyridine (Rubpy), an ECL standard with similar emission profile (shown in Figure 3.16), and a high ECL emission quantum yield. Rubpy is also able to generate a 2e reduced state that produces stable annihilation ECL. Table 3.4 shows that upon comparison of the different possible transients to the total emission in one cycle for **1b**, the results are comparable to the predicted ones, within the standard deviation of the measurements, for both the 1-1 case (T_S : $T_{T(1:1)}$ and T_L : $T_{T(1:1)}$) and the 1-2 case (T_S : $T_{T(1:2)}$ and T_L : $T_{T(1:2)}$).

Table 3.4 Quantitative comparison of experimental and simulated results obtained by numerical integration of ECL transients.

Nomenclature: $T_{T(x:y)}$ = Total transient for one cycle with stoichiometry x:y; T_L = Large transient component, T_S = Small transient component.			
Relation	Species	Predicted	Experimental / Detector*
$T_S : T_{T(1:1)}$	**1b**	0.5	0.47 ± 0.03 PMT
$T_L : T_{T(1:1)}$	**1b**	0.5	0.53 ± 0.017 PMT
$T_S : T_{T(1:2)}$	**1b**	0.25	0.17 ± 0.04 PMT
$T_L : T_{T(1:2)}$	**1b**	0.75	0.83 ± 0.07 PMT
$T_{T(1:1)} : T_{T(1:2)}$	**1b**	1.43	1.3 ± 0.10 PMT
			1.4 ± 0.3 CCD
$T_{T(1:1)} : T_{T(1:2)}$	**Rubpy**	1.43	1.6 ± 0.15 CCD
$T_{T(1:1)} : T_{T(1:1)}$	**Rubpy:1b**	N/A	1.1 ± 0.2 CCD
$T_{T(1:2)} : T_{T(1:2)}$	**Rubpy:1b**	N/A	1.2 ± 0.14 CCD

* PMT and CCD indicate the detector of ECL measurement is a photomultiplier tube or charge coupled device respectively as described in the text. Standard deviations were obtained from three relevant measurements.

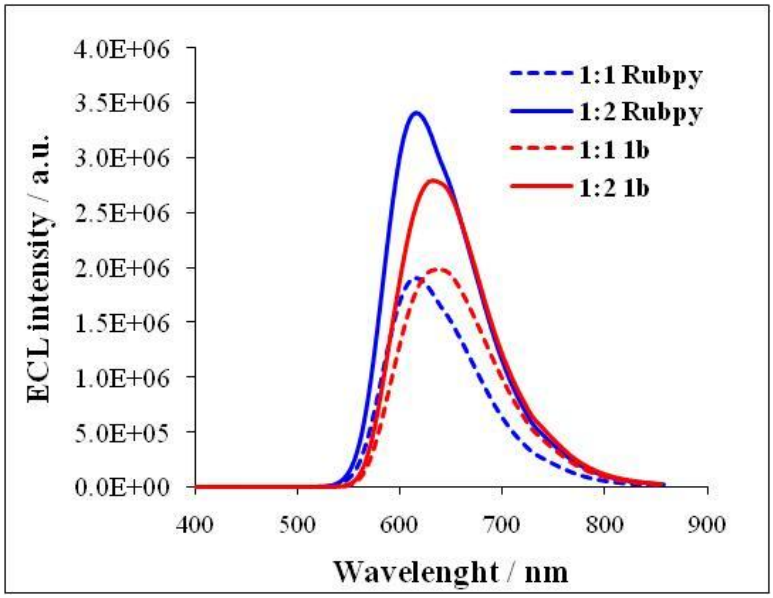

Figure 3.16. Comparison of ECL emission spectra for the 1-1 cases (dotted lines) and 1-2 cases (continuous lines) for Rubpy (blue) and 1b (red).

0.5 mM Rubpy in MeCN and 0.5 mM 1b in CH_2Cl_2 with 0.1 M $TBAPF_6$ as supporting electrolyte. Area of electrode is 0.028 cm^2. Step time = 0.1 s, slit width = 0.5 mm, integration time = 30s. For 1:1 Rubpy: spectrum was generated by pulsing between 1.28 V (80 mV over oxidation peak potential) and –1.53 V (50 mV over first reduction peak potential); for 1:2 Rubpy: spectrum was generated by pulsing between 1.28 V (80 mV over oxidation peak potential) and –1.73 V (50 mV over second reduction peak potential) versus Ag electrode.

The total emission intensity of the 1-1 case with respect to the 1-2 case ($T_{T(1:1)}$: $T_{T(1:2)}$**)** is a useful parameter; a naive expectation might be that the system would show twice the ECL emission for the 1-2 case. However the combined effects of ECL annihilation and diffusion into the bulk of the solution and electrochemical deactivation

of ions must be taken into account (e.g. $\mathbf{1b}^{2+\cdot}$ is prone both to react with $\mathbf{1b}^{-\cdot}$ and to get reduced at the electrode during a cathodic pulse). The simulation predicts a ratio of 1.43 times more total light in the 1-2 case with respect to the 1-1 case, which agrees with the experiment with **1b** and proved by the use of two different signal transducers. Furthermore, this figure is also confirmed within reasonable accuracy in the case of Rubpy. The relationships presented in Table 3.4 are directly comparable to the experiments shown in this study. Nonetheless, simulation of the cases where the diffusion coefficient of the species was increased or decreased by one order of magnitude (e.g. 1×10^{-4} cm^2/s > D > 1×10^{-6} cm^2/s) and in which the step time was changed in the same fashion (e.g. 0.05 s > t > 5 s) revealed no changes in this relative quantification. A final quantitative measurement displayed in Table 3.4 and shown experimentally in Figure 3.16 is the comparison of the total intensity of emission of **1b** in comparison to Rubpy under similar conditions. Rubpy is a good standard for comparison to **1b** because of their similar emission characteristics as shown in Figure 3.16. Our results indicate that the emission produced by **1b** is of comparable intensity to Rubpy.

The simulation presented for the 1-2 case can also be placed in the context of other stoichiometric relationships; Figure 3.17(a) shows the simulated results for the ECL transients when one of the radical ions is produced in excess with respect to the other. The trend observed for the 1-2 case is followed; upon increasing the equivalents of one component with respect to the other, the transients show the narrowing of one part of the ECL emission and the broadening of the other. We found a linear relationship between the total emission intensity of ECL in one cycle compared to the 1-1 case with respect to the excess of equivalents, as shown in Figure 3.17(b), although as already mentioned the slope is not equal to 1 due to a contribution of kinetic, diffusive and electrochemical

factors. Our group is currently involved in the search and study of D-A systems that can fulfill these predictions.

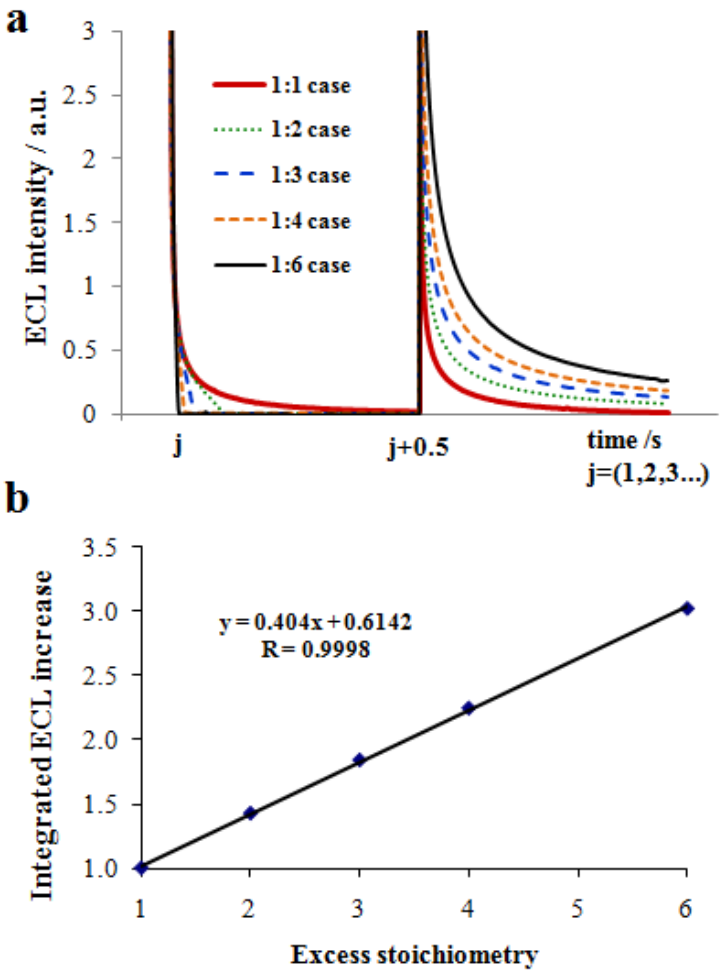

Figure 3.17. Simulated ECL transients for different stoichiometric cases and quantification of the increase in their ECL intensity compared to the 1-1 case.

a) shape of ECL transients for a 0.5 train of pulses; b) Linear plot of the increase of total ECL intensity in one cycle (i.e. both cathodic and anodic pulses) with respect to the 1-1 symmetrical case versus the excess stoichiometry (e.g. for the 1-2 case, x = 2).

3.6 FILM ECL

The ECL properties of **1a** film on FTO were studied in PBS buffer solution with TPrA as the coreactant. Figure 3.18a shows that very strong ECL was generated from **1a** film when scan from 0 V to 2 V vs SCE. As a comparison, Figure 3.18b is the result from a bare FTO electrode in PBS buffer solution with the presence of TPrA(background). It can be seen from Figure 3.18b that no ECL was generated without 1b film. Notice that since **1a** doesn't dissolve in water, there's little chance that ECL could be generated from **1a** dissolved in water.

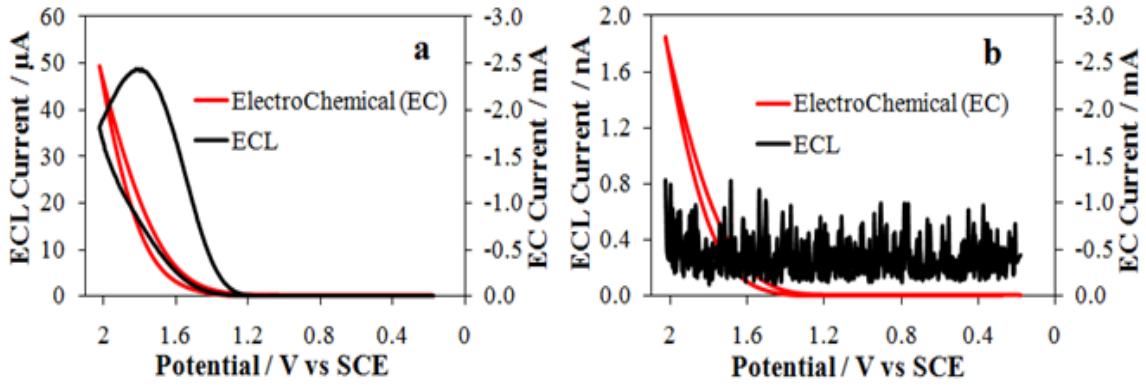

Figure 3.18. ECL coupled with Cyclic Voltammogram (ElectroChemical) of 1**a** film on FTO in PBS buffer with 20 µL TPrA (a) and bare FTO in PBS buffer with 20 µL TPrA (b).

Figure 3.19 shows the ECL spectrum generated from **1a** film, as a comparison, ECL spectrum of **1a** in solution was also shown in Figure 3.19. The thickness of the film measured using profiler is 100-900 nm. From Figure 3.19a, it can be seen that strong ECL was generated from 1a film with maximum emission at 642 nm. Figure 3.19b is the normalized ECL spectra of **1a** film and solution, which indicates that ECL generated from film was red shifted comparing with ECL generated from solution. Around 10 nm red shift in ECL spectrum was observed for **1a** film comparing with **1a** in solution.

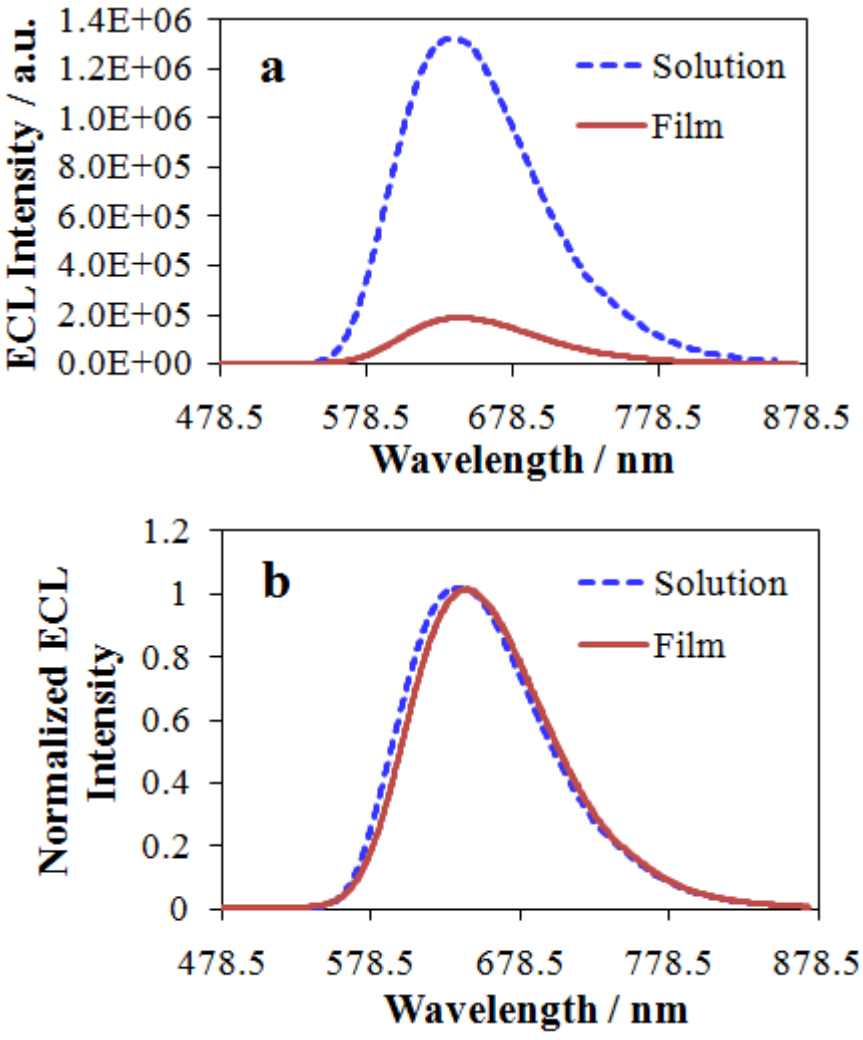

Figure 3.19. ECL spectra (a) and Normalized ECL spectra (b) of 0.5 mM **1a** in 0.1 M $TBAPF_6$ in dichloromethane.

Obtained by pulsing between 80 mV past the reduction peak potential and 80 mV past the first oxidation peak potential (solution) and 1**a** film on FTO in 8 ml PBS buffer with 20 μL TPrA as coreactant. ECL of 1a in film was generated by scanning from 0V to 2 V vs SCE with a scan rate of 0.5 V/s for 20 cycles.

In order to understand the red shifted nature of ECL spectra, absorbance of the film was measured and the results were shown in Figure 3.20. From the normalized absorption spectra in Figure 3.20b that the absorbance of the film was also red shifted comparing with the absorbance of **1a** in solution. A red shift was also observed in fluorescence with maximum emission of 1a film occurring at 624 nm[1] (maximum emission of 1a film occurring at 612 nm). The red shift in ECL spectrum of film is consistent with the red shift in absorbance and fluorescence. Since the ECL, absorbance and fluorescence of the film and solution were measured using the same instrument, the instrument factor cannot account for the red shift. The red-shift of the absorption, emission upon going from solution to film may be attributed to the loss of conformational freedom with the consequent lowering of the energy gap between the HOMO and LUMO orbitals, resulting in a red shift of the absorption and fluorescence spectra.[30, 31]

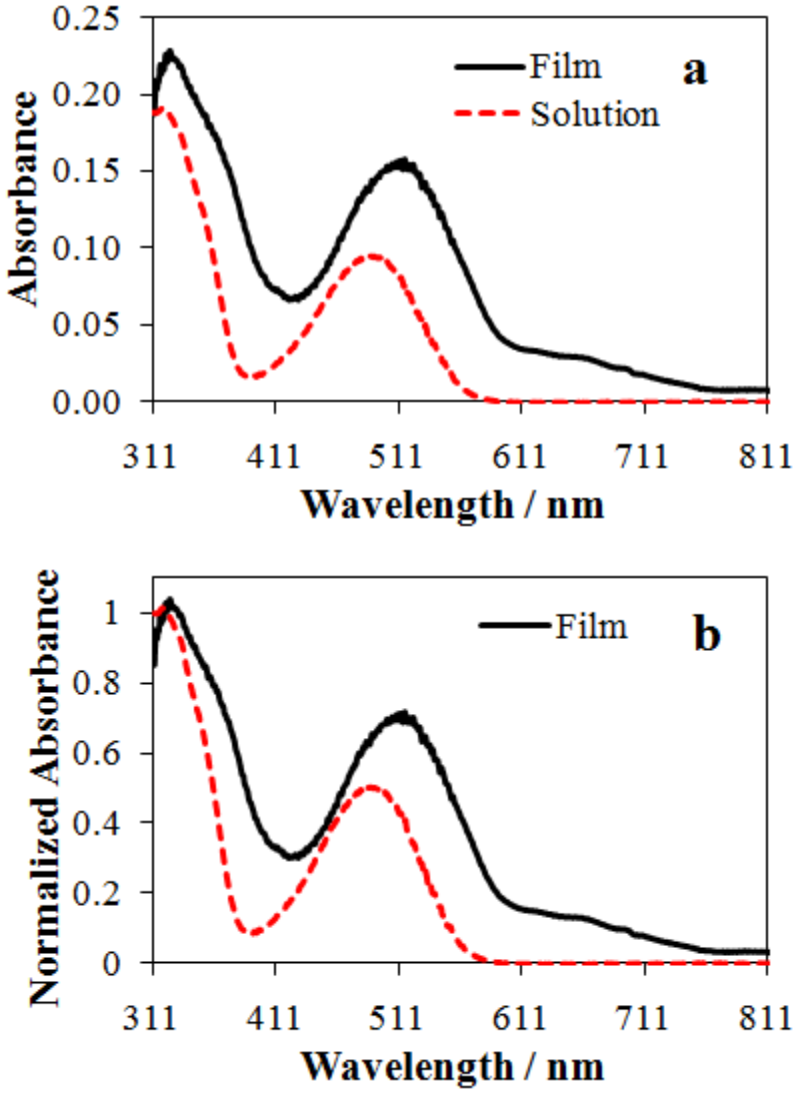

Figure 3.20. Absorbance (a) and Normalized absorbance (b) of 7 μM **1a** in dichloromethane and **1a** film.

3.7 STUDY IN BENZENE AND ACETONITRILE MIXTURE.

CV of **1a** was also studied in a different solvent, a mixture of benzene (PhH) and acetonitrile (MeCN). Figure 3.21 shows the CV result in a 2.33:1 MeCN/PhH. It can be

(A)

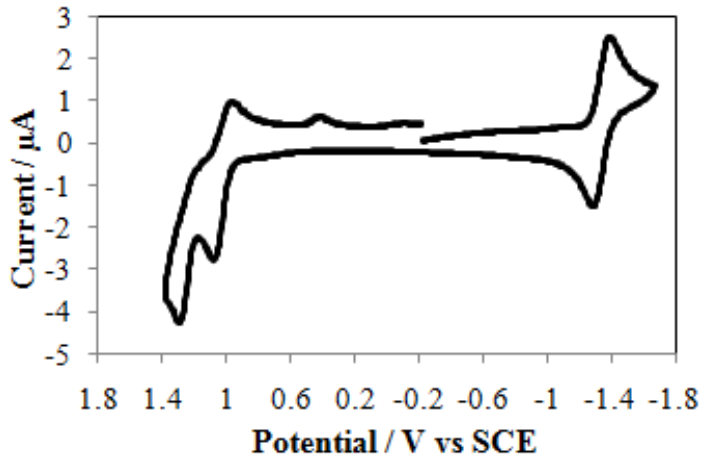

(B)

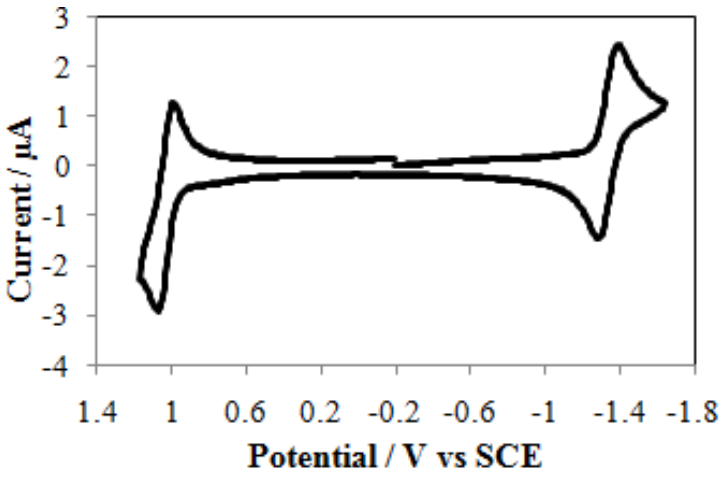

Figure 3.21. Cyclic voltammogram of 0.5 mM **1a** in 2.33:1MeCN/PhH (volume ratio) with 0.1 M $TBAPF_6$.

seen from Figure 3.21 (A) that second oxidation peak is not reversible in 2.33:1 MeCN/PhH mixture and a new peak between 0.2 V and 0.6 V was observed, which could be from the product of the second oxidation peak. This was confirmed by the result in Figure 3.21 (B) that when the scan stops by the first oxidation peak, the peak between 0.2 V and 0.6 V disappears. And the first oxidation peak in 2.33:1 MeCN/PhH is reversible.

Table 3.5 and 3.6 shows $E_{1/2}$ caculated at different scan rates for the reduction and first oxidation respectively. It can be seen that the $E_{1/2}$ almost the same under different scan rates.

Table 3.5 Forward peak potential $\mathbf{E_{pf}}$, reverse peak potential $\mathbf{E_{pb}}$ and $\mathbf{E_{1/2}}$ **/ V** vs Ag wire for reduction of **1a** in 2.33:1MeCN/PhH.

Scan Rate (V/s)	E_{pf} / V	E_{pb} / V	E_{pb} - E_{pf} / V	$E_{1/2}$ / V vs Ag wire
0.02	-1.11	-1.03	0.08	-1.07
0.05	-1.12	-1.02	0.10	-1.07
0.08	-1.12	-1.02	0.10	-1.07
0.1	-1.12	-1.01	0.11	-1.06
0.3	-1.15	-1.00	0.15	-1.07
0.5	-1.16	-0.99	0.17	-1.07
0.75	-1.17	-0.98	0.19	-1.07
1	-1.18	-0.98	0.2	-1.08

Table 3.6 Forward peak potential $\mathbf{E_{pf}}$, reverse peak potential $\mathbf{E_{pb}}$ and $\mathbf{E_{1/2}}$ **/ V** vs Ag wire for first oxidation of **1a** in 2.33:1MeCN/PhH.

Scan Rate (V/s)	E_{pf} / V	E_{pb} / V	E_{pb} - E_{pf} / V	E_0 / V vs Ag wire
0.02	1.29	1.21	0.08	1.25
0.05	1.29	1.21	0.08	1.25
0.08	1.29	1.20	0.09	1.24
0.1	1.30	1.20	0.10	1.25
0.3	1.32	1.19	0.13	1.25
0.5	1.32	1.19	0.13	1.25
0.75	1.33	1.18	0.15	1.25
1	1.34	1.18	0.16	1.26

Table 3.7 and 3.8 shows the peak current with background subtraction for 1a reduction and oxidation, respectively.

Figure 3.22 and 3.23 shows the peak current versus square root of scan rate for reduction and oxidation, respectively. From both figures, it can be seen that reduction current and oxidation current change linearly with square root of scan rate, indicating diffusion control of both reduction and oxidation for 1a in 1.7ml MeCN/0.6 ml PhH.

Table 3.7 Reduction peak currents for 0.435 mM **1a** in 1.7ml MeCN + 0.6 ml PhH with 0.1 M $TBAPF_6$ at different scan rates.

Scan Rate (V/s)	Scan Rate$^{1/2}$ $(V/s)^{1/2}$	$i_{peak,read}$ / A	$i_{background}$ at Ep / A	$i_{peak,read}$ - $i_{background}$ / A
0.02	0.1414	1.07E-06	6.51E-08	1.00E-06
0.05	0.2236	1.61E-06	8.56E-08	1.52E-06
0.08	0.2828	2.04E-06	1.21E-07	1.92E-06
0.1	0.3162	2.18E-06	2.32E-07	1.95E-06
0.3	0.5477	3.61E-06	3.24E-07	3.29E-06
0.5	0.7071	4.79E-06	4.42E-07	4.34E-06
0.75	0.8660	5.58E-06	6.01E-07	4.98E-06
1	1	6.33E-06	7.81E-07	5.55E-06

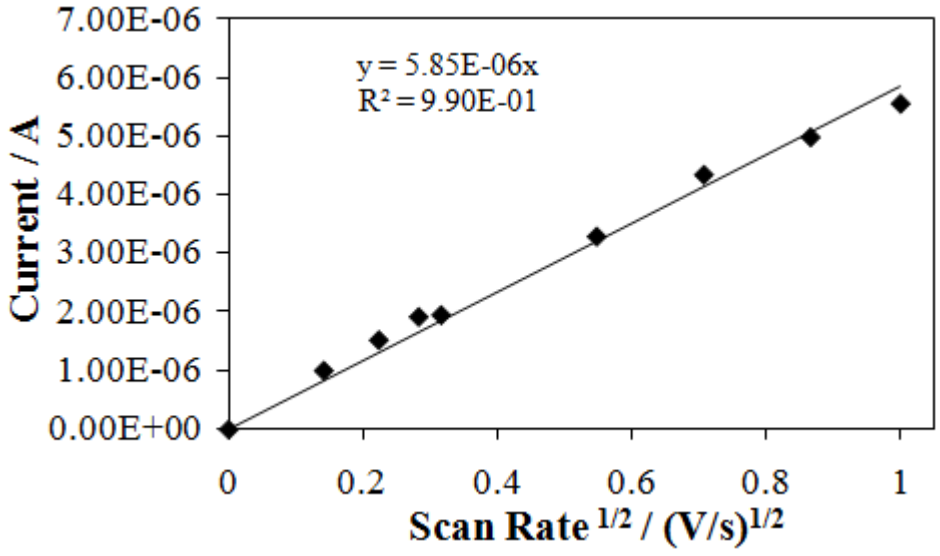

Figure 3.22. Reduction peak current versus square root of scan rate.

Table 3.8 First oxidation peak currents at different scan rates for 0.435 mM **1a** in 1.7ml MeCN + 0.6 ml PhH with 0.1 M $TBAPF_6$.

Scan Rate (V/s)	Scan Rate$^{1/2}$ (V/s)$^{1/2}$	$i_{peak,read}$ / A	$i_{background}$ at Ep / A	$i_{peak,read}$ - $i_{background}$ / A
0.02	0.1414	-1.21E-06	-1.41E-07	-1.06E-06
0.05	0.2236	-1.81E-06	-2.54E-07	-1.55E-06
0.08	0.2828	-2.26E-06	-3.82E-07	-1.88E-06
0.1	0.3162	-2.55E-06	-6.22E-07	-1.93E-06
0.3	0.5477	-4.20E-06	-1.16E-06	-3.03E-06
0.5	0.7071	-5.60E-06	-1.43E-06	-4.17E-06
0.75	0.8660	-6.68E-06	-1.94E-06	-4.74E-06
1	1	-7.68E-06	-2.24E-06	-5.44E-06

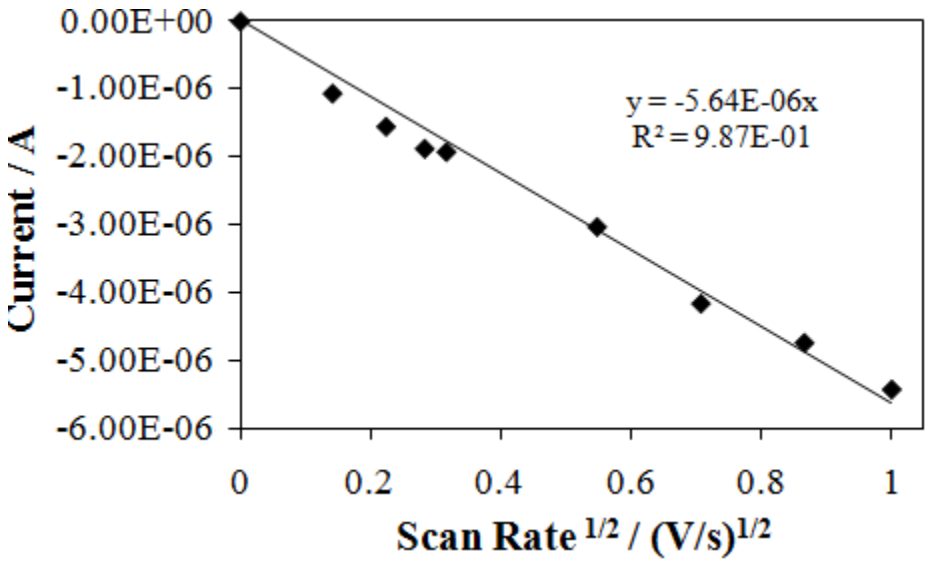

Figure 3.23. Reduction peak current versus square root of scan rate.

Absorbance of **1a** was studied in 2.33:1 MeCN/PhH. Figure 3.24 (A) shows absorbance of **1a** with different concentration and Figure 3.24 (B) is plot of absorbance versus concentration.

(A)

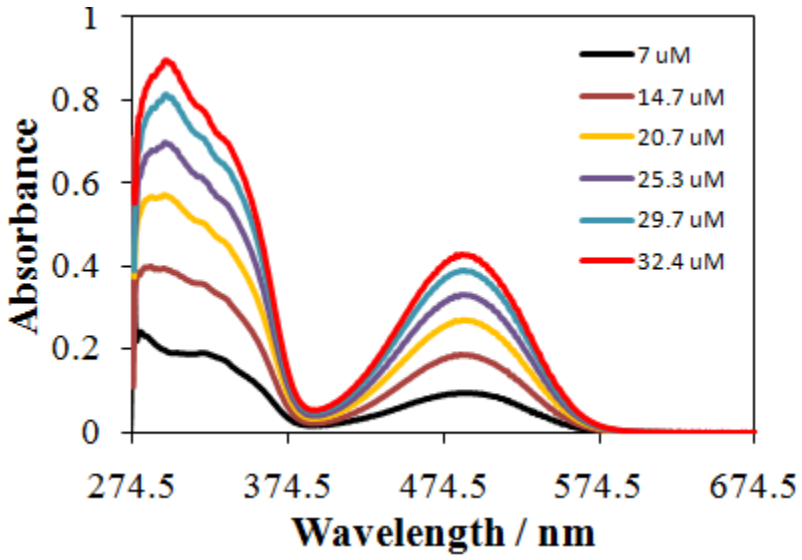

(B)

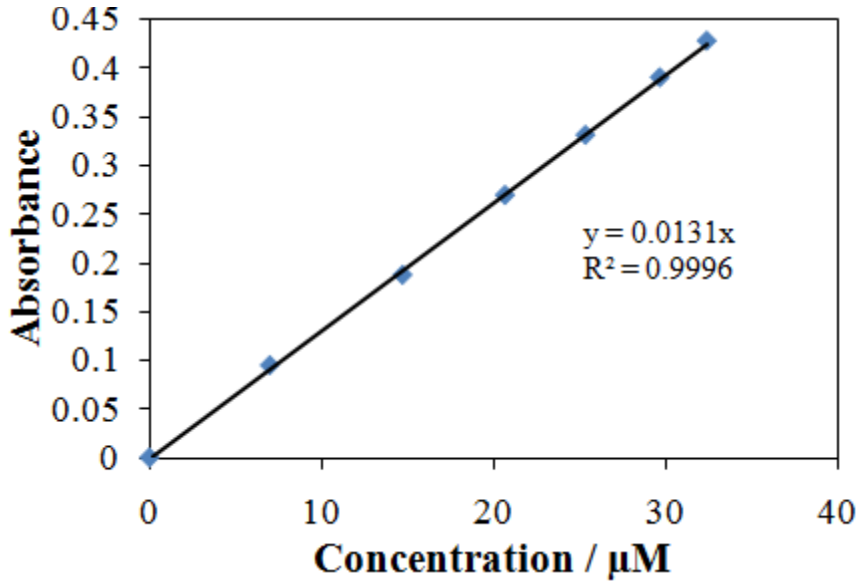

Figure 3.24. (A) Absorbance of different concentration of **1a** in 2.33:1 MeCN/PhH. (B) Absorbance versus concentration of **1a**.

From figure 3.24 (B), molar absorptivity of **1a** at 485 nm is calculated to be 13100 M^{-1} cm^{-1}.

Uncompensated resistance can be calculated from a potential step in a background solution. Figure 3.25 (A) shows the current-time curve in a background solution (2.33:1 MeCN/PhH with 0.1 M $TBAPF_6$) with a step a potential of –0.05 V. And figure 3.25 (B) is the plot of (Ln current) versus time. And the calculated uncompensated resistance from figure 3.25 is 1411 Ω. While the automatic calculated resistance from the instrument are R= 1356 (at 0 V), 1351 (at 0.4V), 1334 (at 1 V).

(A)

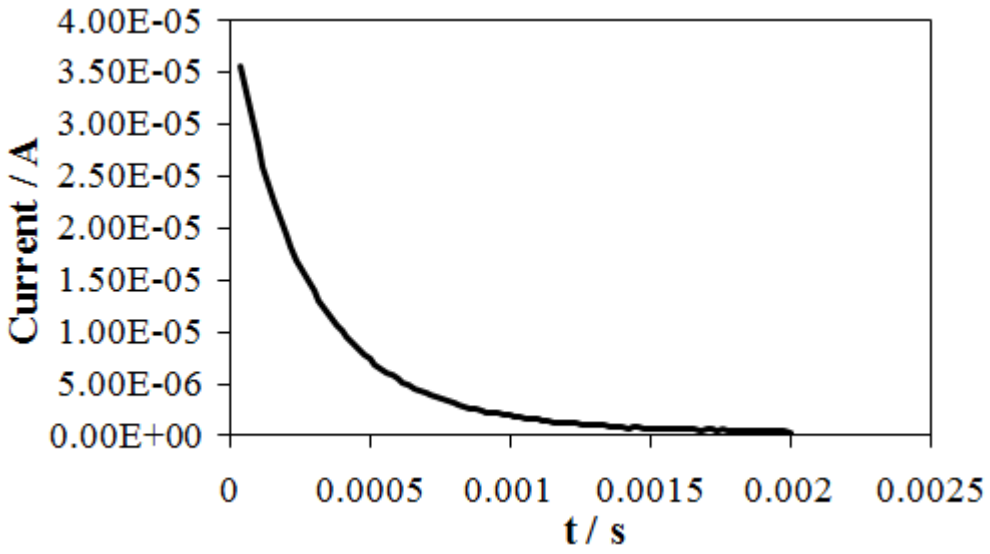

(B)

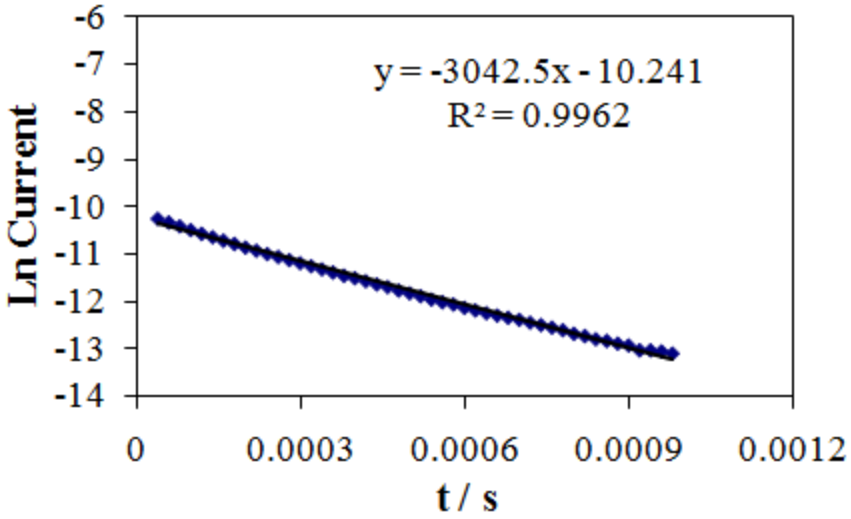

Figure 3.25. (A) Current versus time for background solution (2.33:1 MeCN/PhH with 0.1 M $TBAPF_6$) with a step a potential of –0.05 V. (B) plot of ln (current) versus time.

CV of **1b** was also studied in a different solvent, a mixture of benzene (PhH) and acetonitrile (MeCN). Figure 3.26 shows the CV result in a 2.33:1 MeCN/PhH. It can be seen from Figure 3.26 (A) that second oxidation peak is not reversible in 2.33:1 MeCN/PhH mixture and a new peak between -0.1 V and 0.7V was observed, which could be from the product of the second oxidation peak. This was confirmed by the result in Figure 3.26 (B) that when scan stop by the first oxidation peak, the peak between -0.1 V and 0.7V disappears.

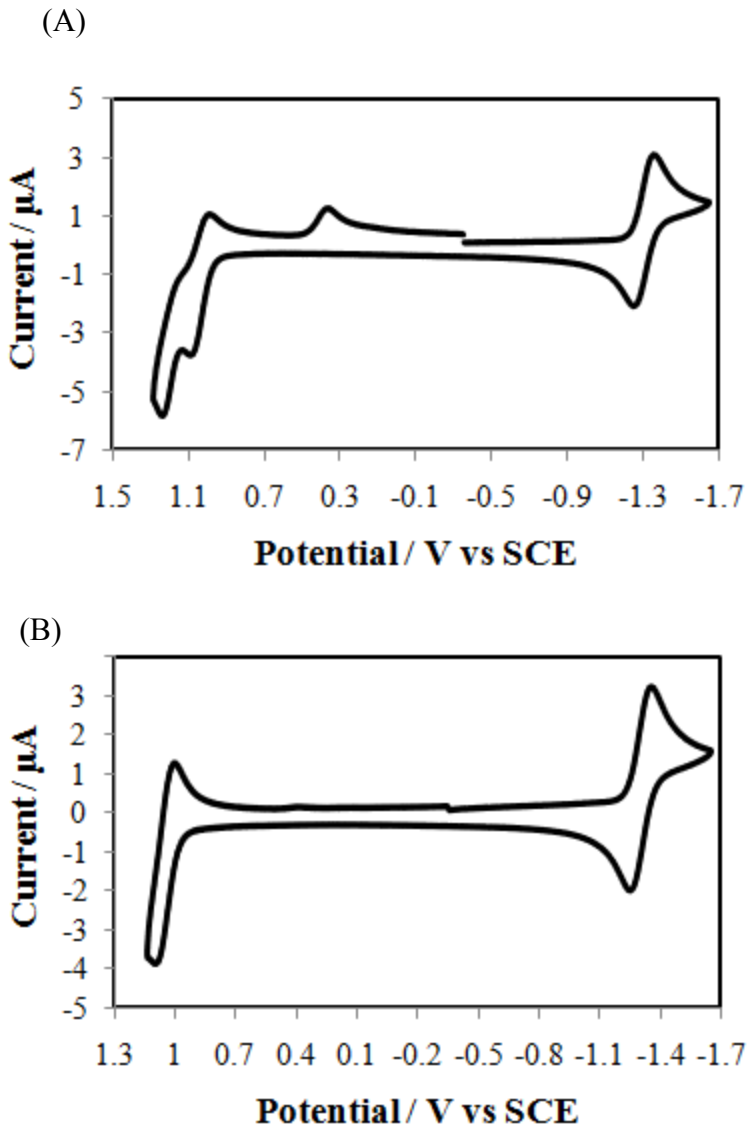

Figure 3.26. Cyclic voltammogram of 0.5 mM **1b** in 2.33:1MeCN/PhH (volume ratio) with 0.1 M $TBAPF_6$.

ECL coupled with CV for **1b** in 2.33:1 MeCN/PhH mixture was shown in Figure 3.27. And maximum ECL intensity of **1a** and **1b** was compared with DPA and the results were shown in Table 3.9.

(A)

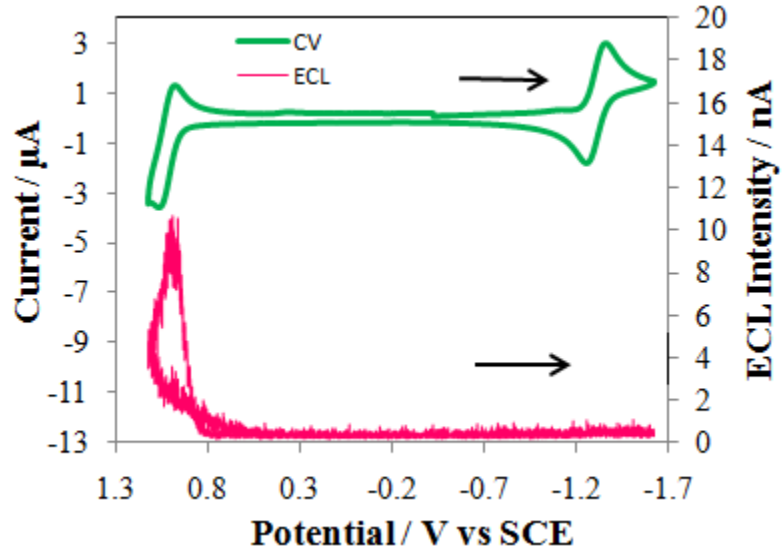

(B)

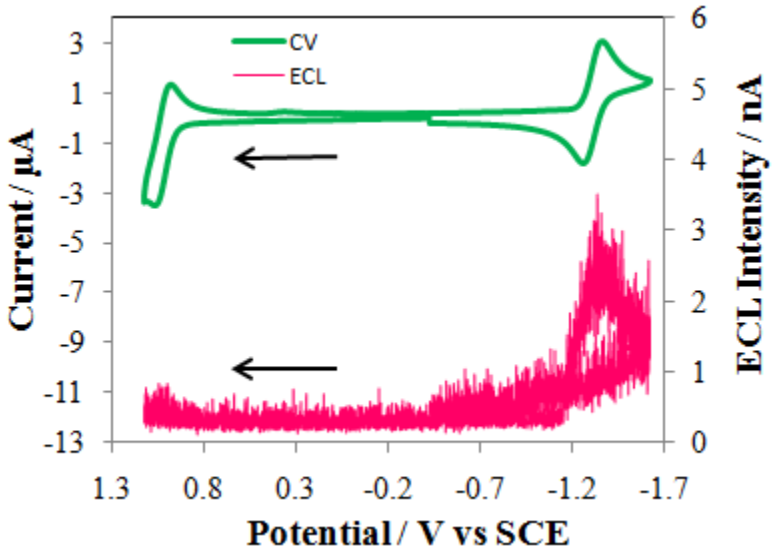

Figure 3.27. ECL coupled with cyclic voltammogram of 0.5 mM **1b** in 2.33:1MeCN/PhH with 0.1 M $TBAPF_6$ with scan rate 0.1 V/s (A) Initial scan direction: negative. (B)Initial scan direction: positive.

Table 3.9 Maximum ECL Emission Intensity of **1a** and **1b**, and Relative Intensity with respect to DPA with different integration time shown in the Table. Slit width: 0.5 mm. ECL of **1a/1b** were generated by pulsing between 80mV pass reduction and first oxidation peak potential.

Time /s	DPA	1a	1a/DPA	1b	1b/DPA
18 s	4.2×10^5	1.5×10^5	37%	2.3×10^5	55%
6s	1.2×10^5	6.1×10^4	49%	8.4×10^4	68%
3s	6.1×10^4	2.9×10^4	48%	4.5×10^4	75%

3.8 CONCLUSIONS

We have studied the electrochemistry and ECL of a red highly fluorescent molecular dye, **1b**, and presented the digital simulation of transient ECL. The cyclic voltammetry (CV) with scan rate ranging from 0.05 V/s to 0.75 V/s of **1b** in DCM shows a single one electron-reduction wave (E^o_{red} = −1.18 V vs SCE) and two nernstian one-electron oxidation waves ($E^o_{1,\ ox}$ = 1.01 V, $E^o_{2,\ ox}$ = 1.24 V vs SCE). Reduction of the unsubstituted 2,1,3-benzothiadiazole center shows nernstian behavior with E^o_{red} = −1.56 V vs SCE. By comparison to a digital simulation, the heterogeneous electron transfer rate constant for reduction, $k_r^o = 1.5 \times 10^{-3}$ cm/s is significantly smaller than those for the oxidations, $k_o^o > 0.1$ cm/s, possibly indicating that the two substituted end groups have a blocking effect on the reduction of the benzothiadiazole center. Electron transfer to a buried acceptor site is slower than oxidation of the more accessible donor sites in the same molecule.

1b can produce strong ECL without a coreactant. The ECL spectrum, produced by electron transfer annihilation of the reduced and oxidized forms, consists of a single peak

with maximum emission at about 635 nm, consistent with the fluorescence of the parent molecule. The ECL intensity of **1b** is higher than the well-known ECL emitter DPA. Relative ECL intensities of **1b** with respect to 9,10-diphenylanthracene (DPA) are 330% and 470% for the radical anion-cation and radical anion-dication annihilation respectively. ECL generated by anion-dication annihilation is stronger than that of anion-cation annihilation. The energies of both of the annihilation reactions are sufficiently high that direct generation of the singlet excited state, with the corresponding ECL emission, is probable.

Transient ECL of **1b** was studied, and transient ECL responses corresponding to anodic and cathodic pulses have equal height and are stable with increasing pulses. Radical anion, cation, dications of **1b** were stable. Transient ECL was successfully simulated using a finite element package. Radical anion ($A^{-\cdot}$)-cation ($A^{+\cdot}$) annihilation produced by potential steps shows symmetric ECL transients during anodic and cathodic pulses while for anion ($A^{-\cdot}$)-dication ($A^{2+\cdot}$) annihilation, transient ECL shows asymmetry in which the anodic pulse is narrower than the cathodic pulse. Digital simulation of the transient ECL experiments showed that the origin of the observed asymmetry is asymmetry in the amount of generated charges rather than instability of the electrogenerated species.

We also studied the electrochemistry and ECL of another red highly fluorescent molecular dye **1a** in dichloromethane (DCM) solution and **1a** film on FTO in PBS buffer solution. A film of **1a** with thickness of 100-900 nm was prepared by drop casting **1a** in DCM on Fluorine-doped Tin Oxide (FTO). The cyclic voltammetry (CV) of **1a** with scan rate ranging from 0.05 V/s to 1 V/s shows a single one-electron reduction wave (E^{o}_{red} = –1.18 V vs SCE) and two nernstian one-electron oxidation waves ($E^{o}_{1,ox}$ = 1.01 V, $E^{o}_{2,ox}$ = 1.24 V vs SCE). By comparison to a digital simulation, the heterogeneous electron

transfer rate constant for reduction, k_r^o = 0.6 × 10^{-3} cm/s is significantly smaller than those for the oxidations, k_o^o = 0.02 cm/s, possibly indicating that the two substituted end groups have a blocking effect on the reduction of the benzothiadiazole center.

1a in solution can produce strong ECL without a coreactant. **1a** film can produce strong ECL in PBS buffer with TPrA as coreactant. ECL generated by anion-dication annihilation is stronger than ECL generated by anion-cation annihilation. The ECL spectrum of **1a** in solution, produced by electron transfer annihilation of the reduced and oxidized forms, consists of a single peak with maximum emission at about 632 nm, consistent with the fluorescence of the parent molecule. While the ECL spectrum of **1a** film produced by reaction with coreactant TPrA consists of a single peak with maximum emission at 642 nm. Around 10 nm red shift in ECL spectrum was observed for **1a** film comparing with **1a** in solution. Absorbance, fluorescence spectra of **1a** film were also red shifted comparing with that of **1a** in solution. Similar amount of red shift was also observed in fluorescence spectrum. Radical anion, cation, dications of the dye were stable. The energies of both of the annihilation reactions are sufficiently high that direct generation of the singlet excited state, with the corresponding ECL emission, is probable. ECL produced from film of **1a** in PBS buffer solution could have possible application in biosensing.

Electrochemistry of **1a** and **1b** in PhH/MeCN mixture shows different behavior as in DCM. The second oxidation **1a** and **1b** in PhH/MeCN mixture is not reversible and the ECL efficiency is lower. This indicates the importance of selecting solvent for electrochemical study.

3.8 REFERENCES

[1] Huang, J.; Liu, Q.; Zou, J.-H.; Zhu, X.-H.; Li, A.-Y.; Li, J.-W.; Wu, S.; Peng, J. B.; Cao, Y.; Xia, R. D.; Bradley, D. D. C.; Roncali, J. *Adv. Funct. Mater.* **2009**, *19*, 2978–2986.

[2] Forster, R. J.; Bertoncello, P.; Keyes, T. E. *Annu. Rev. Anal. Chem.* **2009**, *2*, 359–385.

[3] Bard, A. J. in *Electrogenerated Chemiluminescence*; Bard, A. J., Ed.; Marcel Dekker: New York, 2004.

[4] For reviews on ECL, see: (a)Ref 2. (b) Richter, M. M. *Chem. Rev*. **2004**, *104*, 3003-3036. (c) Knight, A. W.; Greenway, G. M. *Analyst* **1994**, *119*, 879-890. (d) Faulkner, L. R.; Bard, A. J. *Electroanalytical Chemistry*; Marcel Dekker: New York, 1977; Vol. 10, p 1. (e) Bard, A. J.; Debad, J. D.; Leland, J. K.; Sigal, G. B.; Wilbur, J. L.; Wohlstadter, J. N. in *Encyclopedia of Analytical Chemistry: Applications, Theory and Instrumentaion*; Meyers, R. A., Ed.; John Wiley & Sons: New York, 2000; Vol. 11, p 9842.

[5] Maloy, J. T. in *Electrogenerated Chemiluminescence*; Bard, A. J., Ed.; Marcel Dekker: New York, 2004; p 159.

[6] Keszthelyi, C. P.; Tokel-Takvoryan, N. E.; Bard, A. J. *Anal. Chem*. **1975**, *47*, 249-256.

[7] Richter, M. M. in *Electrogenerated Chemiluminescence*; Bard, A. J., Ed.; Marcel Dekker: New York, 2004; p 306.

[8] Tokel, N.; Bard, A. J. *J. Am. Chem. Soc.* **1972**, *94*, 2862-2863.

[9] Juris, A.; Balzani, V.; Barigelletti, F.; Campagna, S.; Belser, P.; Von Zelewsky, A. *Coord. Chem. Rev.* **1988**, *84*, 85-277.

[10] Kapturkiewicz, A.; Grabowski, Z. R.; Jasny, J. *J. Electroanal. Chem.* **1990**, *279*, 55-65.

[11] Kapturkiewicz, A.; Herbich, J.; Nowacki, J. *Chem. Phys. Lett.* **1997**, *275*, 355-362.

[12] Lai, R.Y.; Fabrizio, E. F.; Lu, L.; Jenekhe, S. A.; Bard, A. J. *J. Am. Chem. Soc.* **2001**, *123*, 9112-9118.

[13] Lai, R.Y.; Kong, X. X.; Jenekhe, S. A.; Bard, A. J. *J. Am. Chem.Soc.* **2003**, *125*, 12631–12639.

[14] Omer, K. M.; Ku, S.-Y.; Wong, K.-T.; Bard, A. J. *Angew. Chem. Int. Ed.* **2009**, *48*, 9300-9303.

[15] Sartin, M. M.; Zhang, H. Y.; Zhang, J. Y.; Zhang, P.; Tian, W. J.; Wang, Y.; Bard, A. J. *J. Phys. Chem. C* **2007**, *111*, 16345-16350.

[16] Cardona, C. M.; Mendoza, S.; Kaifer, A. E. *Chem. Soc. Rev.*, **2000**, *29*, 37-42.

[17] Cruser, S. A.; Bard, A. J. *J. Am. Chem. Soc.* **1969**, *91*, 267-275.

[18] Forster, R. J.; Bertoncello, P.; Keyes, T. E. *Annu. Rev. Anal. Chem.* **2009**, *2*, 359-385.

[19] Sartin, M. M.; Shu, C. F.; Bard, A. J. *J. Am. Chem. Soc*. **2008**, *130*, 5354-5360.

[20] Shen, M.; Rodríguez-López, J.; Lee, Y.-T.; Chen, C.-T.; Fan, F.-R. F.; Bard, A. J. *J. Phys. Chem. C* **2010,** *114*, 9772–9780.

[21] Fungo, F.; Wong, K.-T.; Ku, S.-Y.; Hung, Y.-Y.; Bard, A. J. *J. Phys. Chem. B* **2005**, *109*, 3984–3989.

[22] Omer, K. M.; Ku, S.-Y.; Wong, K.-T.; Bard, A. J. *J. Am. Chem. Soc*. **2009**, *131*, 10733-10741.

[23] Kojima, H.; Bard, A. J. *J. Am. Chem. Soc.* **1975**, *97*, 6317-6324.

[24] Bezman, R.; Faulkner, L. R. *J. Am. Chem. Soc.* **1972**, *94*, 3699-3707.

[25] Feldberg, S. W. *J. Am. Chem. Soc*. **1966**, *88*, 390-393.

[26] Ref. 3. Chapter 6 (Forry, S. P.; Wightman, R. M.) and Chapter 7 (Richter, M. M.).

[27] Ref. 3. Chapter 3 (Maloy, J. T.).

[28] Feldberg S. W. *J. Elecroanal. Chem.* **1981**, *127*, 1-10.

[29] Lakowicz, J. R. *Principles of Fluorescence Spectroscopy*, 3rd ed; Springer Science + Business Media: New York, 2006.

[30] Seixas de Melo, J.; Pina, J.; Burrows, H. D.; Di Paolo, R. E.; Maçanita, A. L. *Chem. Phys*. **2006**, *330*, 449–456.

[31] Narwark, O.; Meskers, S.C.J.; Peetz, R.; Thorn-Csányi, E.; Bässler, H. Chem. Phys. **2003**, *294*, 1–15.

Chapter 4. In-situ Electroreductive Synthesis of Carbon Quantum Dots from HOPG and Its Electrochemistry and Electrogenerated Chemiluminescence

4.1 INTRODUCTION

Carbon quantum dots (QDs) and graphene-based nanomaterials have been drawing more and more attention due to their potential applications in energy conversion/storage, bio-labeling/imaging, drug delivery, sensors, diagnostics and composites.[1, 2] Compared with traditional QDs, carbon QDs have the advantages of low toxicity and biocompatibility and are chemically inert.

Many methods have been used to prepare carbon QDs as well as graphene QDs, including arc discharge,[3] laser ablation,[4, 5, 6] supported syntheses,[7, 8] microwave,[9] combustion/thermal decomposition,[10, 11, 12, 13] hydrothermal cutting of graphene sheets,[14] electrooxidation of graphite,[15, 16, 17] electro-redox of multiwalled carbon nanotubes (MWCNTs)[18], oxygen plasma treatment[19] and solution chemistry (bottom-up approaches)[20, 21]. However, all of these methods involved either the oxidation of a carbon source or were done in the atmosphere in the presence of oxygen. Developing better synthetic routes and more detailed fundamental studies of their properties are needed.[1]

The annihilation ECL process for generation of an excited singlet state (S-route) occurs through electron transfer between electrochemically generated species followed by the emission of light. ECL can also be generated by adding a coreactant, when one of the generated radical species is unstable or cannot be generated within the solvent electrochemical window. [22, 23] ECL of carbon QDs or graphene QDs has been generated

through the coreactant route.[17, 24, 25] No one has reported ECL generated through the annihilation route. Electrochemistry (e.g., cyclic voltammograms) of carbon particles in aqueous solution has been reported.[13] Electrochemical studies of carbon/graphene particles in nonaqueous solvent and under inert atmosphere has not been reported and was crucial to understanding the properties of these materials due to broader solvent electrochemical window and zero interference from oxygen and water.

In the present work, we prepared the carbon QDs through the electro-reduction of highly oriented pyrolytic graphite (HOPG) and the whole process was carried out in the absence of oxygen and water. We report here the electrochemistry and ECL of the *in situ* prepared QDs in a nonaqueous solvent under an inert atmosphere. Under such conditions, the ECL results from the annihilation reactions between the radical anions and radical cations generated during electrochemical reduction and oxidation.

4.2 EXPERIMENTAL

Materials. Anhydrous dichloromethane (CH_2Cl_2 or DCM) was obtained from Aldrich (St. Louis, MO) and transferred directly into a helium atmosphere dry box (Vacuum Atmospheres Corp., Hawthorne, CA) without further purification. Electrochemical grade tetra-*n*-butylammonium hexafluorophosphate ($TBAPF_6$) was obtained from Fluka and used as received. HOPG was generously supplied by Arthur W. Moore of Union Carbide Corporation (Parma, OH).

Preparation of Carbon QDs. The electrochemical preparation of carbon QDs was performed in a dichloromethane solution in a helium dry box using 0.1 M $TBAPF_6$ as the supporting electrolyte. HOPG was peeled with scotch tape to reveal the fresh surface

before use. The three-compartment airtight electrochemical cell consisted of the HOPG working electrode, a Pt mesh counter electrode and an Ag wire quasi reference electrode (AgQRE). The Pt mesh counter electrode was separated from the other compartments in the electrochemical cell by a fine glass frit. A negative potential of -1.8 V vs AgQRE was applied to the HOPG electrode for 25 hours. The color of the electrolyte solution gradually changed from colorless to light yellow, which emitted blue luminescence upon irradiation with an UV lamp. The carbon particles retained fluorescence after thoroughly drying, indicating that the fluorescence does not result from an interaction with solvent and is not specific for solvated carbon.[26]

Characterization. The same electrochemical cell was used for both cyclic voltammetry and ECL experiments: it consisted of a coiled Pt wire (0.5 mm in diameter) counter electrode, an Ag QRE (0.5 mm in diameter), and an inlaid Pt disk in glass bent at 90^{o} angle (for the disk to face the light detector) as a working electrode. The geometric area of the Pt disk electrode was 0.028 cm^2. Before each experiment, the working electrode was polished on a felt pad with 0.3 μm alumina (Buehler, Ltd., Lake Bluff, IL), sonicated in Milli-Q deionized water and then in ethanol. The counter and reference electrodes were cleaned by rinsing and sonicating in acetone, water and ethanol. Finally, all the electrodes were rinsed with acetone, dried in the oven and transferred into the glove box.

For measurements made outside of the box, the electrochemical cell was closed with a Teflon cap that had a rubber O-ring to form an airtight seal. Stainless steel rods driven through the cap formed the electrode connections. Cyclic voltammograms (CVs) were obtained on a CH Instruments electrochemical workstation (CHI 660, Austin, TX).

Spectroscopic measurements were done in a 1 cm path length quartz cell. Absorbance spectra were obtained with a Milton Roy Spectronic 3000 diode array

spectrophotometer. Fluorescence spectra were collected on a QuantaMaster spectrofluorimeter (Photon Technology International, Birmingham, NJ). The excitation source was a 70 W xenon lamp (LPS-220B Lamp power supply), and the excitation and emission slits were set at 0.5 mm (2 nm bandwidth).

The ECL spectra were obtained on a Princeton SPEC-10 Instruments using a charge-coupled device (CCD) camera (Trenton, NJ) cooled to -100 ^{o}C, coupled with an Acton SpectraPro-150 monochromator (Acton, MA) as the detector. The wavelength scale of the CCD camera and grating system were calibrated using an Hg/Ar pen-ray lamp from Oriel (Stratford, CT). ECL intensity-time curves were collected on an Autolab potentiostat (Ecochemie, Netherlands) connected to a photomultiplier tube (PMT, Hamamatsu, R4220p, Japan). The PMT was powered at -750 V with a Kepco (New York) high voltage power supply.

The prepared carbon QD solution was purified by evaporating the original solvent (DCM), then adding ethanol, shaking and using argon to evaporate some of the ethanol. Crystallization of supporting electrolyte occurred during solvent evaporation; centrifugation (VWR Galaxy 16D) at 14000 RPM was then used to remove the supporting electrolyte. The same procedure was repeated several times until no supporting electrolyte crystals were detected by TEM (coupled with EDS). The TEM image before the separation of the supporting electrolyte is shown in Figure 4.1(using a Hitachi S-5500 SEM equipped with STEM), in which crystals of supporting electrolyte were observed. The TEM of the nanoparticles after the separation of supporting electrolyte was shown in Figure 4.5.

After separating the supporting electrolyte and evaporating all of the ethanol, the remaining solid was dissolved in THF for mass spectroscopy measurement. Solvent extraction methods were used to prepare the sample for FT-IR, TEM and Raman

measurements: DCM from the prepared carbon QDs solution was first evaporated and acetonitrile was then added; then hexane was added to extract the carbon QDs. Since the prepared carbon QDs are not soluble in water, we cannot dissolve the carbon QDs solution in water and use dialysis to get rid of the supporting electrolyte as reported previously.[18]

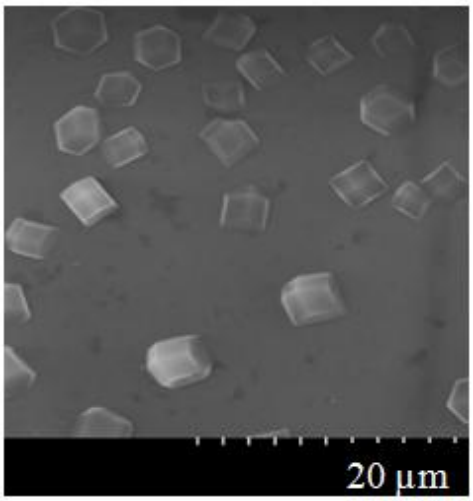

Figure 4.1. TEM image before separation of supporting electrolyte.

Raman spectra were acquired using a Renishaw inVia Microscope using a 514.5 nm argon laser. TEM images were obtained using a FEI Tecnai Transmission Electron Microscope and HR-TEM images were obtained using a JEOL 2010F transmission electron microscope (JEOL Ltd.). The TEM grids were carbon films supported on 200 mesh copper (Electron Microscope Sciences). The TEM sample was prepared by holding the TEM grid to touch a µL droplet from a micropipette. The FT-IR spectrum was recorded with a Fourier transform infrared spectrometer (Thermo Mattson Infinity Gold FTIR) using attenuated total reflectance (ATR) mode. The optical dense crystal used is

ZnSe crystal. Carbon NPs in hexane was dropped cast directly on the ZnSe crystal, then the FT-IR spectrum was measured after hexane evaporated. Low-resolution desorption chemical ionization (CI) mass spectra were obtained with an Agilent 6130 Quadrupole LC/MS spectrometer. High-resolution mass spectra were recorded with a Varian 9.4T HiRes ESI-QFT ion cyclotron resonance mass spectrometer. After separation of supporting electrolyte, the carbon QDs solution retained its fluorescence and emitted blue luminescence upon irradiation with an UV lamp. The absorbance and fluorescence emission spectra after separation of supporting electrolyte are shown in Figure 4.2. The comparison of the fluorescence emission spectra before and after separation of the supporting electrolyte was shown in Figure 4.3. It can be seen from Figure 4.3 that the feature of the fluorescence emission spectra maintained after the separation of the supporting electrolyte.

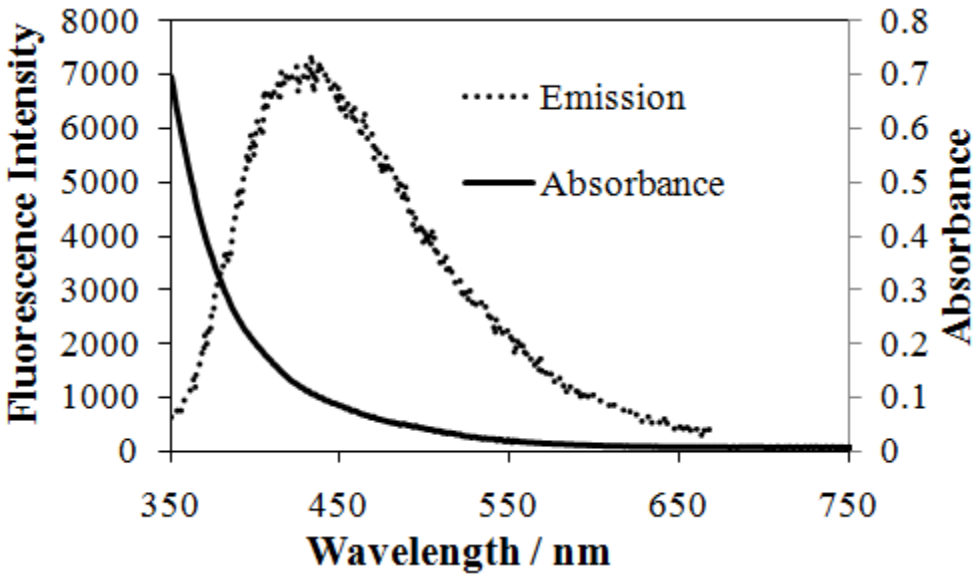

Figure 4.2. Absorbance and fluorescence emission spectra of carbon QDs solution in THF after separation of supporting electrolyte. (Excitation wavelength: 340 nm).

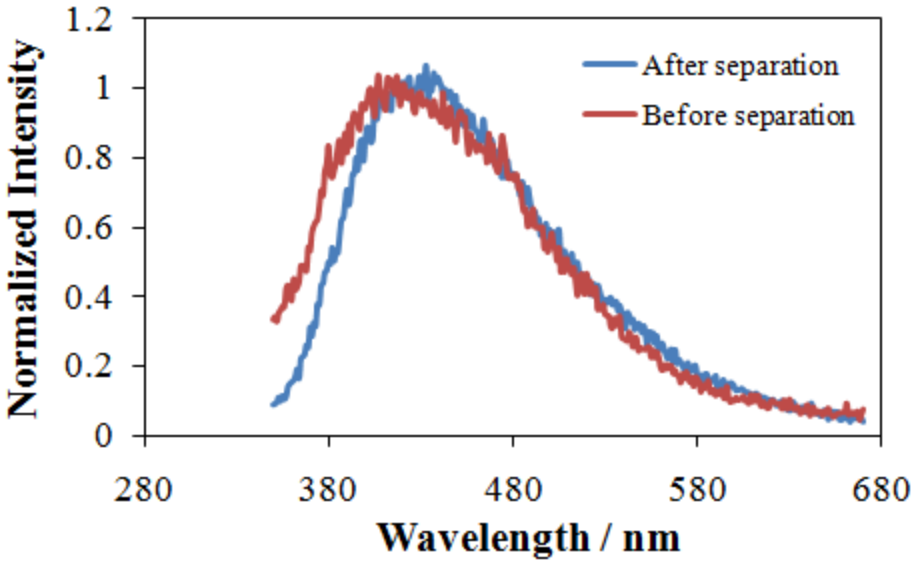

Figure 4.3. Fluorescence emission spectra of carbon QDs solution in DCM before and in THF after separation of supporting electrolyte. (Excitation wavelength: 340 nm).

4.3 CHARACTERIZATION

The prepared carbon QDs solution was characterized with mass spectroscopy, TEM, FT-IR and Raman. Since preliminary high resolution MALDI analysis with tetracyanoquinodimethane as matrix showed only matrix ions and GCMS experiment didn't show any discrete peaks, we ran desorption chemical ionization (CI) (as shown in Figure 4.4). Both positive and negative ion modes suggest the presence of something with a MW of 546. In the positive ion mode, there's a weak signal at m/z of 547 that probably corresponds to an $(M+H)^+$ ion, while in the negative ion mode, the strong signal at m/z 546 probably represents an electron capture product $M^{-\cdot}$. A possible reason why we didn't see it in the MALDI experiment is that the NPs are too small and too non-polar to be ionized effectively. CI analysis of another carbon QDssolution prepared in different batch using the same method also shows MW of 546/547. High resolution CI experiment in both positive and negative ion modes were performed to elucidate possible formula and shows

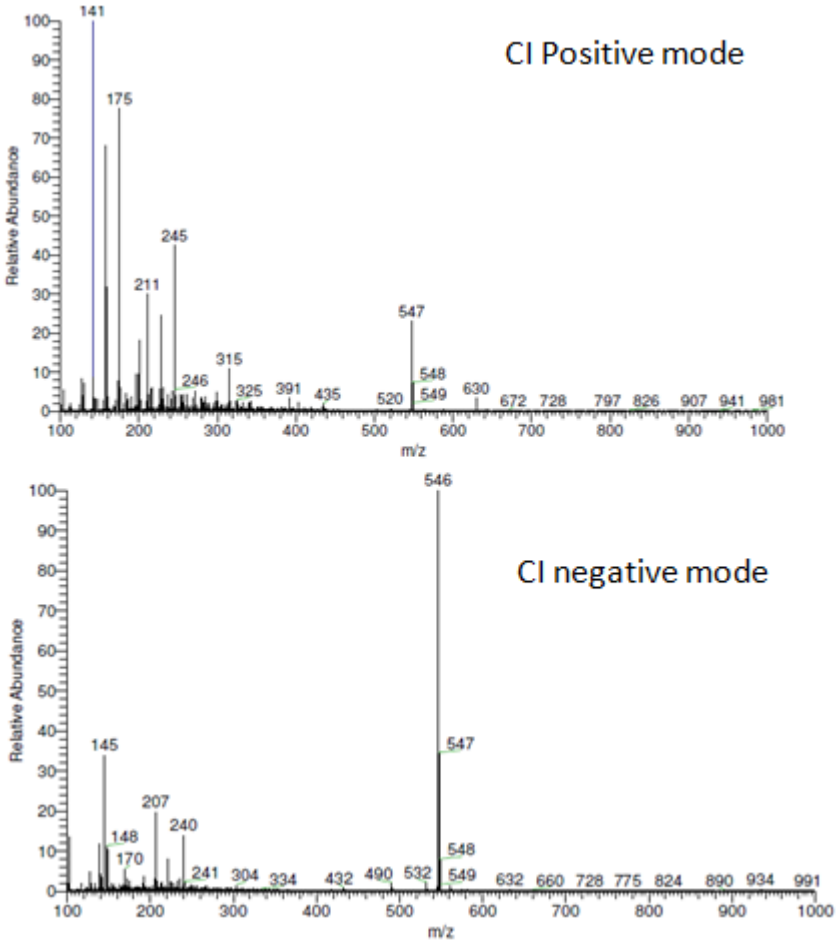

Figure 4.4. Mass Spectra (Desorption Chemical Ionization) of carbon QDs.

consistent MW results as low resolution CI experiment. A formula search with the negative mode data is consistent with the positive mode data; negative mode suggests a formula of $C_{33}H_{54}O_6$ with 1.1 ppm error and positive mode suggests a formula of $C_{33}H_{55}O_6$ with 2.7 ppm error.

The TEM image (Figure 4.5, left) shows particles with a size distribution ranging from 2 to 6 nm; the observed lattice spacing distance from HR-TEM result (Figure 4.5, right) is 3 Å, very close to that reported previously.[18]

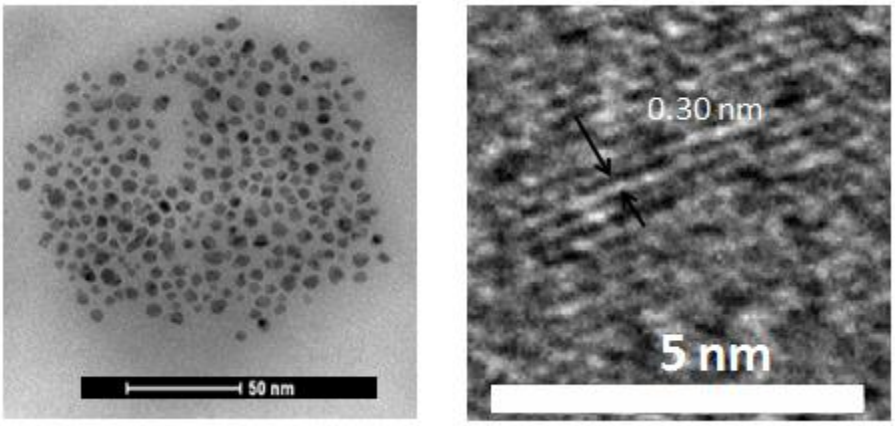

Figure 4.5. TEM image (left) and HR-TEM (right) of carbon QDs.

The FT-IR spectrum was used to investigate the functional groups of the synthesized carbon QDs and the result was shown in Figure 4.6. The assignments for the bands were summarized in Table 4.1.

Table 4.1. Bands assignment for the FT-IR spectrum of carbon QDs.

Wave number / cm^{-1}	Bands Assignment
2848, 2914, 2952	Stretching vibration of C-H bond from the solvent[26]
1620	Vibration of C=C bond from aromatic rings
1375, 1460	Vibration of C-H bond from the solvent
1008, 1077	Vibrations of C=C bond from alkenes
794, 843 (shoulder)	C-H vibration on aromatic rings[27]
1258 (very weak)	C-O vibration[13, 26, 28]
1710 (very weak)	Stretching vibration of C=O[13, 26, 28]

No stretching vibration of O-H bond[28,14,13] (at 3385/3400/3440 cm^{-1}) was observed and very weak bands from C-O bond and C=O bond vibrations were observed, which means partial oxidation of as-prepared carbon QDs occurs during the separation process which is performed under atmospheric environment. The absence and lack of the oxygen-containing functional groups can explain why the as-prepared carbon QDs are not soluble in water.

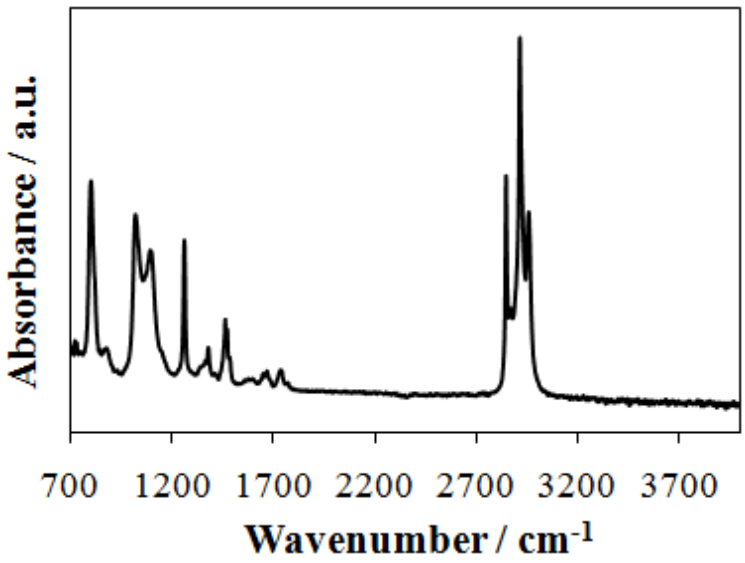

Figure 4.6. FT-IR spectrum of carbon QDs in hexane after evaporating hexane.

The observed strong band from the C-H bond vibration could be from the solvent (hexane) trapped by the carbon QDs. FT-IR spectrum was also measured immediately after dropping cast carbon NPs in hexane on the optical crystal ZnSe, and the result is in shown in Figure 4.7 (indicated as "before"). As a comparison, the FT-IR spectrum after evaporation of hexane was also shown as "after". It can be seen from Figure 4.7 that the intensity of FT-IR band from C-H vibration was decreased dramatically after evaporating hexane. As a control experiment, the FT-IR spectrum for the background (only the optical crystal) was also shown, which is pretty good.

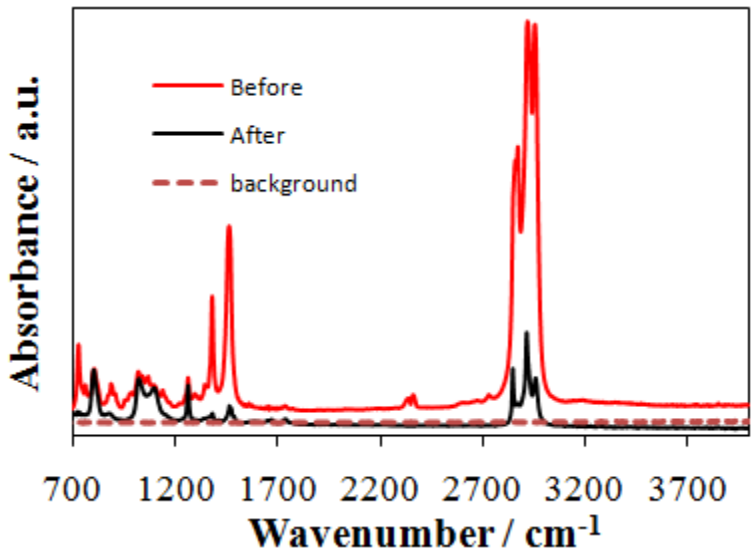

Figure 4.7. FT-IR spectrum of carbon QDs in hexane before and after evaporating hexane as well as FT-IR spectrum of background with only ZnSe optical crystal.

The Raman spectrum of the carbon QDs shows a very high photoluminescence background as shown in Figure 4.8, which has been observed for luminescent graphene and carbon.[12, 19]

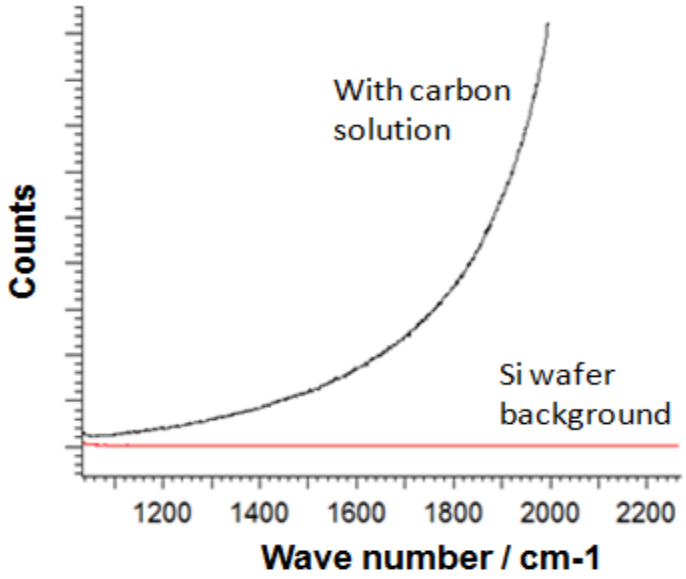

Figure 4.8. Raman Spectrum of Carbon QDs on Si wafer and background (Si wafer).

4.4 ELECTROCHEMISTRY

Figure 4.9 shows the cyclic voltammograms (CVs) of the as-prepared carbon QDs solution recorded on a Pt working electrode. The CVs were characterized by irreversible oxidation and reduction peaks.

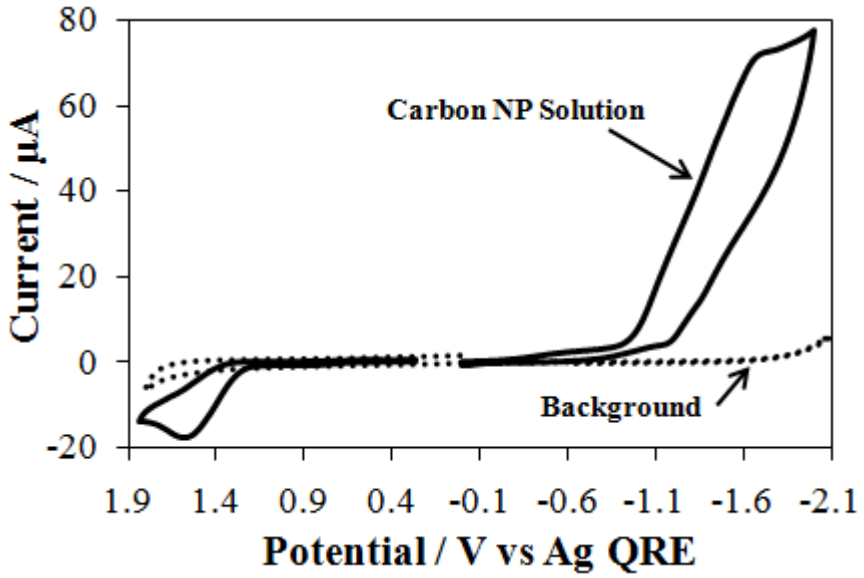

Figure 4.9. Cyclic voltammogram of the carbon QDs solution and background solution.

The carbon QDs solution was prepared by electrochemical reduction of HOPG in dichloromethane with 0.1 M $TBAPF_6$ as the supporting electrolyte. Then background solution contains 0.1 M $TBAPF_6$ in dichloromethane. Scan rate = 50 mV/s.

The scan rate was varied to study the reduction and oxidation peaks of the carbon QDs solution. Scan-rate-dependent CVs for the oxidation peak are presented in Figure 4.10a. The peak current was plotted against square root of scan rate and the result was shown in Figure 4.10b. From Figure 4.10b, it can be seen that the peak current changed linearly with the square root of the scan rate and intercepted near zero for the oxidation, indicating diffusion control of the current.

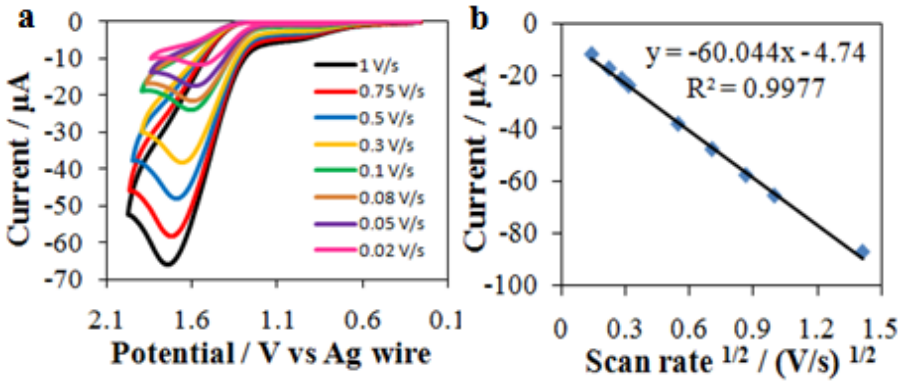

Figure 4.10. (a) Oxidation CV of carbon QDs solution in dichloromethane at various scan rates. (b) Oxidation peak current versus (scan rate)$^{1/2}$.

The reduction peak current didn't change linearly with either the scan rate or its square root (results not shown). The reduction was studied with continuous sweeping on a freshly polished electrode at a scan rate of 0.05 V/s with the solution stirred between runs. The results of the first and second run are shown in Figure 4.11a.

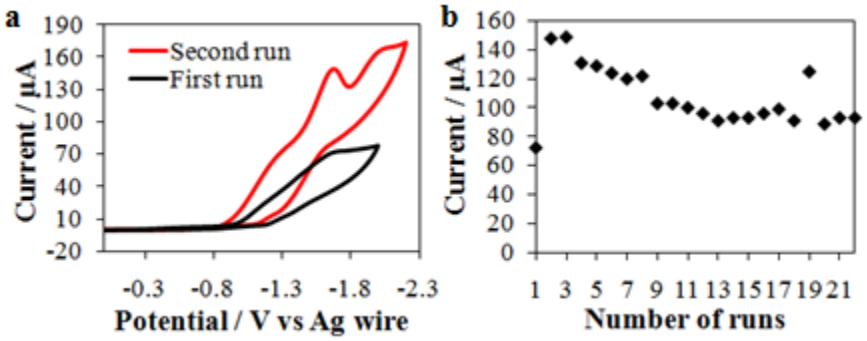

Figure 4.11. Reduction CV and peak current.

(a) First run of reduction CV of carbon QDs solution in dichloromethane at 0.05 V/s on a freshly polished Pt working electrode and the second run after stirring solution following the first run. (b) The peak current around -1.6 V versus the number of runs. Scan rate = 0.05 V/s.

It can be seen from Figure 4.11a that both the shape and the magnitude of the reduction current changed dramatically on the second run, indicating a surface process is involved in the reduction. This was further confirmed by the peak current at – 1.6 V obtained for different runs shown in Figure 4.11b.

4.4 ABSORBANCE, PL AND ECL

The UV-vis absorption and fluorescence spectra of the carbon QDs are shown in Figure 4.12. From Figure 4.12, it can be seen that the carbon QDs show strong optical absorption in the UV region, with a tail extending out into the visible range. An absorption peak was observed around 280 nm. This is consistent with the UV-vis absorption spectra of other carbon dots reported.[1, 10, 15, 5, 6] Figure 4.13 shows the fluorescence emission spectra with different excitation wavelength and it shows clear excitation wavelength dependence of emission wavelength and intensity, which has been an unifying feature of fluorescence emission of carbon dots. Whether this occurs because of optical selection of differently sized nanoparticles (quantum effect) and/or different emissive traps on the carbon-dot surface or another mechanism altogether is currently unresolved. Knowledge into the origins of fluorescence emission of carbon-dots is a

matter of current debate and requires greater clarification.[1] From Figure 4.13, it can be seen that the highest fluorescent intensity was achieved at the excitation wavelength of 340 nm and from Figure 4.12, it can be seen that the fluorescence emission maximum occurred at 408 nm. Figure 4.12 also shows the fluorescence excitation spectrum, which is different from the absorption spectrum.[17, 16, 29]

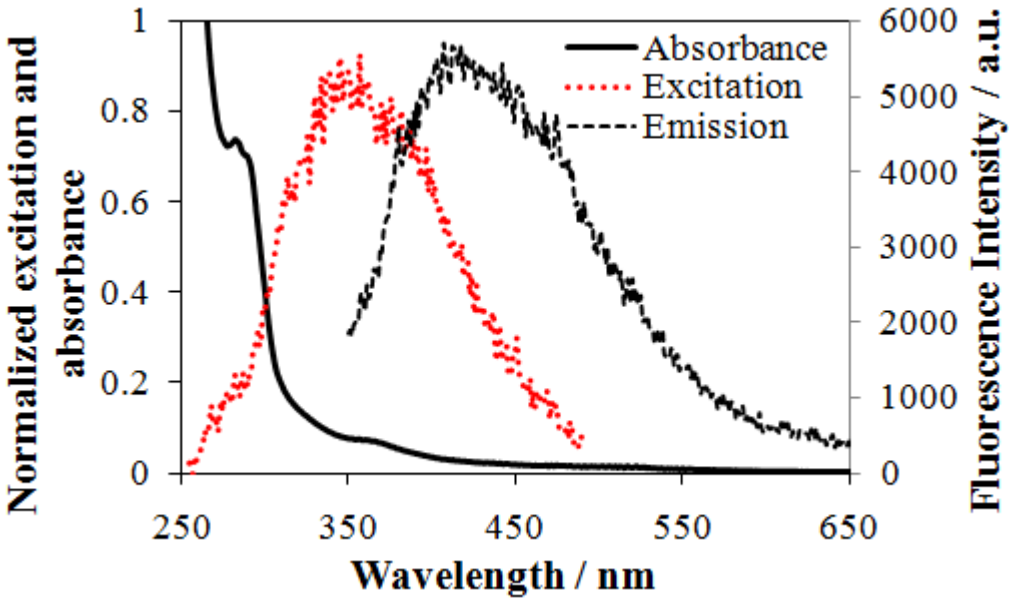

Figure 4.12. Absorbance and fluorescence emission spectra of carbon QDs solution.

Concentration is 0.57 times of the concentration used for electrochemistry and ECL study. (Excitation wavelength: 340 nm).

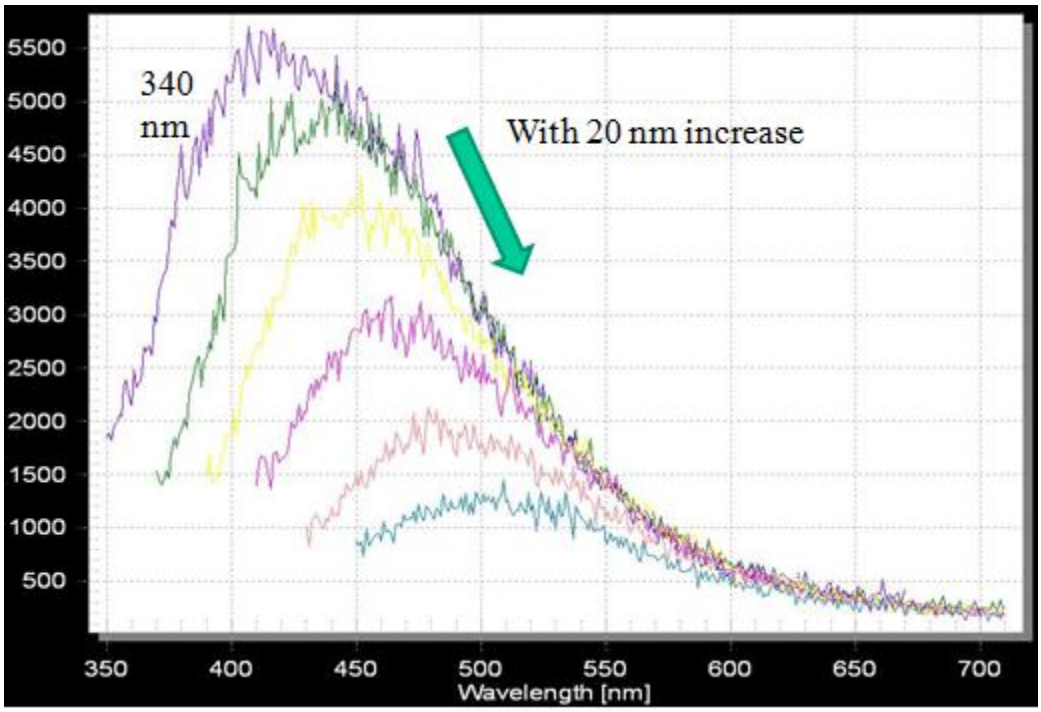

Figure 4.13. Fluorescence emission spectra with different excitation wavelength shown in the graph.

The annihilation ECL properties of as-prepared carbon QDs solutions were tested. The ECL coupled with CV, scanning from 0 V to -2 V then going to 1.8 V, was studied with two continuous cycles (see Figure 4.14). During the first cycle, no light was detected, while in the second cycle, ECL light was detected during reduction (around -1.6 V). In our experiment, we varied the scan rate of CV and found that the ECL light intensity increased as we increased the scan rate. This phenomenon correlates with the CV feature that oxidation is irreversible.

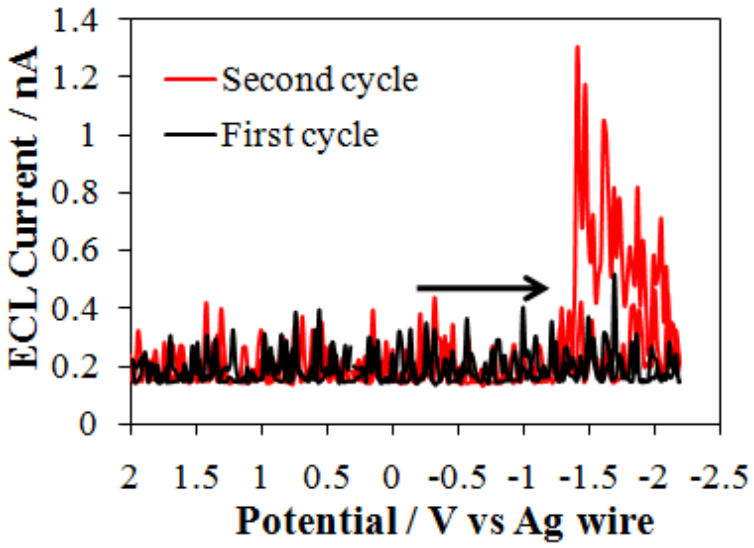

Figure 4.14. Electrogenerated chemiluminescence (ECL) coupling with cyclic voltammogram of carbon solution.

Initial scan polarity is negative as shown by the arrow. Two scans are done continuously. Scan rate = 3 V/s.

Transient ECL coupled with multipotential step chronoamperometry (see Figure 4.15) show that strong ECL light was produced during negative pulses and no light was detected during positive pulses, which is consistent with what was observed in ECL coupled with CV experiment. Possible reason could be that the product of reduction of carbon QDs precipitates on electrode surface. After reduction, there's no radical anions left in solution to react with the radical cations produced during oxidation of carbon QDs, thus no ECL was produced detected during positive pulses. A decrease in ECL intensity was observed with an increase in pulse duration, which is frequently observed in annihilation ECL when the radical ions are not stable. This is because when the radical ions are not stable, the longer the pulse duration, the less of the radical ions will be left

for the annihilation reaction to generate ECL. The ECL light lasted as long as 2s of pulsing before it was at a negligible level.

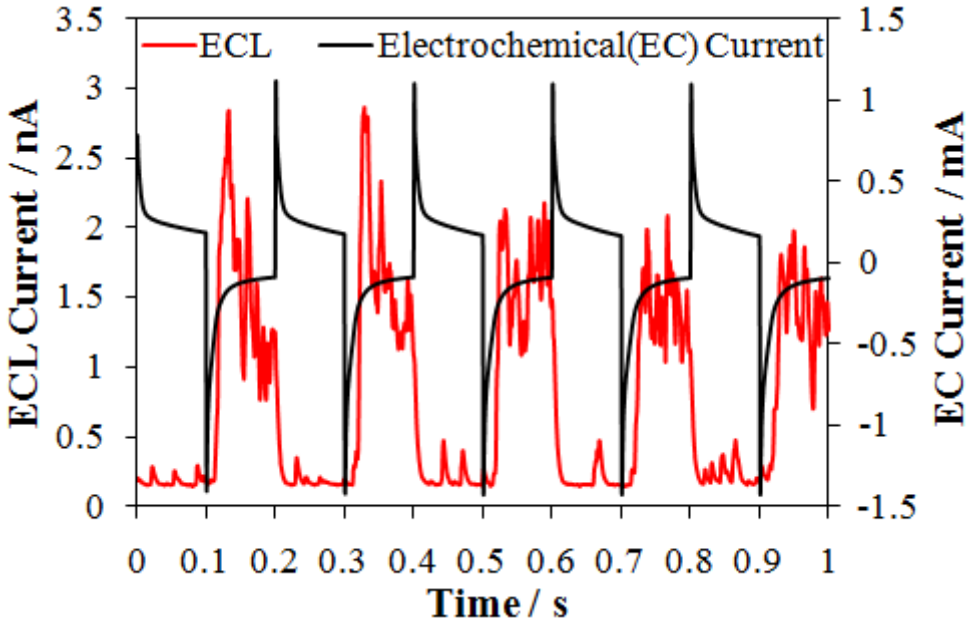

Figure 4.15. Coupled electrochemical current and ECL intensity of carbon solution.

Pulsed alternately between 2 V and -2 V with pulse duration time of 0.1 s. At 0 s, pulsed at 2 V and at 0.1 s, pulsed at -2 V and so on.

The normalized ECL spectra are shown in Figure 4.16. ECL spectra before normalization are shown in Figure 4.17. ECL light with very broad wavelength ranging from 400 nm to 890 nm was generated by annihilation mode. The ECL peak shifted toward red with time (perhaps increasing cycles) and maximum ECL emission wavelength could reach as high as 630 nm. The change in ECL spectrum was

accompanied with the change in the reduction CV after ECL measurements, which is consistent with the reduction CV results shown in Figure 4.11. The red shift in wavelength of ECL spectrum could be related with the formation of carbon QDs (C-QDs) film on the electrode surface. During oxidation, radical cations ($C\text{-}QD^{+\cdot}$) of C-QDs were produced, while radical anions ($C\text{-}QD^{-\cdot}$) of C-QDs were formed during reduction. The formed radical cations and formed radical anions react to form the excited state, which emit ECL light. The whole process could be expressed from equations 4.1-4.4:

$$C\text{-}QD + e^- \rightarrow C\text{-}QD^{-\cdot} \text{ (reduction at electrode)} \quad (4.1)$$

$$C\text{-}QD - e^- \rightarrow C\text{-}QD^{+\cdot} \text{ (oxidation at electrode)} \quad (4.2)$$

$$C\text{-}QD^{+\cdot} + C\text{-}QD^{-\cdot} \rightarrow C\text{-}QD^{*} + C\text{-}QD \text{ (excited state formation)} \quad (4.3)$$

$$C\text{-}QD^{*} \rightarrow C\text{-}QD + h\nu \text{ (light emission)} \quad (4.4)$$

Notice that in one of the products in both reaction 4.3 and 4.4 is C-QD, which could precipitate on electrode surface. The red shift of ECL spectrum generated from the film of an organic compound comparing with the ECL generated from the solution species has been observed in our previous study. [30] A red-shift of the absorption, emission was also observed upon going from solution to film, which may be attributed to the loss of conformational freedom with the consequent lowering of the energy gap between the HOMO and LUMO orbitals, resulting in a red shift of the absorption and fluorescence spectra.[31, 32] The red shift in ECL spectrum could be because of similar reason for the red shift in absorption and fluorescence spectra.

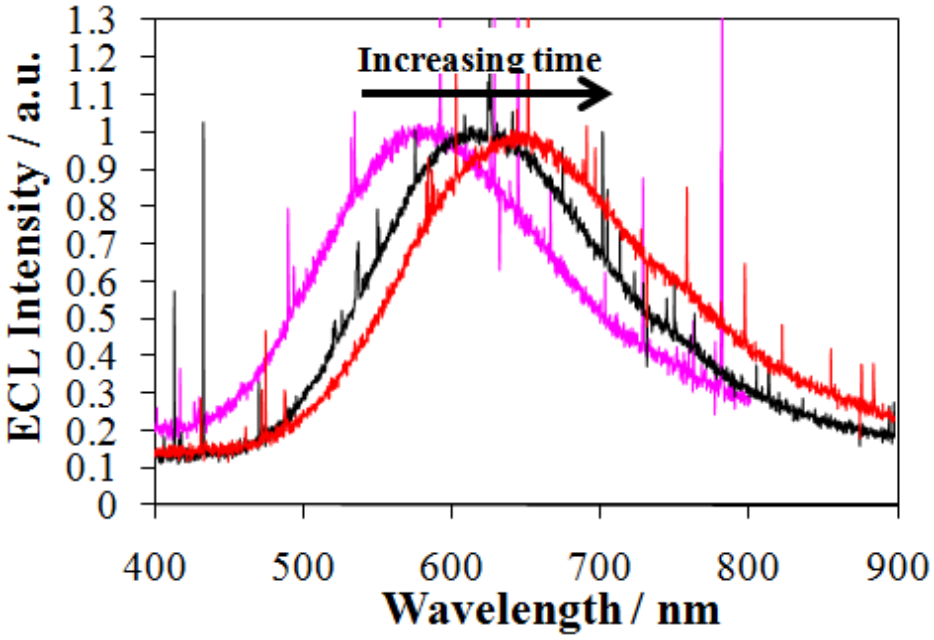

Figure 4.16. Normalized ECL spectra of carbon solution.

Obtained by pulsing between +2 V and -2 V vs. AgQRE. ECL spectra were integrated for 10 min using a 2 mm slit width. Pink: the first 10 min cycle; black: the second 10 min cycle; red: the third 10 min cycle.

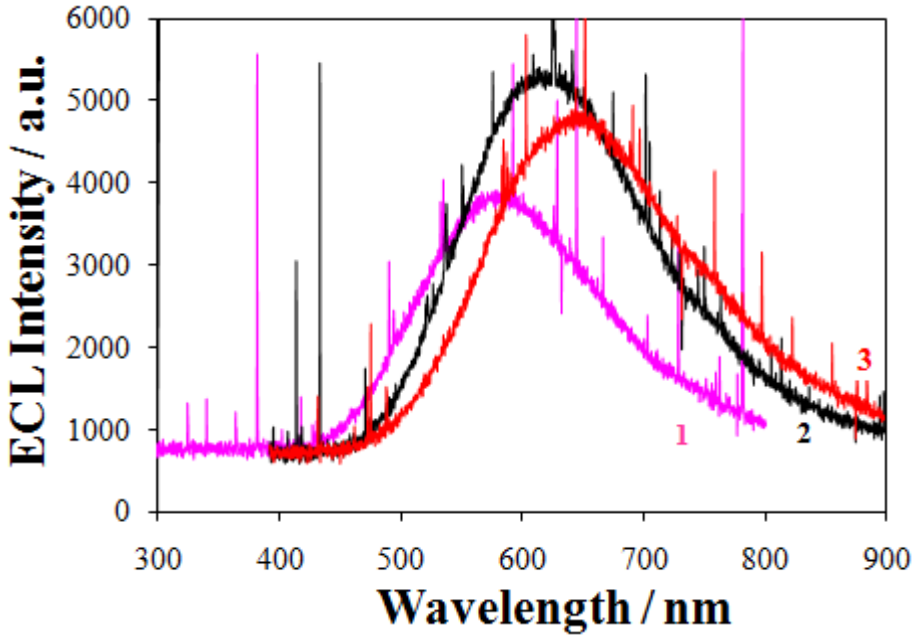

Figure 4.17. ECL spectra of carbon solution.

Obtained by pulsing between +2 V and -2 V vs. an AgQRE. ECL spectra were integrated for 10 min using a 2 mm slit width. Pink (1): the first 10 min cycle; black (2): the second 10 min cycle; red (3): the third 10 min cycle.

4.5 CONCLUSIONS

In conclusion, highly fluorescent carbon quantum dots (QDs) with no –OH group were prepared through electrochemical reduction of HOPG in dichloromethane under inert atmosphere in a three compartment cell. The absence of –OH groups confirms the success in the preparation methodology for non-oxidized C-QDs, which may provide as a

model system to understand the properties of C-QDs. Irreversible reduction and oxidation were observed. The anodic current shows diffusion-limited behavior, while surface process may be involved during reduction of C-QDs. ECL was produced by annihilation reaction of radical ions. Precipitation of carbon-QDs on electrode surface may occur during ECL process, which may cause ECL spectrum progressively red-shifted with cycles. Highest fluorescent intensity was observed at an excitation wavelength of 340 nm and the corresponding maximum fluorescence occurred at 408 nm.

4.6 REFERENCES

[1] Baker, S. N.; Baker, G. A. *Angew. Chem. Int. Ed*. **2010**, *49*, 2-21.

[2] Pumera, M. *Chem. Soc. Rev.* **2010**, *39*, 4146-4157.

[3] Xu, X. Y.; Ray, R.; Gu, Y. L.; Ploehn, H. J.; Gearheart, L.; Raker, K.; Scrivens, W. A. *J. Am. Chem. Soc.* **2004**, *126*, 12736 – 12737.

[4] Hu, S.-L.; Niu, K.-Y.; Sun, J.; Yang, J.; Zhao, N.-Q.; Du, X.-W. *J. Mater. Chem.* **2009**, *19*, 484 – 488.

[5] Sun, Y.-P.; Wang, X.; Lu, F.; Cao, L.; Meziani, M. J.; Luo, P. G.; Gu, L.; Veca, L. M. *J. Phys. Chem. C* **2008**, 112, 18295 – 18298.

[6] Sun, Y. P.; Zhou, B.; Lin, Y.; Wang, W.; Fernando, K. A. S.; Pathak, P.; Meziani, M. J.; Harruff, B. A.; Wang, X.; Wang, H. F.; Luo, P. G.; Yang, H.; Kose, M. E.; Chen, B.; Veca, L. M.; Xie, S.-Y. *J. Am. Chem. Soc*. **2006**, *128*, 7756 – 7757.

[7] Bourlinos, A. B.; Stassinopoulos, A.; Anglos, D.; Zboril, R.; Georgakilas, V.; Giannelis, E. P. *Chem. Mater.* **2008**, *20*, 4539 – 4541.

[8] Liu, R. L.; Wu, D. Q.; Liu, S. H.; Koynov, K.; Knoll, W.; Li, Q. *Angew. Chem.* **2009**, *121*, 4668 – 4671; *Angew. Chem. Int. Ed.* **2009**, *48*, 4598 – 4601.

[9] Zhu, H.; Wang, X.; Li, Y.; Wang, Z.; Yang, F.; Yang, X. *Chem. Commun.* **2009**, 5118 – 5120.

[10] Bourlinos, A. B.; Stassinopoulos, A.; Anglos, D.; Zboril, R.; Karakassides, M.; Giannelis, E. P. *Small* **2008**, *4*, 455 – 458.

[11] Liu, H. P.; Ye, T.; Mao, C. D.; *Angew. Chem.* **2007**, *119*, 6593 – 6595; *Angew. Chem. Int. Ed.* **2007**, *46*, 6473 – 6475.

[12] Ray, S. C.; Saha, A.; Jana, N. R.; Sarkar, R. *J. Phys. Chem. C* **2009**, *113*, 18546 – 18551.

[13] Tian, L.; Ghosh, D.; Chen, W.; Pradhan, S.; Chang, X.; Chen, S. *Chem. Mater.* **2009**, *21*, 2803 – 2809.

[14] Pan, D.; Zhang, J.; Li, Z.; Wu, M. *Adv. Mater.* **2010**, *22*, 734-738.

[15] Lu, J.; Yang, J.-X.; Wang, J.; Lim, A.; Wang, S.; Loh, K. P. *ACS Nano* **2009**, *3*, 2367 – 2375.

[16] Zhao, Q.-L.; Zhang, Z.-L.; Huang, B.-H.; Peng, J.; Zhang, M.; Pang, D.-W. *Chem. Commun.* **2008**, 5116 – 5118.

[17] Zheng, L. Y.; Chi, Y.W.; Dong, Y. Q.; Lin, J. P.; Wang, B. B. *J. Am. Chem. Soc.* **2009**, *131*, 4564 – 4565.

[18] Zhou, J. G.; Booker, C.; Li, R. Y.; Zhou, X. T.; Sham, T. K.; Sun, X. L.; Ding, Z. F. *J. Am. Chem. Soc.* **2007**, *129*, 744 – 745.

[19] Gokus, T.; Nair, R. R.; Bonetti, A.; Böhmler, M.; Lombardo, A.; Novoselov, K.; Geim, A. K.; Ferrari, A. C.; Hartschuh, A. *ACS Nano*, **2009**, *3*, 3963-3968.

[20] Wu, J.; Pisula, W.; Müllen, K. *Chem. Rev*. **2007**, *107*, 718-747.

[21] Yan, X.; Cui, X.; Li, L.-S. *J. Am. Chem. Soc.* **2010**, *132*, 5944–5945.

[22] Bard, A. J. in *Electrogenerated Chemiluminescence*; Bard, A. J., Ed.; Marcel Dekker: New York, 2004.

[23] For reviews on ECL, see: (a) Richter, M. M. *Chem. Rev*. **2004**, *104*, 3003-3036. (b) Knight, A. W.; Greenway, G. M. *Analyst* **1994**, *119*, 879-890. (c) Faulkner, L. R.; Bard, A. J. *Electroanalytical Chemistry*; Marcel Dekker: New York, 1977; Vol. 10, p 1. (d) Bard, A. J.; Debad, J. D.; Leland, J. K.; Sigal, G. B.; Wilbur, J. L.; Wohlstadter, J. N. in *Encyclopedia of Analytical Chemistry: Applications, Theory and Instrumentaion*; Meyers, R. A., Ed.; John Wiley & Sons: New York, 2000; Vol. 11, p 9842.

[24] Dong, Y.; Zhou, N.; Lin, X.; Lin, J.; Chi, Y.; Chen, G. *Chem. Mater*. **2010**, *22*, 5895-5899.

[25] Fan, F.-R. F.; Park, S; Zhu, Y.; Ruoff, R. S.; Bard, A. J. *J. Am. Chem. Soc.*, **2009**, *131*, 937-939.

[26] Mochalin, V. N.; Gogotsi, Y. *J. Am. Chem. Soc*. **2009**, *131*, 4594-4595.

[27] Yan, X.; Cui, X.; Li, B.; Li, L.-S. *Nano Lett.* **2010**, *10*, 1869-1873.

[28] Wang, Z.; Xiao, P.; He, N. *Carbon.* **2006**, *44*, 3277-3284.

[29] Mao, X.-J.; Zheng, H.-Z.; Long, Y.-J.; Du, J.; Hao, J.-Y.; Wang, L.-L.; Zhou, D.-B. Spectrochimica Acta Part A, **2010**, *75*, 553–557.

[30] Shen, M.; Huang, J.; Liu, Q.; Zhu, X.-H.; Bard, A. J. Electrochemistry and Electrogenerated Chemiluminescence Study of Film and Solution of Substituted Thiophene Red Fluorophore. *In preparation.*

[31] Seixas de Melo, J.; Pina, J.; Burrows, H. D.; Di Paolo, R. E.; Maçanita, A. L. *Chem. Phys.* **2006**, *330*, 449–456.

[32] Narwark, O.; Meskers, S.C.J.; Peetz, R.; Thorn-Csányi, E.; Bässler, H. Chem. Phys. **2003**, *294*, 1–15.

Chapter 5. Localized Electron Transfer and the Role of Tunneling on the Rates of $Ru(bpy)_3^{2+}$ Oxidation and Reduction as Measured by Scanning Electrochemical Microscopy

5.1 INTRODUCTION

In considering heterogeneous electron transfer (ET), molecules where different moieties are not conjugated with one another often show electrochemistry in which the each moiety behaves independently and resembles that of that portion alone. Such localized ET is seen for example in oligomers and polymers, e.g. poly(vinylferrocene), where each monomer unit behaves independently. Many donor-acceptor molecules, with general structures that involve the linking of a donor group (D) to an acceptor group (A), D~(L)~A, where L represents the linker, also show localized ET to A and D. For example in dithienylbenzothiadiazole-based molecule, **1b** (4,7-bis(4-(4-sec-butoxyphenyl)-5-(3,5-di(1-naphthyl)phenyl)thiophen-2-yl)-2,1,3-benzothiadiazole) shown in scheme 1, the benzothiadiazole (A) and the two thienyl moieties (D) are weakly coupled, even though they are directly linked, probably because of steric interactions.[1] In this D-A molecule the heterogeneous ET rate constants, k^o, for the oxidation of D and the reduction of A were different. This was ascribed to differences in the ET distances involved, where the A, with the smaller k^o, was blocked by the bulky D groups from close approach to the electrode surface, while the D groups themselves were accessible. Thus differences in tunneling, rather than differences in reorganization energies, were taken as the main factor to explain the results.

Tunneling effects can be important factors influencing the rates of electron transfer and are described by equation 5.1.1 where k_{ET} is the effective rate of electron transfer, k^0_{ET} is the rate of electron transfer in the absence of barrier effects, β is the tunneling constant and x is the tunneling distance:

$$k_{ET} = k^0_{ET} e^{-\beta x} \qquad (5.1.1)$$

The impact of tunneling effects on the rates of electrochemical processes have been studied by making use of the exponential dependence on distance shown in equation 5.1.1; this is accomplished generally by separating the electrode surface from the electroactive species by using a spacer e.g. a self-assembled monolayer or by connecting the electroactive species at the end of a linker. [2,3,4,5]

An advantage of studying tunneling effects in D-A molecules is that comparison of oxidation and reduction rate constants can be made on the same molecule under identical electrode and solution conditions, thus minimizing impacts of electrode surface blockage, uncompensated resistance effects, and other variables that might affect the measured value of the heterogeneous rate constant. The extensively-studied molecule tris(2,2'-bipyridine)ruthenium (II) (Rubpy) (see scheme 1)) is in fact also a D-A complex that consists of an oxidizable ruthenium center (D) coordinated by three 2,2'-bipyridine ligands (A) that can be reduced in MeCN solution.[6] Surprisingly the rate constants for the reduction and oxidation of Rubpy at an electrode in MeCN have not been measured previously, perhaps because these rates are high. Sun and Mirkin[7] tried to measure the rate constants for Rubpy oxidation in aqueous and organic solvents at a nm ultramicroelectrode, but a decrease in the limiting current, probably because of impurities, prevented quantitative studies. We show here that scanning electrochemical

microscopy (SECM) can be employed to measure the relative rates and propose that the difference in the rate constants can arise from tunneling effects.

SECM has been used to study the kinetics of heterogeneous electron transfer with high accuracy.[7,8,9,10,11] In SECM, a µm-size ultramicroelectrode (UME or tip) is approached to a substrate electrode held at a potential where the product of the half reaction at the tip is reversed. The rate of electron transfer of a solution species at the tip can be measured by observing the feedback current detected as a function of distance between tip and substrate, *d*, and noting deviations from the behavior for a diffusion-controlled reaction.[12] Because the tip current is measured at steady state and small currents (~nA) are detected, fast kinetics can be measured without the problem of dealing with electrode capacitive effects and uncompensated resistance, that can be especially important in nonaqueous solvents. However to measure large heterogeneous rate constants, the mass transfer rate, proportional to D/d, where D is the diffusion coefficient of the molecule under study, must be large compared with k^o, so the tip-substrate distance must be small compared with the tip radius, a.[13]

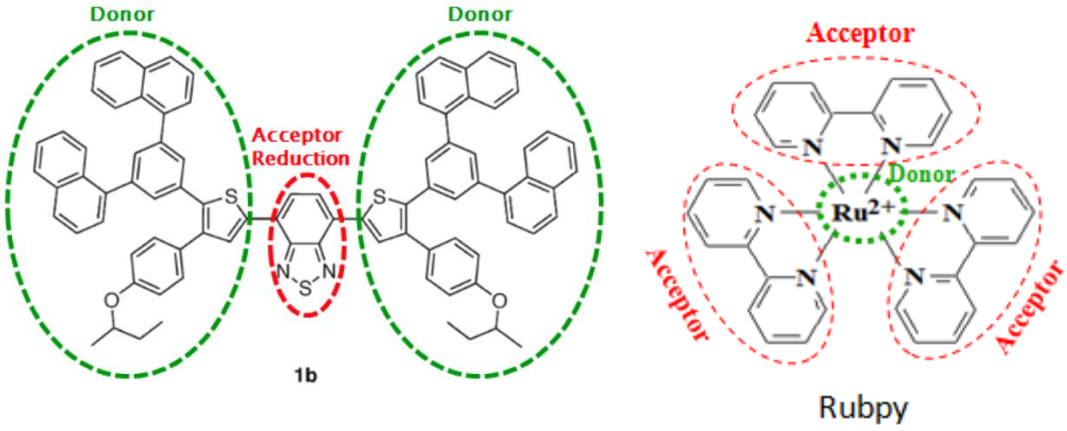

Scheme 1

5.2 EXPERIMENTAL

Chemicals. Anhydrous acetonitrile (MeCN) was obtained from Aldrich (St. Louis, MO) and transferred directly into an argon atmosphere drybox (MBraun Inc., Stratham, NH) without further purification. Electrochemical grade tetra-*n*-butylammonium hexafluorophosphate ($TBAPF_6$) was obtained from Fluka and used as received. Tris(2,2'-bipyridine)ruthenium (II) perchlorate (Rubpy) was obtained from GFS Chemicals, Inc. (Powell, OH).

Setup. All SECM and other electrochemical measurements were carried out with a CHI 920C SECM station bipotentiostat (CH Instruments, Austin, TX). The SECM scanning head and cell were placed inside the drybox and connected to the controller and bipotentiostat outside the glovebox via electric feedthroughs. This was necessary to avoid contamination of the solution with water and oxygen. A partially-inflated inner tube was placed beneath the SECM to minimize vibrations from the glovebox blower and a metal plate was placed on the top of the tire as a stand support. A diagram of the setup is shown below in Figure 5.1.

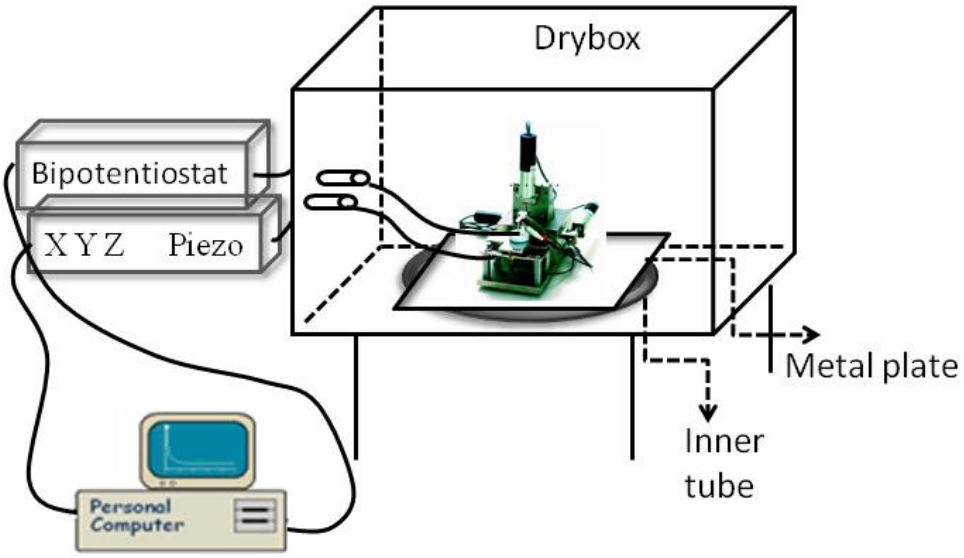

Figure 5.1. Diagram of the SECM inside a drybox.

Electerodes. Platinum (99.99%) 10 μm diameter wire from Goodfellow (Devon, PA) was used to fabricate the SECM electrodes by procedures described elsewhere.[13, 14] The glass surrounding the tip was made as small as possible by careful polishing, holding the tip at an angle with respect to the polishing disk. Making such a tip and careful alignment with respect to the substrate was necessary to obtain the very small *d/a*-values required in the measurement. Details about the tip construction and simulations of the tip behavior with geometric variations will be published elsewhere.[15] An SEM was used to check the tip geometry, where the tip was initially placed flat (horizontal) and then tilted to different angles to find the optimum one (tilted at 5 and 15 degrees) to best characterize the tip end (Figure 5.2).

(A)

(B)

(C)

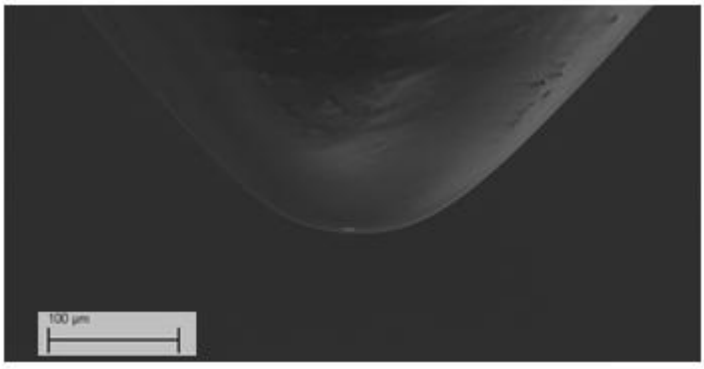

Figure 5.2. SEM pictures of UME tip tilted at (A) 5 degrees. (B)5 degrees (higher magnification of (A). (C)15 degrees.

The brighter area at the end of the tip is the 10 µm diameter Pt and the remainder is glass.

The substrate electrode was a Pt disk (2mm in diameter, CH Instruments, Austin, TX) sealed in Teflon. The tip and substrate electrodes were polished prior to use with alumina paste (0.3 μm and 0.05 μm) on microcloth pads (Buehler, Lake Bluff, IL), and sonicated in Milli-Q deionized water and then in ethanol. The substrate electrode was polished to a mirror-finish. The measurement was done in a Teflon cell, a Pt wire (0.5 mm in diameter) was used as a counter electrode and an Ag wire (1 mm in diameter) was used as a quasi-reference electrode. The thermodynamic potential of ferrocene in acetonitrile vs this Ag reference electrode is 0.356 V. The counter and reference electrodes were cleaned by rinsing and sonicating in acetone, water and ethanol. Finally, all the electrodes were rinsed with acetone, dried in the oven and transferred into the glove box. To make the measurements, very careful alignment of the tip and substrate and imaging to find the highest point on the substrate was required.[15] The experimental approach curves before and after alignment of the tip and the substrate was shown in Figure 5.3. From Figure 5.3, it can be seen that after aligning the tip and the substrate, a higher positive feedback current was reached, which means that the tip is getting closer to the substrate after aligning the tip and the substrate.

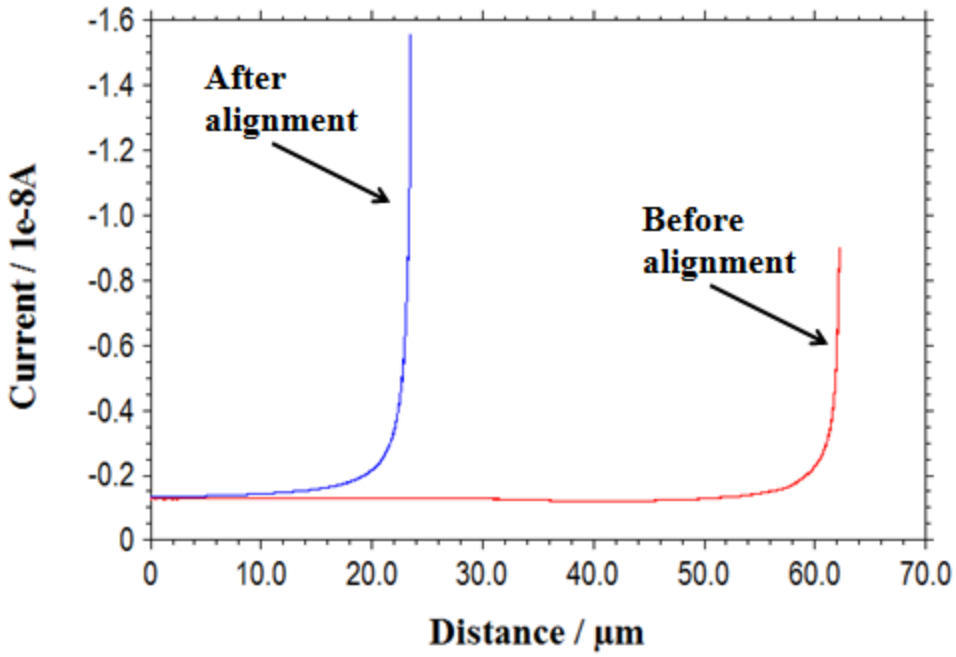

Figure 5.3. Experimental approach curves before and after alignment of the tip and substrate. Note: 0 µm is when the tip is far from the substrate.

Figure 5.4 and 5.5 shows the process of alignment for the tip and substrate. A good approach curve was acquired (Figure 5.4A), then the tip was withdrawn and approach to a position (indicated by the arrow in Figure 5.4 A) where the tip current is very sensitive to the change in the distance between the tip and the substrate. The result is shown in Figure 5.4 B. 5.4 C is the zoom of 5.4 B. Then the SECM imaging was performed at this position.

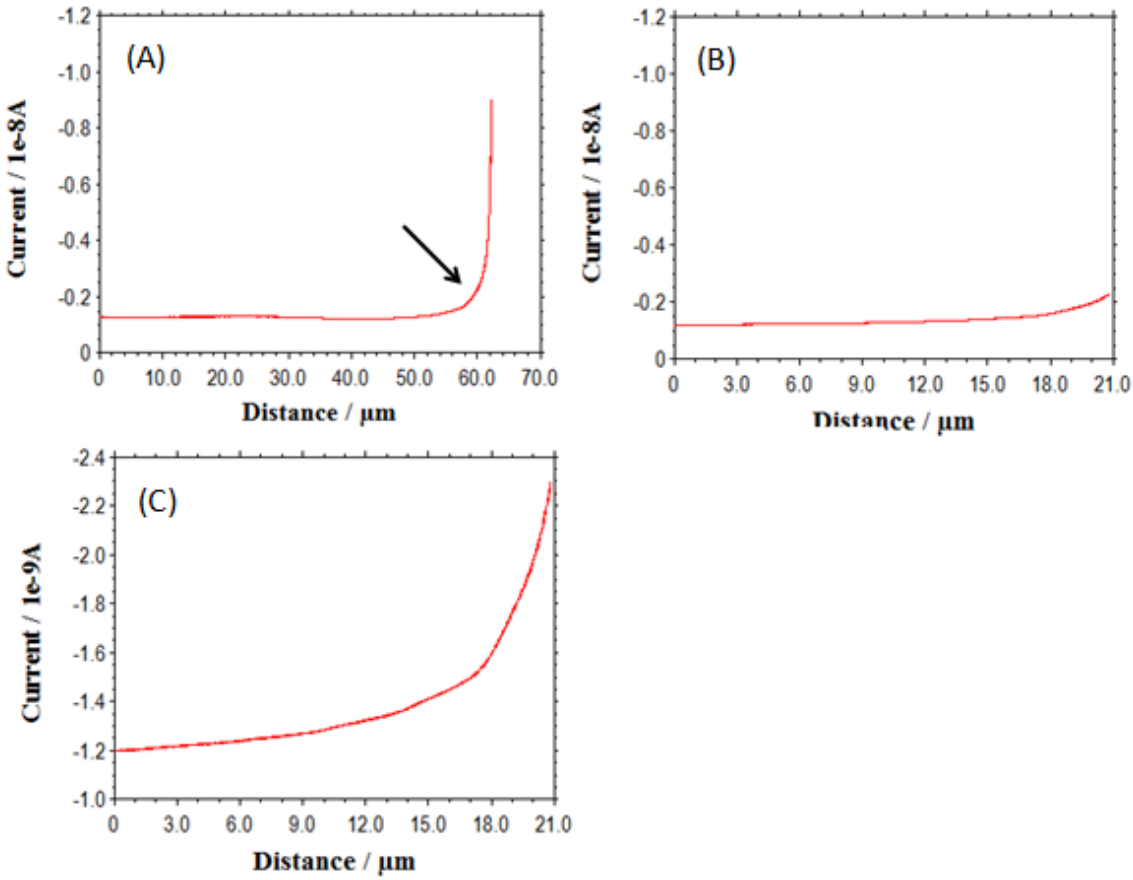

Figure 5.4. (A) Approach curve used for aligning the tip and the substrate. (B) Approach curve stopped at the current indicated by arrow in Figure 5.4(A). (C) Zoom of Figure 5.4 (B). Note: 0 µm is when the tip is far away from the substrate.

The SECM imaging results were shown in Figure 5.5. Figure 5.5A is the result scanning in y direction, and Figure 5.5B is the result scanning in x direction. Finally the experiment was performed on the top plateau.

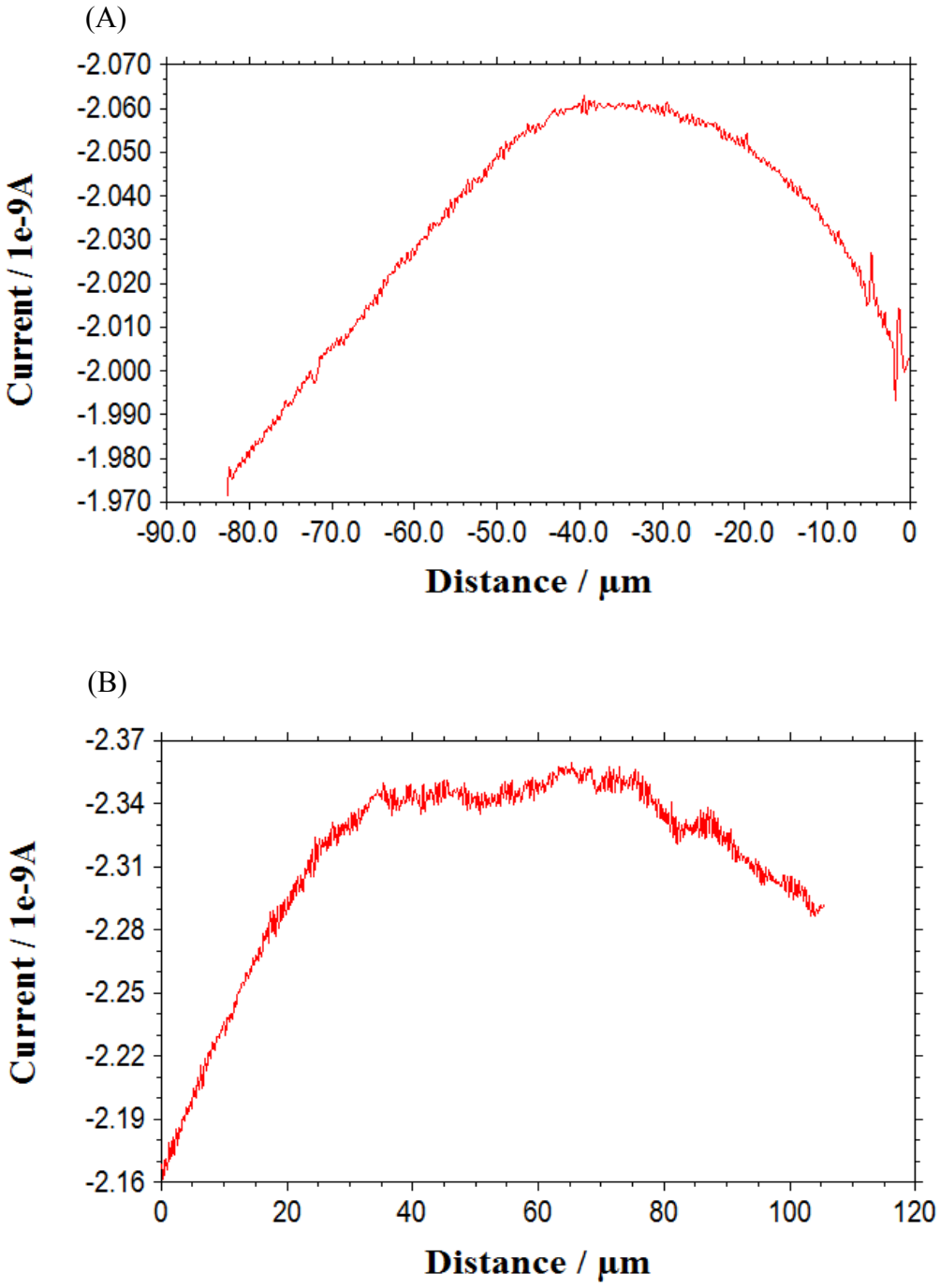

Figure 5.5. SECM Imaging (A) Scan in y direction. (B) Scan in x direction.

The electrodes and cell configuration are shown in Figrue 5.6.

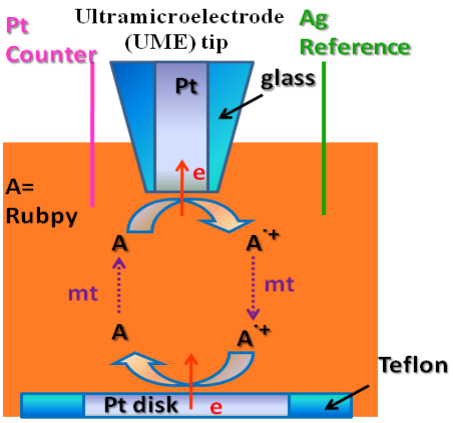

Figure 5.6. Electrodes and cell configuration.

5.3 Results and Discussion

Figure 5.7 shows the steady state voltammogram for the tip when the tip is far away from the substrate.

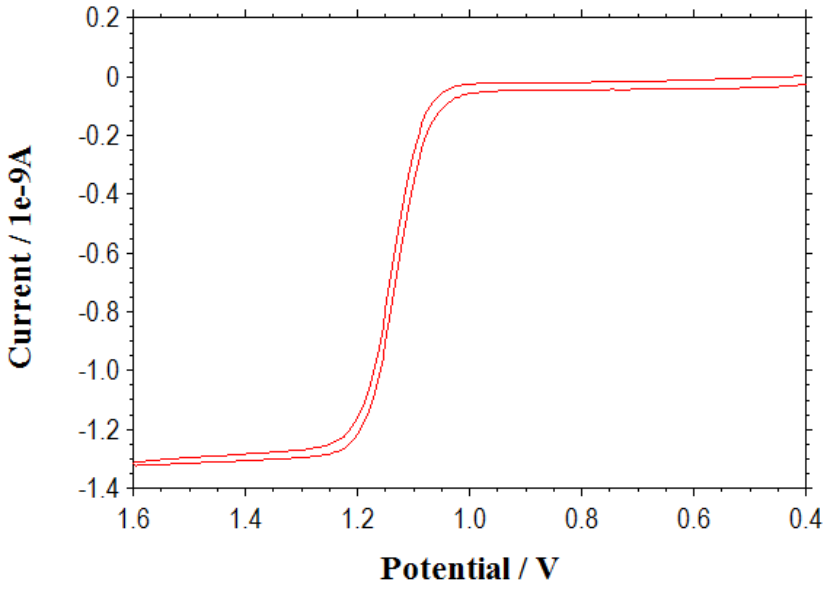

Figure 5.7. Tip steady state voltammogram of 0.38 mM Rubpy in MeCN with 0.1 M $TBAPF_6$ as supporting electrolyte at 5-µm-radius Pt tip when the tip is far away from the substrate. $i_{T,\infty}$= 1.3 nA. Scan rate: 50 mV/s.

Figure 5.8A shows the approach curve acquired experimentally and Figure 5.8B shows the normalized approach curve and the simulated approach curve. It can be seen from figure 5.8B that the experimental approach curve fits very well with the simulated approach curve. Table 5.1 to 5.4 shows the absolute and relative error of the experimental and simulated normalized tip current at different L values. It can be seen from Tables 5.1 to 5.4 that the errors are very small.

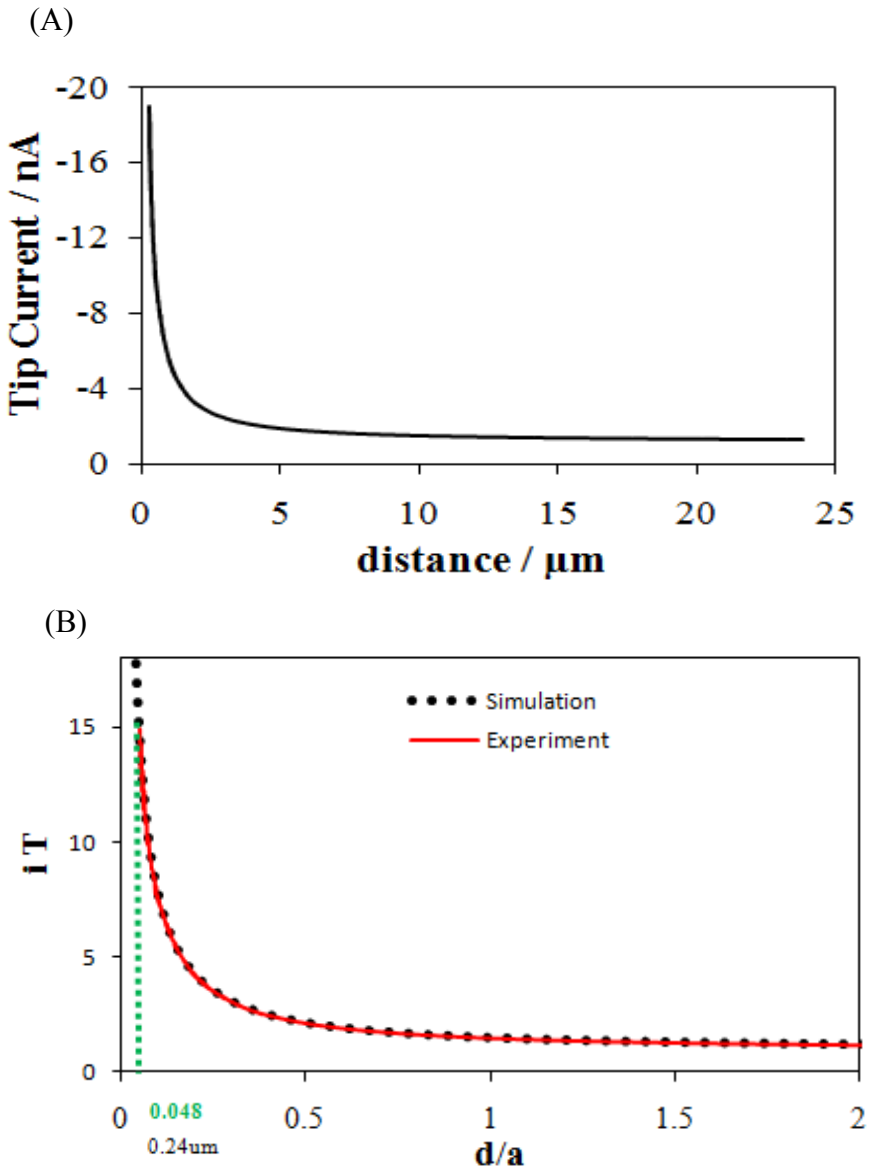

Figure 5.8. (A) Approach curve acquired after aligning the tip and the substrate. (B) Experimentally normalized approach curve and simulated approach curve. Note: the distance is the real distance between the tip and the substrate.

Table 5.1. Absolute error (I_{Experi}- I_{Theory}) and relative error ((I_{Experi}- I_{Theory}) / I_{Theory}) of the normalized experimental tip current (I_{Experi}) with respect to the simulated normalized tip current (I_{Theory}) with L value from 8.52 to 17.01.

L	Normalized Current (I_{Theory})	Normalized Current (I_{Experi})	I_{Experi}- I_{Theory}	(I_{Experi}- I_{Theory}) / I_{Theory}
8.52	7.89	7.50	-0.38	-0.05
8.68	8.03	7.39	-0.65	-0.08
8.84	8.19	7.71	-0.48	-0.06
9.02	8.35	7.60	-0.75	-0.09
9.20	8.52	8.11	-0.41	-0.05
9.39	8.69	7.78	-0.91	-0.10
9.59	8.88	8.49	-0.39	-0.04
9.79	9.07	8.40	-0.67	-0.07
10.01	9.27	8.61	-0.65	-0.07
10.24	9.48	8.83	-0.65	-0.07
10.48	9.70	8.84	-0.86	-0.09
10.73	9.93	9.24	-0.69	-0.07
10.99	10.18	9.27	-0.91	-0.09
11.27	10.44	9.57	-0.87	-0.08
11.57	10.71	10.08	-0.63	-0.06
11.88	11.00	10.24	-0.75	-0.07
12.21	11.30	9.97	-1.33	-0.12
12.56	11.63	10.98	-0.65	-0.06
12.93	11.97	10.84	-1.13	-0.09
13.32	12.33	11.00	-1.33	-0.11
13.74	12.72	12.27	-0.46	-0.04
14.19	13.14	11.45	-1.69	-0.13
14.68	13.59	13.14	-0.45	-0.03
15.19	14.07	12.28	-1.79	-0.13
15.75	14.59	14.31	-0.28	-0.02
16.36	15.14	12.97	-2.18	-0.14
17.01	15.75	14.96	-0.79	-0.05

Table 5.2. Absolute error (I_{Experi}- I_{Theory}) and relative error ((I_{Experi}- I_{Theory}) / I_{Theory}) of the normalized experimental tip current (I_{Experi}) with respect to the simulated normalized tip current (I_{Theory}) with L value from 5.7 to 8.36.

L	Normalized Current (I_{Theory})	Normalized Current (I_{Experi})	I_{Experi}- I_{Theory}	(I_{Experi}- I_{Theory}) / I_{Theory}
5.70	5.28	5.18	-0.10	-0.02
5.77	5.34	5.22	-0.12	-0.02
5.84	5.40	5.25	-0.15	-0.03
5.91	5.47	5.37	-0.09	-0.02
5.98	5.53	5.46	-0.08	-0.01
6.05	5.60	5.40	-0.20	-0.04
6.12	5.67	5.65	-0.02	0.00
6.20	5.74	5.52	-0.22	-0.04
6.28	5.81	5.74	-0.07	-0.01
6.36	5.89	5.76	-0.13	-0.02
6.44	5.97	5.79	-0.18	-0.03
6.53	6.05	5.90	-0.15	-0.02
6.62	6.13	5.93	-0.20	-0.03
6.71	6.21	6.23	0.01	0.00
6.80	6.30	6.07	-0.22	-0.04
6.90	6.39	6.23	-0.16	-0.02
7.00	6.48	6.16	-0.32	-0.05
7.10	6.58	6.48	-0.10	-0.01
7.21	6.68	6.36	-0.31	-0.05
7.32	6.78	6.49	-0.29	-0.04
7.44	6.89	6.63	-0.26	-0.04
7.56	7.00	6.75	-0.25	-0.04
7.68	7.11	6.86	-0.25	-0.03
7.81	7.23	6.78	-0.44	-0.06
7.94	7.35	7.06	-0.29	-0.04
8.07	7.48	7.05	-0.42	-0.06
8.22	7.61	7.27	-0.34	-0.04
8.36	7.74	7.22	-0.52	-0.07

Table 5.3. Absolute error (I_{Experi}- I_{Theory}) and relative error ((I_{Experi}- I_{Theory}) / I_{Theory}) of the normalized experimental tip current (I_{Experi}) with respect to the simulated normalized tip current (I_{Theory}) with L value from 3.11 to 5.58.

L	Normalized Current (I_{Theory})	Normalized Current (I_{Experi})	I_{Experi}- I_{Theory}	(I_{Experi}- I_{Theory}) / I_{Theory}
3.11	2.88	2.87	-0.01	0.00
3.14	2.91	2.92	0.01	0.00
3.17	2.94	2.97	0.03	0.01
3.27	3.03	3.03	0.00	0.00
3.30	3.06	3.06	0.00	0.00
3.34	3.09	3.10	0.01	0.00
3.37	3.12	3.11	-0.01	0.00
3.41	3.16	3.16	0.00	0.00
3.45	3.19	3.21	0.02	0.01
3.49	3.23	3.24	0.02	0.00
3.53	3.27	3.31	0.05	0.01
3.55	3.28	3.25	-0.04	-0.01
3.57	3.30	3.33	0.03	0.01
3.59	3.32	3.29	-0.03	-0.01
3.61	3.34	3.36	0.01	0.00
4.28	3.96	3.97	0.01	0.00
4.34	4.02	4.01	-0.01	0.00
4.41	4.09	4.06	-0.03	-0.01
4.49	4.15	4.13	-0.03	-0.01
4.56	4.22	4.12	-0.11	-0.03
4.64	4.30	4.17	-0.13	-0.03
4.76	4.41	4.39	-0.02	-0.01
4.85	4.49	4.41	-0.08	-0.02
4.94	4.57	4.50	-0.07	-0.02
5.04	4.66	4.55	-0.12	-0.02
5.13	4.75	4.68	-0.07	-0.01
5.24	4.85	4.76	-0.09	-0.02
5.35	4.95	4.83	-0.12	-0.02
5.46	5.06	4.96	-0.09	-0.02
5.58	5.17	5.07	-0.10	-0.02

Table 5.4. Absolute error (I_{Experi}- I_{Theory}) and relative error ((I_{Experi}- I_{Theory}) / I_{Theory}) of the normalized experimental tip current (I_{Experi}) with respect to the simulated normalized tip current (I_{Theory}) with L value from 2.63 to 2.99.

L	Normalized Current (I_{Theory})	Normalized Current (I_{Experi})	I_{Experi}- I_{Theory}	(I_{Experi}- I_{Theory}) / I_{Theory}
2.63	2.43	2.46	0.02	0.01
2.65	2.46	2.49	0.04	0.01
2.68	2.48	2.50	0.01	0.01
2.69	2.49	2.50	0.01	0.00
2.71	2.51	2.50	-0.01	0.00
2.73	2.53	2.54	0.01	0.00
2.75	2.55	2.55	0.00	0.00
2.77	2.57	2.59	0.02	0.01
2.78	2.58	2.55	-0.03	-0.01
2.79	2.59	2.60	0.01	0.00
2.81	2.60	2.59	-0.01	0.00
2.82	2.61	2.61	0.00	0.00
2.83	2.62	2.63	0.01	0.00
2.85	2.64	2.65	0.01	0.00
2.86	2.65	2.64	-0.01	0.00
2.87	2.66	2.67	0.01	0.00
2.89	2.67	2.67	-0.01	0.00
2.91	2.69	2.70	0.00	0.00
2.92	2.71	2.69	-0.01	0.00
2.94	2.72	2.71	0.00	0.00
2.95	2.73	2.71	-0.02	-0.01
2.96	2.74	2.75	0.01	0.00
2.97	2.75	2.74	-0.02	-0.01
2.99	2.77	2.76	0.00	0.00

The kinetics of Rubpy oxidation and reduction at the tip were obtained by a previously described SECM technique in which the tip voltammograms obtained under positive feedback conditions at different tip-substrate distances are fit to a model assuming Butler-Volmer kinetics. [16, 17, 18, 10] Figure 5.9a shows tip voltammograms obtained at different *d*-values for the oxidation of the 2^+ to 3^+ form, while holding the substrate potential where the reaction is diffusion controlled at 0.4 V vs Ag wire. The results show that a higher current was generated when the tip is closer to the substrate, as expected from feedback theory. Note that in this experiment, the a=5 μm tip could approach to 0.45 μm. Figure 5.9b presents the normalized voltammograms derived from Figure 5.9a, where the tip current was normalized with respect to the maximum current, $i_{T,max}$, (the steady state limiting current) in the voltammograms in Figure 5.9a. As shown in Figure 5.9b the voltammograms become more and more drawn out with a decrease of *d*. Rubpy oxidation shows a diffusion –controlled (nernstian) voltammogram at large *d* but as the mass transfer coefficient is increased with a decrease of *d*, the kinetics of ET make a greater contribution and kinetic information can be extracted.

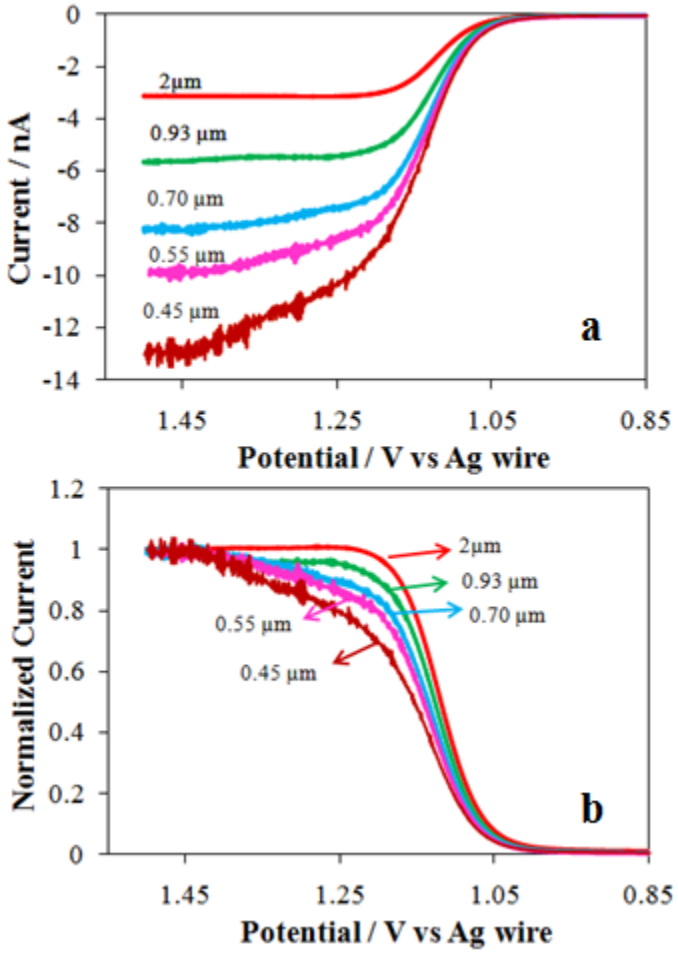

Figure 5.9. (a) Tip steady state voltammograms. (b) Normalized tip steady state voltammograms. The distance (d) between the tip and the substrate are shown in the Figure.

For 0.38 mM Rubpy in MeCN with 0.1 M $TBAPF_6$ as supporting electrolyte at 5-µm-radius Pt tip inside a glovebox. $i_{T,\infty}$= 1.3 nA.

The kinetic parameters for the oxidation were obtained through the use of eqns.5.3.2-5.3.5: [16, 13]

$$I_T(E, L) = \frac{0.68 + \frac{0.78377}{L} + 0.3315\, e^{-\frac{1.0672}{L}}}{\theta + \frac{1}{\kappa}} \quad (5.3.2)$$

$$\theta = 1 + \frac{D_o}{D_R}\, e^{\left(nf\left(E - E^{0\prime}\right)\right)} \quad (5.3.3)$$

$$\kappa = \frac{k^o e^{-\alpha nf\left(E - E^{o\prime}\right)}}{m_o} \quad (5.3.4)$$

$$m_o = \frac{4D_o}{\pi a}\left(0.68 + \frac{0.78377}{L} + 0.3315e^{-1.0672/L}\right) \quad (5.3.5)$$

Where κ is the kinetic parameter and m_o is the effective mass-transfer coefficient. The standard rate constant k^0 and the transfer coefficient α can be measured in terms of known quantities such as distance, d (where $L = d/a$), the potential E and standard potential of reaction E^0 and the steady state tip current at infinite distance, $i_{T,\infty}$. The experimental tip current can be treated with the relation $i_T = I_T(E,L)\ i_{T,\infty}$.[19] Figure 5.10 shows the fit obtained for the experimental scans at different distances, and Table 5.5 summarizes the electrochemical parameters obtained for a series of experiments. The diffusion coefficient (D) of 1.76×10^{-5} cm^2/s for Rubpy in MeCN, calculated from the tip steady-state CV and was used for the calculations, is very close to the D value reported in the literature (e.g. D = 1.8×10^{-5} cm^2/s).[20] The average standard reaction rate constant, k^0, and transfer coefficient, α, for the oxidation of Rubpy are 0.7 ± 0.1 cm/s and 0.28 ± 0.03, respectively. These results are in agreement with those obtained from the quartile potential approach. [9] (where $E_{1/4}$, $E_{1/2}$, $E_{3/4}$ are the potentials at which the tip current is 1/4, 1/2 and 3/4 of the diffusion-limiting current). The dimensionless parameter $k^0/(D/d)$ is also listed in Table 5.5; the values are <5, as required to obtain kinetic information.

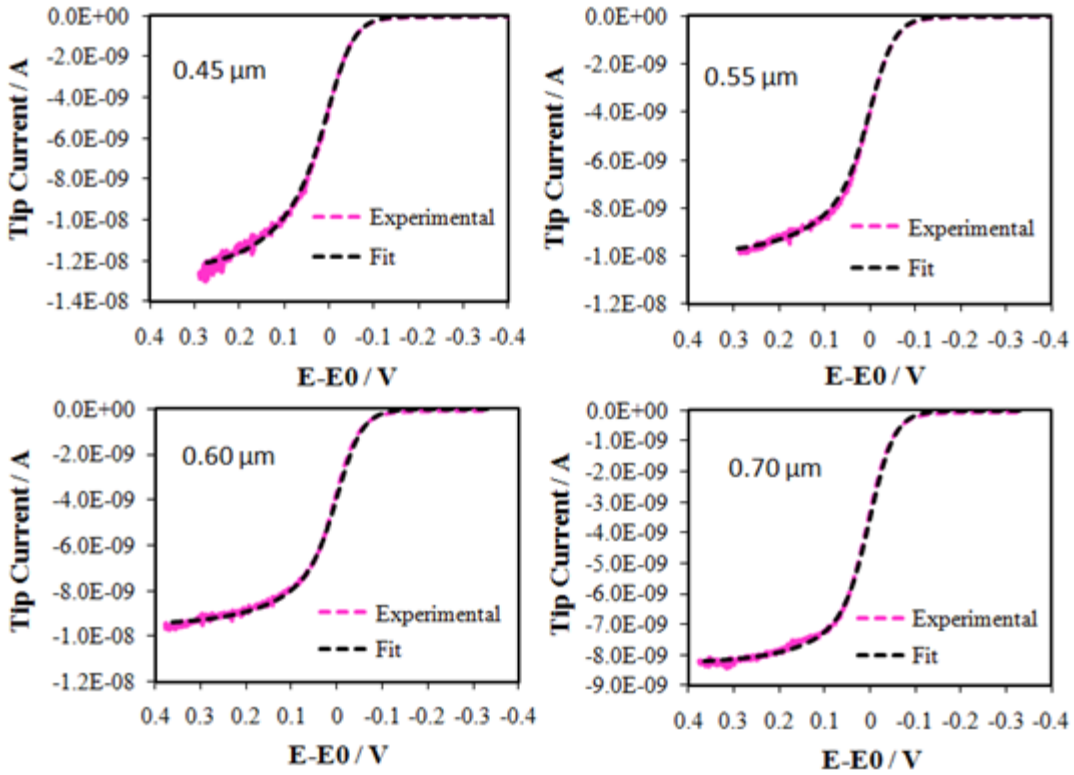

Figure 5.10. Determination of tip kinetic parameters for Rubpy oxidation with tip-substrate distance.

Table 5.5. Kinetic parameters for oxidation of Rubpy at Pt tip electrode from SECM steady-state voltammograms.

No	$\Delta E_{1/4}$,mV	$\Delta E_{3/4}$, mV	L	i_T	k^0, cm/s	α	$k^0/(D/d)$
1	32	38	0.14	6.1	0.8	0.25	3.1
2	33	42	0.13	6.9	0.8	0.25	3.0
3	34	55	0.12	7.3	0.7	0.32	2.4
4	36	47	0.11	7.7	0.6	0.27	2.0
5	41	69	0.09	10	0.5	0.30	1.2

The rate constants for Rubpy reduction were obtained by the same approach under identical experimental conditions by examining the negative potential region. However the reduction was more difficult to study, because, as is well known, it is characterized by three consecutive waves (roughly corresponding to successive electron transfers to the three bpy ligands). The spacing of the second wave from the first of about 0.2 V perturbs the first wave, especially in the limiting current region. This is illustrated by a comparison of the steady state oxidation voltammogram with the substrate biased at 0.4 V and, at the exactly same distance, L, for the reduction with the substrate biased at -0.4V is shown in Figures 5.11a and b. For the oxidation, the experimental data (pink dotted curve) fit very well to the simulated curve with rate constant of 0.7 ± 0.1 cm/s (black curve) in good agreement with results discussed above and showing a clear deviation from nernstian behavior (red curve). To treat the reduction with the same diffusion coefficient, and tip-substrate separation distance, it was necessary to take account of the second wave. If the successive ETs were represented as two steady-state voltammetric waves spaced 0.2 V (the experimentally-measured difference between the half wave potentials of the first and second reduction waves). The normalized waves fit very well (Figure 5.11c) with the experimental data, showing that at this distance, where clear kinetic effects are shown for the oxidation, the reduction is essentially nernstian, i.e. with rate constant $\geq$ 3 cm/s. Thus the reduction reaction, measured under the same conditions, is at least 4 times larger than that of the oxidation.

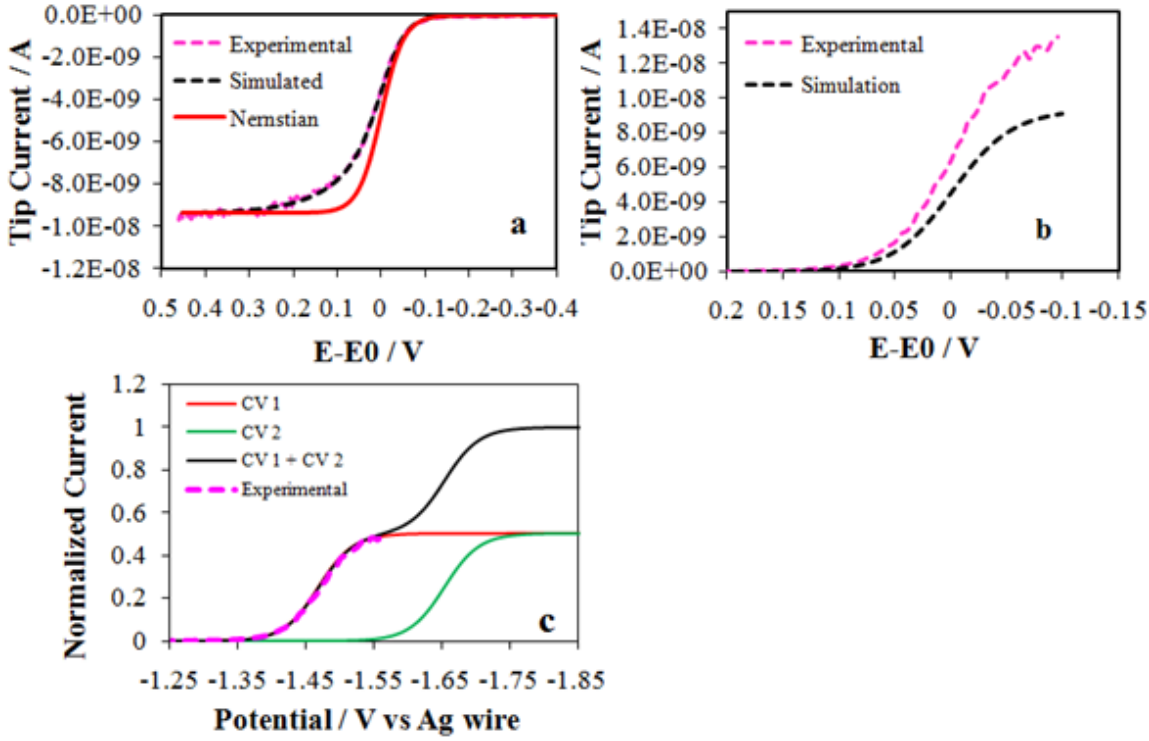

Figure 5.11. Determination of tip kinetic parameters for Rubpy reduction.

The observed difference between the rates of ET between the oxidation and reduction on the same molecule and obtained at the same time under the same conditions, is consistent with the model where the bpy ligands act as a barrier for ET to the Ru(II) center. Oxidation via the ligands cannot occur, because the oxidation of the bpy ligands occurs at significantly more positive potentials.[21] The reduction of the exposed ligands occurs with the possibility of a closer approach of the acceptor group to the electrode. The blocking effects of the ligands have been observed in the study of photo-induced electron transfer reaction between ruthenium bpy complexes and methyl viologen, where the 2, 2'-bipyridines were substituted with propyl, hexyl or adamantyl groups. [22] The rate constant of ET reaction decreased with increasing size of the alkyl substituent. Since the

other factors in a treatment of ET via Marcus theory were essentially the same, the authors ascribed this trend to the fact that a "bulky substituent decreases the orbital overlap between donor and acceptor," i.e. between the Ru(bpy) (D) and MV^{2+} (A) and treated this by a tunneling effect (the electronic coupling matrix elements, H_{rp}).[22] Although the ET here involves oxidation of the Ru(II) center, it demonstrates the importance of distance effects in ET rates with Ru(bpy) complexes. These findings encouraged us to estimate how the difference in rate relates to the difference in ET distance and the β value in equation 5.1. The distance from the Ru center to the H atom para to the N on the pyridine ring is 4.746 Å from the bond distances and bond angles reported by Rillema et al.[23] The approach of the molecule to an electrode may be slightly smaller, so we take a distance, x, or 4 Å. From the minimum difference between the rate constant for oxidation, 0.7 cm/s, and that for reduction, 3 cm/s, a β value of 0.4 $Å^{-1}$ is found. This number is smaller than that expected for transfer through an alkyl chain, where $\beta \sim 1$ $Å^{-1}$. This suggests either that the actual reduction rate constant is considerably larger, e.g. 20 to 30 cm/s or the bpy ligands can behave as conjugated spacers. [3, 4]

5.4 CONCLUSIONS

The kinetics of a donor-acceptor molecule-tris(2,2'-bipyridine)ruthenium (II) (Rubpy) oxidation and reduction in acetonitrile were investigated by steady state voltammetry using scanning electrochemical microscopy (SECM). The SECM setup was placed inside a drybox for carrying out experiments in an anhydrous atmosphere and in the absence of oxygen. The standard rate constant, k^0, for Rubpy oxidation at a Pt

electrode (radius, a = 5 μm) was 0.7 ± 0.1 cm/s, which is smaller than k^0 for Rubpy reduction measured under the same conditions (≥ 3 cm/s). This is attributed to the 2,2'-bipyridine ligands having an electron-transfer blocking effect on the oxidation of the ruthenium(II) center, as opposed to the reduction, which involves electron transfer to the exposed ligands. Differences in the rate of heterogeneous ET from the buried Ru(II) center and to the more available bpy ligand suggests that effects of tunneling may be important. Donor-Acceptor based molecules with the configuration in which the Donor occupies a central position and is connected to bulky acceptors on the ends, or vice versa, could possibly be used as model molecules to study the effects of tunneling on electron transfer processes.

5.7 REFERENCES

[1] Shen, M.; Rodríguez-López, J.; Huang, J.; Liu, Q.; Zhu, X.-H.; Bard, A. J. *J. Am. Chem. Soc.* **2010**, *132*, 13453-13461.

[2] Finklea, H. O. Electroanal. Chem. 1996, 19, 109

[3] Smalley, J. F.; Feldberg, S. W.; Chidsey, C. E. D.; Linford, M. R.; Newton, M. D.; Liu, Y.-P. *J. Phys. Chem.* **1995**, *99*, 13141

[4] Sachs, S. B.; Dudek, S. P.; Hsung, R. P.; Sita, L. R.; Smalley, J. F.; Newton, M. D.; Feldberg, S. W.; Chidsey, C. E. D. *J. Am. Chem. Soc.* **1997**, *119*, 10563.

[5] Creager, S.; Yu, S. J.; Bamdad, D.; O'Conner, S.; MacLean, T.; Lam, E.; Chong, Y.; Olsen, G. T.; Luo, J.; Gozin, M.; Kayyem, J. F. *J. Am. Chem. Soc.* **1999**, *121*, 1059

[6] Juris, A.; Balzani, V.; Barigelletti, F.; Campagna, S.; Belser, P.; Von Zelewsky, A. *Coord. Chem. Rev.* **1988**, *84*, 85-277.

[7] Sun, P.; Mirkin, M.V. *Anal. Chem* .**2006**, *78*, 6526-6534

[8] Zhou, J. F.; Zu, Y. B.; Bard, A. J. *J. Electroanal. Chem.* **2000**, *491*, 22-29.

[9] Mirkin, M. V.; Bard, A. J. *Anal. Chem.* **1992**, *64*, 2293-2302.

[10] Mirkin, M. V.; Bulhões, L. O. S.; Bard, A. J. *J. Am.Chem. Soc.* **1993**, *115*, 201-204.

[11] Ding, Z. F.; Quinn, B. M.; Bard, A. J. *J. Phys. Chem. B* **2001**, *105*, 6367-6374.

[12] Bard, A. J. ; Mirkin, M. V.; Unwin, P. R.; Wipf, D. O. *J. Phys. Chem.* **1992,***96*, 1861.

[13] *Scanning Electrochemical Microscopy*; Bard, A. J., Mirkin, M. V., Eds.; Marcel Dekker: New York, 2001.

[14] Bard, A. J.; Fan, F.-R. F.; Mirkin, M. V. Scanning Electrochemical Microscopy. In *Electroanalytical Chemistry*; Bard, A. J., Ed.; Marcel Dekker: New York, 1993, Vol. 18, pp 243-373.

[15] Shen , M.; Netzahualcoyotl A. C.; Bard, A. J., manuscript in preparation.

[16] Mirkin, M. V.; Richards, T. C.; Bard, A. J. *J. Phys. Chem.* **1993**, *97*, 7672-7677.

[17] Mirkin, M. V.; Bard, A. J. *Anal. Chem.* **1993**, *97*, 7672-7677.

[18] Mirkin, M. V.; Bard, A. J. *J. Electrochem. Soc.* **1992**, *139*, 3535—3539.

[19] Rodríguez-López, J.; Minguzzi, A.; Bard, A. J. *J. Phys. Chem. C* **2010**, *114*, 18645-18655.

[20] Wipf, D. O.; Kristensen, E. W.; Deakin, M. R.; Wightman, R. M. *Anal. Chem.* **1988**, *60*, 306-310.

[21] (a) Gaudiello, J. G; Sharp, P. R; Bard, " A. J. *J. Am. Chem. Soc.*, **1982**, *104*, 6367-6377; (b) Gaudiello, J. G. ; Bradley, P. G;. Norton, K. A.; Woodruff, W. H.; Bard, A. J. *Inorg. Chem*, **1984**,*23*, 3.

[22] Hamada, T.; Tanaka, S.; Koga, H.; Sakai, Y.; Sakaki, S. *Dalton Trans.* **2003**, 692-698.

[23]Rillema, D. P.; Jones, D. S.; Woods, C.; Levy, H. A. *Inorg. Chem.* **1992**, *31*, 2935-2938.

Outlook

A very strong ECL emitter was discovered in the process of ECL study, (4,7-bis(4-(4-sec-butoxyphenyl)-5-(3,5-di(1-naphthyl)phenyl)thiophen-2-yl)-2,1,3-benzothiadiazole), **1b**. Its ECL could have potential application in biosensing. **1b** has the configuration of D-A-D. Its annihilation ECL was generated through anion-cation and anion-dication reactions. Radical anion-cation annihilation produced by potential steps shows symmetric ECL transients during anodic and cathodic pulses while for anion-dication annihilation, transient ECL shows asymmetry in which the anodic pulse is narrower than the cathodic pulse. The transient ECL was successfully simulated using COMSOL Multiphysics ® Software v.3.2. Digital simulation of the transient ECL experiments showed that the origin of the observed asymmetry is asymmetry in the amount of generated charges rather than instability of the electrogenerated species. Other novel ECL system was explored, such as generation of annihilation ECL from carbon quantum dots prepared through electrochemical reduction of HOPG in organic solvent under inert atmosphere. Another interesting phenomenon was observed in the electrochemical study of **1b**, the kinetics of heterogeneous electron transfer for the reduction and oxidation of **1b** are different. Since the bulky donor on the sides have blocking effect on the acceptor in the center, the reduction rate constant is smaller than the oxidation rate constant. This observation leads us to think about the electron transfer kinetics of another D-A molecule, Rubpy, which is a famous dye producing strong ECL. It has Ru in the center connected to 3 bpy ligands on the sides, since the ligands are pretty small, and no one has studied the rate of this molecule before, probably because the electron transfer rate is pretty fast. Thus SECM, a technique used to study kinetics of fast

reaction, was used to study the reduction and oxidation kinetics of Rubpy. During the kinetics study of Rubpy, I polished the 5μm-radius Pt tip very carefully, use SEM to check the tip and explored new way to align the tip and the substrate by SECM imaging to find the top plateau to bring the tip to very close distance to the substrate (240nm). The methodology to polish, check and align the tip could be used in other studies, like STM.

Appendix A. Publications derived from ECL and SECM work

In this section are listed the publications derived from the work presented in this dissertation at the time of completion. Other project in which SECM was used for the study of annihilation electrogenerated chemiluminescence is listed. In this project, the author participated through experimentation, simulations and scientific discussion.

Chapters 2

Shen, M.; Rodríguez-López, J.; Lee, Y.-T.; Chen, C.-T.; Fan, F.-R. F.; Bard, A. J. Electrochemistry and Electrogenerated Chemiluminescence of a Novel Donor-Acceptor FPhSPFN Red Fluorophore. *J. Phys. Chem. C* **2010,** *114*, 9772–9780.

Chapter 3

Shen, M.; Rodríguez-López, J.; Huang, J.; Liu, Q.; Zhu, X.-H.; Bard, A. J. "Electrochemistry and Electrogenerated Chemiluminescence of Dithienylbenzothiadiazole Derivative. Differential Reactivity of Donor and Acceptor Groups and Simulations of Radical Cation-Anion and Dication- Radical Anion Annihilations." *J. Am. Chem. Soc.* **2010**, *132*, 13453–13461.

Shen, M.; Huang, J.; Liu, Q.; Zhu, X.-H.; Bard, A. J. Electrochemistry and Electrogenerated Chemiluminescence Study of Film and Solution of Substituted Thiophene Red Fluorophore. *In preparation.*

Chapter 4

Shen, M.; Fan, F.-R. F.; Bard, A. J. In situ Electro-Reduction Synthesis of Carbon Quantum Dots from HOPG and its Electrogenerated Chemiluminescence study. *In preparation.*

Chapter 5

Shen, M.; Bard, A. J. Localized Electron Transfer and the Role of Tunneling on the Rates of $Ru(bpy)_3^{2+}$Oxidation and Reduction as Measured by Scanning Electrochemical Microscopy**.** *In preparation.*

Shen, M.; Netzahualcoyotl A. C.; Bard, A. J. Tip Construction and Simulations of the Tip Approach Curve with Geometric Variations**.** *In preparation.*

Other works

Rodríguez-López, J.; Shen, M.; Nepomnyashchii, A.; Bard, A. J. Scanning Electrochemical Microscopy studies of Radical Annihilation Electrogenerated Chemiluminescence. *In preparation.*

References

Chapter 1

Dufford, R. T.; Nightingale, D.; Gaddum, W. L. *J. Am. Chem. Soc.* **1927**, *49*, 1858.

Harvey, N. *J. Phys. Chem.* **1929**, *33*, 1456.

Hercules, D. M. *Science.* **1964**, *145*, 808.

Bard, A. J. in *Electrogenerated Chemiluminescence*; Bard, A. J., Ed.; Marcel Dekker: New York, 2004.

For reviews on ECL, see: (a)Ref 2. (b) Richter, M. M. *Chem. Rev*. **2004**, *104*, 3003-3036. (c) Knight, A. W.; Greenway, G. M. *Analyst* **1994**, *119*, 879-890. (d) Faulkner, L. R.; Bard, A. J. *Electroanalytical Chemistry*; Marcel Dekker: New York, 1977; Vol. 10, p 1. (e) Bard, A. J.; Debad, J. D.; Leland, J. K.; Sigal, G. B.; Wilbur, J. L.; Wohlstadter, J. N. in *Encyclopedia of Analytical Chemistry: Applications, Theory and Instrumentaion*; Meyers, R. A., Ed.; John Wiley & Sons: New York, 2000; Vol. 11, p 9842.

Forry, S. P.; Wightman, R. M. in *Electrogenerated Chemiluminescence*; Bard, A. J., Ed.; Marcel Dekker: New York, 2004; p 277.

Maloy, J. T. in *Electrogenerated Chemiluminescence*; Bard, A. J., Ed.; Marcel Dekker: New York, 2004; p 159.

Keszthelyi, C. P.; Tokel-Takvoryan, N. E.; Bard, A. J. *Anal. Chem*. **1975**, *47*, 249-256.

Sartin, M. M.; Zhang, H. Y.; Zhang, J. Y.; Zhang, P.; Tian, W. J.; Wang, Y.; Bard, A. J. *J. Phys. Chem. C* **2007**, *111*, 16345-16350.

Choi, J.-P.; Wong, K.-T.; Chen, Y.-M.; Yu, J.-K.; Chou, P.-T.; Bard, A. J. *J. Phys. Chem. B.* **2003**, *107*, 14407-14413.

Bard, A. J. In *Scanning Electrochemical Microscopy*; Bard, A. J.; Mirkin, M. V., Eds,; Marcel Dekker: New York, 2001, pp 1.

Borgwarth, K.; Heinze, J. In *Scanning Electrochemical Microscopy*; Bard, A. J.; Mirkin, M. V., Eds,; Marcel Dekker: New York, 2001, pp 217-219.

Mirkin, M. V.; Richards, T. C.; Bard, A. J. *J. Phys. Chem.* **1993**, *97*, 7672-7677.

Scanning Electrochemical Microscopy; Bard, A. J.; Mirkin, M. V., Eds,; Marcel Dekker: New York, 2001.Dufford, R. T.; Nightingale, D.; Gaddum, W. L. *J. Am. Chem. Soc.* **1927**, *49*, 1858.

Chapter 2

Lai, R. Y.; Kong, X. X.; Jenekhe, S. A.; Bard. A. J. *J. Am. Chem. Soc.* **2003**, *125*, 12631-12639.

Lai, R.Y.; Fabrizio, E. F.; Lu, L.; Jenekhe, S. A.; Bard, A. J. *J. Am. Chem. Soc.* **2001**, *123*, 9112-9118.

Izadyar, A.; Omer, K. M.; Liu, Y. Q.; Chen, S. Y.; Xu, X. J.; Bard, A. J. *J. Phys. Chem. C* **2008**, *112*, 20027-20032.

Fungo, F.; Wong, K.-T.; Ku, S.-Y.; Hung, Y.-Y.; Bard, A. J. *J. Phys. Chem. B* **2005**, *109*, 3984-3989.

Pan, Y.; Zhao, J. S.; Ji, Y. Y.; Yan, L.; Yu, S. Q. *Chem. Phys*. **2006**, *320*, 125-132.

Izadyar, A.; Omer, K. M.; Liu, Y. Q.; Chen, S. Y.; Xu, X. J.; Bard, A. J. *J. Phys. Chem. C* **2008**, *112*, 20027-20032.

Chiu, K.Y.; Su, T. X.; Li, J. H.; Lin, T.-H.; Liou, G.-S.; Cheng, S.-H. *J. Electroanal. Chem*. **2005**, *575*, 95-101.

Zou, Y. P.; Sang, G. Y.; Wan, M. X.; Tan, S. T.; Li, Y. F. *Macromol. Chem. Phys.*, **2008**, *209*, 1454-1462.

Hancock, J. M.; Gifford, A. P.; Zhu, Y.; Lou, Y.; Jenekhe, S. A. *Chem. Mater*. , **2006**, *18*, 4924-4932.

Sartin, M. M.; Shu, C. F.; Bard, A. J. *J. Am. Chem. Soc*. **2008**, *130*, 5354-5360.

Fungo, F.; Wong, K.-T.; Ku, S.-Y.; Hung, Y.-Y.; Bard, A. J. *J. Phys. Chem. B* **2005**, *109*, 3984-3989.

Natera, J.; Otero, L.; D'Eramo, F.; Sereno, L.; Fungo, F.; Wang, N.-S.; Tsai, Y.-M.; Wong, K.-T. *Macromolecules*, **2009**, *42*, 626-635.

Lee, Y.-T.; Chiang, C.-L.; Chen, C.-T. *Chem. Commun.* **2008**, 217–219.

Sartin, M. M.; Shu, C. F.; Bard, A. J. *J. Am. Chem. Soc*. **2008**, *130*, 5354-5360.

Denuault, G.; Mirkin, M. V.; Bard, A. J. *J. Electroanal. Chem.* **1991**, *308*, 27-38.

Grimshaw, J. *Electrochemical Reactions and Mechanisms in Organic Chemistry*. Elsevier: Amsterdam, 2000; P 66.

Rashidnadimi, S.; Hung, T. H.; Wong, K.-T.; Bard, A. J. *J. Am. Chem. Soc.* **2008**, *130*, 634-639.

Berlman, I. B. *Handbook of Fluorescence Spectra of Aromatic Molecules*, 2nd ed.; Academic Press: New York, 1971.

Bard, A. J. in *Electrogenerated Chemiluminescence*; Bard, A. J., Ed.; Marcel Dekker: New York, 2004.

Lakowicz, J. R. *Principles of Fluorescence Spectroscopy*, 3rd ed; Springer Science + Business Media: New York, 2006.

Nigam, S.; Rutan, S. *Appl. Spectrosc*. **2001**, *55*, 362A-370A.

Kapturkiewicz, A.; Herbich, J.; Nowacki, J. *Chem. Phys. Lett*. **1997**, *275*, 355-362.

Itaya, K.; Toshima, S. *Chem. Phys. Lett*. **1977**, *51*, 447-452.

Bard, A. J. in *Electrogenerated Chemiluminescence*; Bard, A. J., Ed.; Marcel Dekker: New York, 2004. Chapters 2 (Fan, F.-R. F.) and 3 (Maloy, J. T.).

Cruser, S. A; Bard, A. J. *J. Am. Chem. Soc.* **1969**, *91*, 267.

Chapter 3

Huang, J.; Liu, Q.; Zou, J.-H.; Zhu, X.-H.; Li, A.-Y.; Li, J.-W.; Wu, S.; Peng, J. B.; Cao, Y.; Xia, R. D.; Bradley, D. D. C.; Roncali, J. *Adv. Funct. Mater.* **2009**, *19*, 2978–2986.

Forster, R. J.; Bertoncello, P.; Keyes, T. E. *Annu. Rev. Anal. Chem.* **2009**, *2*, 359–385.

Bard, A. J. in *Electrogenerated Chemiluminescence*; Bard, A. J., Ed.; Marcel Dekker: New York, 2004.

For reviews on ECL, see: (a)Ref 2. (b) Richter, M. M. *Chem. Rev*. **2004**, *104*, 3003-3036. (c) Knight, A. W.; Greenway, G. M. *Analyst* **1994**, *119*, 879-890. (d) Faulkner, L. R.; Bard, A. J. *Electroanalytical Chemistry*; Marcel Dekker: New York, 1977; Vol. 10, p 1. (e) Bard, A. J.; Debad, J. D.; Leland, J. K.; Sigal, G. B.; Wilbur, J. L.; Wohlstadter, J. N. in *Encyclopedia of Analytical Chemistry: Applications, Theory and Instrumentaion*; Meyers, R. A., Ed.; John Wiley & Sons: New York, 2000; Vol. 11, p 9842.

Maloy, J. T. in *Electrogenerated Chemiluminescence*; Bard, A. J., Ed.; Marcel Dekker: New York, 2004; p 159.

Keszthelyi, C. P.; Tokel-Takvoryan, N. E.; Bard, A. J. *Anal. Chem*. **1975**, *47*, 249-256.

Richter, M. M. in *Electrogenerated Chemiluminescence*; Bard, A. J., Ed.; Marcel Dekker: New York, 2004; p 306.

Tokel, N.; Bard, A. J. *J. Am. Chem. Soc.* **1972**, *94*, 2862-2863.

Juris, A.; Balzani, V.; Barigelletti, F.; Campagna, S.; Belser, P.; Von Zelewsky, A. *Coord. Chem. Rev.* **1988**, *84*, 85-277.

Kapturkiewicz, A.; Grabowski, Z. R.; Jasny, J. *J. Electroanal. Chem.* **1990**, *279*, 55-65.

Kapturkiewicz, A.; Herbich, J.; Nowacki, J. *Chem. Phys. Lett.* **1997**, *275*, 355-362.

Lai, R.Y.; Fabrizio, E. F.; Lu, L.; Jenekhe, S. A.; Bard, A. J. *J. Am. Chem. Soc.* **2001**, *123*, 9112-9118.

Lai, R.Y.; Kong, X. X.; Jenekhe, S. A.; Bard, A. J. *J. Am. Chem.Soc.* **2003**, *125*, 12631–12639.

Omer, K. M.; Ku, S.-Y.; Wong, K.-T.; Bard, A. J. *Angew. Chem. Int. Ed.* **2009**, *48*, 9300-9303.

Sartin, M. M.; Zhang, H. Y.; Zhang, J. Y.; Zhang, P.; Tian, W. J.; Wang, Y.; Bard, A. J. *J. Phys. Chem. C* **2007**, *111*, 16345-16350.

Cardona, C. M.; Mendoza, S.; Kaifer, A. E. *Chem. Soc. Rev.*, **2000**, *29*, 37-42.

Cruser, S. A.; Bard, A. J. *J. Am. Chem. Soc.* **1969**, *91*, 267-275.

Forster, R. J.; Bertoncello, P.; Keyes, T. E. *Annu. Rev. Anal. Chem.* **2009**, *2*, 359-385.

Sartin, M. M.; Shu, C. F.; Bard, A. J. *J. Am. Chem. Soc*. **2008**, *130*, 5354-5360.

Shen, M.; Rodríguez-López, J.; Lee, Y.-T.; Chen, C.-T.; Fan, F.-R. F.; Bard, A. J. *J. Phys. Chem. C* **2010,** *114*, 9772–9780.

Fungo, F.; Wong, K.-T.; Ku, S.-Y.; Hung, Y.-Y.; Bard, A. J. *J. Phys. Chem. B* **2005**, *109*, 3984–3989.

Omer, K. M.; Ku, S.-Y.; Wong, K.-T.; Bard, A. J. *J. Am. Chem. Soc*. **2009**, *131*, 10733-10741.

Kojima, H.; Bard, A. J. *J. Am. Chem. Soc.* **1975**, *97*, 6317-6324.

Bezman, R.; Faulkner, L. R. *J. Am. Chem. Soc.* **1972**, *94*, 3699-3707.

Feldberg, S. W. *J. Am. Chem. Soc*. **1966**, *88*, 390-393.

Bard, A. J. in *Electrogenerated Chemiluminescence*; Bard, A. J., Ed.; Marcel Dekker: New York, 2004.Chapter 6 (Forry, S. P.; Wightman, R. M.), Chapter 7 (Richter, M. M.) and Chapter 3 (Maloy, J. T.).

Feldberg S. W. *J. Elecroanal. Chem.* **1981**, *127*, 1-10.

Lakowicz, J. R. *Principles of Fluorescence Spectroscopy*, 3rd ed; Springer Science + Business Media: New York, 2006.

Seixas de Melo, J.; Pina, J.; Burrows, H. D.; Di Paolo, R. E.; Maçanita, A. L. *Chem. Phys.* **2006**, *330*, 449–456.

Narwark, O.; Meskers, S.C.J.; Peetz, R.; Thorn-Csányi, E.; Bässler, H. Chem. Phys. **2003**, *294*, 1–15.

Chapter 4

Baker, S. N.; Baker, G. A. *Angew. Chem. Int. Ed*. **2010**, *49*, 2-21.

Pumera, M. *Chem. Soc. Rev.* **2010**, *39*, 4146-4157.

Xu, X. Y.; Ray, R.; Gu, Y. L.; Ploehn, H. J.; Gearheart, L.; Raker, K.; Scrivens, W. A. *J. Am. Chem. Soc.* **2004**, *126*, 12736 – 12737.

Hu, S.-L.; Niu, K.-Y.; Sun, J.; Yang, J.; Zhao, N.-Q.; Du, X.-W. *J. Mater. Chem.* **2009**, *19*, 484 – 488.

Sun, Y.-P.; Wang, X.; Lu, F.; Cao, L.; Meziani, M. J.; Luo, P. G.; Gu, L.; Veca, L. M. *J. Phys. Chem. C* **2008**, 112, 18295 – 18298.

Sun, Y. P.; Zhou, B.; Lin, Y.; Wang, W.; Fernando, K. A. S.; Pathak, P.; Meziani, M. J.; Harruff, B. A.; Wang, X.; Wang, H. F.; Luo, P. G.; Yang, H.; Kose, M. E.; Chen, B.; Veca, L. M.; Xie, S.-Y. *J. Am. Chem. Soc*. **2006**, *128*, 7756 – 7757.

Bourlinos, A. B.; Stassinopoulos, A.; Anglos, D.; Zboril, R.; Georgakilas, V.; Giannelis, E. P. *Chem. Mater.* **2008**, *20*, 4539 – 4541.

Liu, R. L.; Wu, D. Q.; Liu, S. H.; Koynov, K.; Knoll, W.; Li, Q. *Angew. Chem.* **2009**, *121*, 4668 – 4671; *Angew. Chem. Int. Ed.* **2009**, *48*, 4598 – 4601.

Zhu, H.; Wang, X.; Li, Y.; Wang, Z.; Yang, F.; Yang, X. *Chem. Commun.* **2009**, 5118 – 5120.

Bourlinos, A. B.; Stassinopoulos, A.; Anglos, D.; Zboril, R.; Karakassides, M.; Giannelis, E. P. *Small* **2008**, *4*, 455 – 458.

Liu, H. P.; Ye, T.; Mao, C. D.; *Angew. Chem.* **2007**, *119*, 6593 – 6595; *Angew. Chem. Int. Ed.* **2007**, *46*, 6473 – 6475.

Ray, S. C.; Saha, A.; Jana, N. R.; Sarkar, R. *J. Phys. Chem. C* **2009**, *113*, 18546 – 18551.

Tian, L.; Ghosh, D.; Chen, W.; Pradhan, S.; Chang, X.; Chen, S. *Chem. Mater.* **2009**, *21*, 2803 – 2809.

Pan, D.; Zhang, J.; Li, Z.; Wu, M. *Adv. Mater.* **2010**, *22*, 734-738.

Lu, J.; Yang, J.-X.; Wang, J.; Lim, A.; Wang, S.; Loh, K. P. *ACS Nano* **2009**, *3*, 2367 – 2375.

Zhao, Q.-L.; Zhang, Z.-L.; Huang, B.-H.; Peng, J.; Zhang, M.; Pang, D.-W. *Chem. Commun.* **2008**, 5116 – 5118.

Zheng, L. Y.; Chi, Y.W.; Dong, Y. Q.; Lin, J. P.; Wang, B. B. *J. Am. Chem. Soc.* **2009**, *131*, 4564 – 4565.

Zhou, J. G.; Booker, C.; Li, R. Y.; Zhou, X. T.; Sham, T. K.; Sun, X. L.; Ding, Z. F. *J. Am. Chem. Soc.* **2007**, *129*, 744 – 745.

Gokus, T.; Nair, R. R.; Bonetti, A.; Böhmler, M.; Lombardo, A.; Novoselov, K.; Geim, A. K.; Ferrari, A. C.; Hartschuh, A. *ACS Nano*, **2009**, *3*, 3963-3968.

Wu, J.; Pisula, W.; Müllen, K. *Chem. Rev*. **2007**, *107*, 718-747.

Yan, X.; Cui, X.; Li, L.-S. *J. Am. Chem. Soc.* **2010**, *132*, 5944–5945.

Bard, A. J. in *Electrogenerated Chemiluminescence*; Bard, A. J., Ed.; Marcel Dekker: New York, 2004.

For reviews on ECL, see: (a) Richter, M. M. *Chem. Rev*. **2004**, *104*, 3003-3036. (b) Knight, A. W.; Greenway, G. M. *Analyst* **1994**, *119*, 879-890. (c) Faulkner, L. R.; Bard, A. J. *Electroanalytical Chemistry*; Marcel Dekker: New York, 1977; Vol. 10, p 1. (d) Bard, A. J.; Debad, J. D.; Leland, J. K.; Sigal, G. B.; Wilbur, J. L.; Wohlstadter, J. N. in *Encyclopedia of Analytical Chemistry: Applications, Theory and Instrumentaion*; Meyers, R. A., Ed.; John Wiley & Sons: New York, 2000; Vol. 11, p 9842.

Dong, Y.; Zhou, N.; Lin, X.; Lin, J.; Chi, Y.; Chen, G. *Chem. Mater*. **2010**, *22*, 5895-5899.

Fan, F.-R. F.; Park, S; Zhu, Y.; Ruoff, R. S.; Bard, A. J. *J. Am. Chem. Soc.*, **2009**, *131*, 937-939.

Mochalin, V. N.; Gogotsi, Y. *J. Am. Chem. Soc*. **2009**, *131*, 4594-4595.

Yan, X.; Cui, X.; Li, B.; Li, L.-S. *Nano Lett.* **2010**, *10*, 1869-1873.

Wang, Z.; Xiao, P.; He, N. *Carbon.* **2006**, *44*, 3277-3284.

Mao, X.-J.; Zheng, H.-Z.; Long, Y.-J.; Du, J.; Hao, J.-Y.; Wang, L.-L.; Zhou, D.-B. Spectrochimica Acta Part A, **2010**, *75*, 553–557.

Shen, M.; Huang, J.; Liu, Q.; Zhu, X.-H.; Bard, A. J. Electrochemistry and Electrogenerated Chemiluminescence Study of Film and Solution of Substituted Thiophene Red Fluorophore. *In preparation.*

Seixas de Melo, J.; Pina, J.; Burrows, H. D.; Di Paolo, R. E.; Maçanita, A. L. *Chem. Phys.* **2006**, *330*, 449–456.

Narwark, O.; Meskers, S.C.J.; Peetz, R.; Thorn-Csányi, E.; Bässler, H. Chem. Phys. **2003**, *294*, 1–15.Baker, S. N.; Baker, G. A. *Angew. Chem. Int. Ed*. **2010**, *49*, 2-21.

Chapter 5

Finklea, H. O. Electroanal. Chem. 1996, 19, 109

Smalley, J. F.; Feldberg, S. W.; Chidsey, C. E. D.; Linford, M. R.; Newton, M. D.; Liu, Y.-P. *J. Phys. Chem.* **1995**, *99*, 13141

Sachs, S. B.; Dudek, S. P.; Hsung, R. P.; Sita, L. R.; Smalley, J. F.; Newton, M. D.; Feldberg, S. W.; Chidsey, C. E. D. *J. Am. Chem. Soc.* **1997**, *119*, 10563.

Creager, S.; Yu, S. J.; Bamdad, D.; O'Conner, S.; MacLean, T.; Lam, E.; Chong, Y.; Olsen, G. T.; Luo, J.; Gozin, M.; Kayyem, J. F. *J. Am. Chem. Soc.* **1999**, *121*, 1059

Shen, M.; Rodríguez-López, J.; Huang, J.; Liu, Q.; Zhu, X.-H.; Bard, A. J. *J. Am. Chem. Soc.* **2010**, *132*, 13453-13461.

Sun, P.; Mirkin, M.V. *Anal. Chem* .**2006**, *78*, 6526-6534.

Zhou, J. F.; Zu, Y. B.; Bard, A. J. *J. Electroanal. Chem.* **2000**, *491*, 22-29.

Mirkin, M. V.; Bard, A. J. *Anal. Chem.* **1992**, *64*, 2293-2302.

Mirkin, M. V.; Bulhões, L. O. S.; Bard, A. J. *J. Am.Chem. Soc.* **1993**, *115*, 201-204.

Ding, Z. F.; Quinn, B. M.; Bard, A. J. *J. Phys. Chem. B* **2001**, *105*, 6367-6374.

Scanning Electrochemical Microscopy; Bard, A. J., Mirkin, M. V., Eds.; Marcel Dekker: New York, 2001.

Juris, A.; Balzani, V.; Barigelletti, F.; Campagna, S.; Belser, P.; Von Zelewsky, A. *Coord. Chem. Rev.* **1988**, *84*, 85-277.

Bard, A. J.; Fan, F.-R. F.; Mirkin, M. V. Scanning Electrochemical Microscopy. In *Electroanalytical Chemistry*; Bard, A. J., Ed.; Marcel Dekker: New York, 1993, Vol. 18, pp 243-373.

Mirkin, M. V.; Richards, T. C.; Bard, A. J. *J. Phys. Chem.* **1993**, *97*, 7672-7677.

Mirkin, M. V.; Bard, A. J. *Anal. Chem.* **1993**, *97*, 7672-7677.

Mirkin, M. V.; Bard, A. J. *J. Electrochem. Soc.* **1992**, *139*, 3535—3539.

Rodríguez-López, J.; Minguzzi, A.; Bard, A. J. *J. Phys. Chem. C* **2010**, *114*, 18645-18655.

Wipf, D. O.; Kristensen, E. W.; Deakin, M. R.; Wightman, R. M. *Anal. Chem.* **1988**, *60*, 306-310.

Hamada, T.; Tanaka, S.; Koga, H.; Sakai, Y.; Sakaki, S. *Dalton Trans.* **2003**, 692-698.
Rillema, D. P.; Jones, D. S.; Woods, C.; Levy, H. A. *Inorg. Chem.* **1992**, *31*, 2935-2938.

Vita

Mei Shen was born in Shanxi, China in 1982. After completing her high school work, she entered Sichuan University in 2000. She received a Bachelor of Science in Chemistry from Sichuan Unverstiy in 2004 and a Master of Science in Physical Chemistry in 2007 with honors. Her bachelor's thesis about high performance rare earth oxygen storage materials as catalyst support for three-way catalyst used for automotive waste conversion, directed by Prof. Yaoqiang Chen, was awarded third prize in 2004 by Sichuan Universtiy. Her master study was about Catalytic combustion of volatile organic compounds (VOCs), advised by Prof. Yaoqiang Chen. She moved to Austin, Texas in August 2007 to begin her Ph.D. studies under the direction of Prof. Allen J. Bard at the University of Texas at Austin.

Permanent e-mail: meishen@utexas.edu, mei20078@hotmail.com

This dissertation was typed by the author.